Stress Conditioning Controls Differentiation, Organization, and Maturation of Functional Bioengineered Human Cardiovascular Tissue

Nathaniel Lindsay Tulloch

A dissertation

submitted in partial fulfillment of the

requirements for the degree of

Doctor of Philosophy

University of Washington

2012

Charles E Murry, Chair

Randall T Moon

Michael A Laflamme

Program Authorized to Offer Degree:

Molecular and Cellular Biology

Abstract

Stress Conditioning Controls Differentiation, Organization, and Maturation of Functional Bioengineered Human Cardiovascular Tissue

Nathaniel Lindsay Tulloch

University of Washington

The regulation of heart growth through the interaction of cell types, matrix molecules, and mechanical cues is poorly understood, yet is necessary for the heart to reach its proper size and function. This body of work focuses on the directive cues necessary for differentiation, organization, and maturation of developing human cardiac tissue through proliferation, cellular and matrix alignment, hypertrophy, contractility, and force generation. Using mechanical stress conditioning and vascular cell co-culture in the context of tissue engineering approaches that utilize human cardiomyocytes within 3-dimensional scaffolds, we have been able to generate organized human myocardium *in vitro* and, further, to modulate cardiomyocyte differentiation, proliferation, and hypertrophy, as well as improve the maturation and contractile function of the engineered tissue as a whole. First, we found that stress conditioning and the presence of human endothelium both increased cardiomyocyte proliferation, and that stress conditioning and a 3-dimensional scaffold environment increased hypertrophy and cell alignment of cardiomyocytes, as well as cardiomyocyte differentiation from cardiovascular progenitor cells. We also observed that these vascularized engineered cardiac tissue constructs could be engrafted onto the heart *in vivo* and quickly perfused by host circulation through connection to the pre-formed human vascular networks within the constructs, indicating that these pre-vascularized cardiac tissues may have potential for therapeutic applications. Finally, as these bioengineered tissues are able to contract spontaneously and synchronously, we were able to observe and measure calcium transients as well as active twitch force production within the intact cardiac tissue constructs. Quantification of active force allowed us to determine Force/Length Relationships analogous to Frank-Starling Curves generated in the intact heart. Not only did these constructs become more contractile when stretched to greater lengths, as native myocardium does, but 14 days of stress pre-conditioning markedly potentiated this tissue-level response. The goal of these studies has been to characterize *in vitro* models of human cardiac development and to work towards human therapeutics using organized, vascularized, contractile human cardiac tissue.

Table of Contents

List of Figures

List of Tables

Acknowledgements

I would first and foremost like to thank my advisor Charles Murry, and to recognize the unique and incomparable training environment provided within the context of the Murry lab, as well as my extended second homes of the Regnier and Laflamme labs. I would like to directly acknowledge my publication co-authors, without whose efforts these studies would not be possible, and who wear, often at the same time, the various hats of coworker, mentor, and friend. In alphabetical order, they are Hans Reinecke, Jia-Ling Ruan, Kip Hauch, Lil Pabon, Maria Razumova, Mark Saiget, Michael Regnier, Sarah Fernandes, Sharon Paige, Steven Korte, and Veronica Muskheli. I would also specifically like to thank my reading committee members Michael Laflamme and Randall Moon, as well as my other supervisory committee members: Michael Regnier, David Russell, and Patrick Paddison, for their critical thinking and advice. I very much appreciate the funding support of the Cardiovascular Pathology Training grant overseen by Stephen Schwartz and administered by J.P. Paredes, as well the support and encouragement of the Medical Scientist Training Program, led by Marshall Horowitz and managed by Marcie Buckner, and the structure of the Molecular and Cellular Biology Program here at the University of Washington through whose framework I have been able to pursue this degree. And lastly, I would like to again recognize Dr. Charles Murry for creating and maintaining such an outstanding group of people who are able to produce amazing science while working together in camaraderie and friendship.

Dedication

I would like to dedicate this to my grandmother Mamine, who taught me about crows, and to hate grackles and love robins.

Chapter 1: Introduction

Engineered cardiovascular tissue has been an important goal for the field of cardiac biology for three distinct reasons: it provides a model system for investigating normal human myocardial development, it is required for the development of models of cardiomyopathies and other cardiovascular diseases and, lastly, it has alluring potential for the creation of cell and tissue-based therapies for patients with cardiovascular disease.

Cardiac tissue engineering has traditionally had its roots in both matrix-based[1-10] and scaffold-free approaches,[11, 12] often using readily available rat neonatal cardiomyocytes[5, 8-10] or mouse embryonic stem cell-derived cardiomyocytes.[6, 13] A large body of work has been created using collagen-based scaffolding,[8-10, 14, 15] although work has been done as well with alginate,[4] fibrin,[5-7] or PEG-based scaffolding.[16-18] Comprehensive studies by Eschenhagen and Zimmermann, especially, have demonstrated that – at least in the rat neonatal cardiomyocyte-based system – stress conditioning can provide cues for alignment and maturation,[8] for generating force-producing functional tissue,[8, 10, 15] and for scaling engineering efforts into the range necessary for *in vivo* heart repair, at least in the context of a small animal model.[9, 10, 14] Additionally, it has been reported that highly purified cardiomyocytes underperform on a number of parameters compared to those in mixed cultures of naturally associating cell types, such as neonatal cardiomyocytes and cardiac fibroblasts.[15, 19] Other groups, such as Caspi and Levenberg's, have created mixed tissues by using non-degradable scaffolds, human cardiomyocytes generated using a low purity serum-derived differentiation method followed by micro-dissection of beating clusters, human umbilical vein endothelial cells (HUVEC), and mouse embryonic fibroblasts (MEFs) as a stromal cell type, in order to build a hybrid tri-cell tissue.[2] They found that endothelial cell viability and proliferation were increased by the presence of a stromal cell type (fibroblasts) and that nascent endothelial structures were stabilized in the tri-cell mixture, compared to the bi-cell mixture of endothelial cells and cardiomyocytes.

The techniques available for differentiation of human cardiomyocytes have markedly improved over the years,[20-24] from the early serum-based embryoid body differentiation methods with only 1-2% differentiation purity,[2] and a number of protocols have been published, by our group[25] and others,[26] for

differentiating human endothelial cells as well. Two robust protocols, in particular, have been used to generate large numbers of human cardiomyocytes from human embryonic stem cells (ES cells)[20, 22] and, more recently, even from human induced pluripotent stem cells (iPS cells),[27] reprogrammed from differentiated adult tissues to the pluripotent state.

In the studies presented here, we have built upon these earlier important endeavors, demonstrating that it is now possible to generate all human tri-cell based tissues, in a collagen scaffold, using either human ES cell-derived or human iPS cell-derived cardiomyocytes, along with human endothelial cells and at times utilizing human MSCs as a preferred stromal cell type. We first validated previous findings of the influence of stress conditioning on rat neonatal cardiomyocyte-based engineered tissue and then established that human cardiomyocytes respond similarly, quantifying intracellular alignment, proliferation, and hypertrophy within the bioengineered tissue. We found that stress conditioning and the presence of human endothelium increased cardiomyocyte proliferation, that stress conditioning increased hypertrophy and cell alignment, and that the presence of endothelium and nascent vascular structures did not markedly decrease the extent of cardiomyocyte alignment. Furthermore, we found that static stress conditioning and exogenously provided 1 Hz cyclic stress conditioning were similar in their ability to promote alignment and hypertrophy over no stress conditions, likely because the cardiomyocytes themselves within the engineered tissue are synchronously contracting, providing, in the "static stress" condition, their own endogenously produced cyclic stress as an organizing cue.

Furthermore, we found that the addition of a stromal cell type markedly increased the number of vascular structures formed within the tissue. The species origin of the stromal cell was relatively unimportant – with similar results from both human mesenchymal stem cells (MSCs) and mouse embryonic fibroblasts (MEFs) on the extent of human endothelial-derived vascular structure – and these interactions occurred in both the human cardiomyocyte-derived and rat neonatal cardiomyocyte-derived engineered cardiovascular tissue. This nascent vasculature appeared histologically as networks of cord structures and structures with lumens throughout the bioengineered tissue *in vitro*, but the functionality of these networks for hemodynamic perfusion remained unknown from *in vitro* experiments.

We implanted both human ES cell-derived and iPS cell-derived cardiovascular tissue into the myocardium of immuno-compromised athymic rats and assayed for success of engraftment. After as little

as one week we found healthy human myocardium engrafted in the host tissue. In addition, we observed that within the grafts were vessels of both human and rodent origin, apparently anastomosed with the host circulation and perfused with circulating red blood cells.

We next examined whether complex, mixed cell-type human myocardium could be generated from a single genotype, through a human cardiovascular progenitor cell population and employing our engineered tissue production techniques. Finding our initial results promising, we went on to delineate the effects of stress conditioning both on fate specification and on maturation of resulting cell types within the bioengineered human cardiovascular tissue. Through a series of experiments comparing standard 2-dimensional (2-D) culture and 3-dimensional (3-D) tissue engineering, as well as the application of no stress, static stress and cyclic stress conditioning regimes, we were able to demonstrate that human cardiovascular progenitors in a 3-D bioengineered tissue environment develop into differentiated human cardiovascular tissue composed of multiple cell types, with cardiomyocyte specification and maturation significantly increased in the 3-D environment while smooth muscle specification and maturation were greatly diminished (endothelial cell population dynamics did not change markedly). Furthermore, these experiments revealed that mechanical stress conditioning in the 3-D bioengineered tissue environment strongly increased maturation of the cardiomyocyte subset on a per-cell basis, without differentially affecting specification to the cardiac fate. Finally, we demonstrated by calcium transient analysis of the intact engineered cardiovascular tissue that contractility is markedly increased by cyclic stress conditioning, in comparison to static stress or no stress conditioned counterparts.

In addition to our efforts to produce homogenic vasculature within engineered human cardiac tissue by controlling differentiation of cardiovascular progenitors and maturation of their progeny, we examined the contractile function of engineered human myocardium *in vitro*. We used human iPS cell-derived cardiomyocytes, reprogrammed from human fibroblasts, then differentiated into human cardiomyocytes, to generate force-producing engineered human cardiac tissue. Spontaneous, synchronous contraction was observed in stress-conditioned and unconditioned tissue, but calcium transient characteristics proved to be more mature in stress-conditioned tissue. We were also able to measure active twitch force and found that the amplitude of twitch force height increased up to 8-fold over stepwise length increases starting from slack length. This force-length relationship is analogous to Frank-

Starling curves generated in the intact heart, and is also markedly improved with stress pre-conditioning. We hope to convince the reader that stress conditioning is a viable and validated method for improving the maturity of human myocardium generated *in vitro*.

Chapter 2: Growth of Engineered Human Myocardium with Mechanical Loading and Vascular Co-culture

Summary

The developing heart requires both mechanical load and vascularization to reach its proper size, yet the regulation of human heart growth by these processes is poorly understood. We seek to elucidate the responses of immature human myocardium to mechanical load and vascularization using tissue engineering approaches. Using human embryonic stem cell and human induced pluripotent stem cell-derived cardiomyocytes in a 3-dimensional collagen matrix, we show that uniaxial mechanical stress conditioning promotes 2-fold increases in cardiomyocyte and matrix fiber alignment and enhances myofibrillogenesis and sarcomeric banding. Furthermore, cyclic strain markedly increases cardiomyocyte hypertrophy (2.2-fold) and proliferation rates (21%) vs. unstrained constructs. Addition of endothelial cells enhances cardiomyocyte proliferation under all stress conditions (14% to 19%), and addition of stromal supporting cells enhances formation of vessel-like structures by ~10-fold. Furthermore, these optimized human cardiac tissue constructs generate Starling curves, increasing their active force in response to increased resting length. When transplanted onto hearts of athymic rats, the human myocardium survives and forms grafts closely apposed to host myocardium. The grafts contain human microvessels that are perfused by the host coronary circulation. Our results indicate that both mechanical load and vascular cell co-culture control cardiomyocyte proliferation, and that mechanical load further controls the hypertrophy and architecture of engineered human myocardium. Such constructs may be useful for studying human cardiac development as well as for regenerative therapy.

Introduction

The developing heart is exquisitely sensitive to its mechanical environment, and studies in model organisms such as chick or mouse indicate that mechanical loading is required for cardiac growth and morphogenesis.[28-31] Similarly, the heart requires a rich coronary vascular supply for its normal growth, with the coronaries providing both nutrient exchange and paracrine growth signals.[32-34] While model organism studies shed light onto general mechanisms of vertebrate development, they do not perfectly model human cardiac growth. For example, the human heart is thousands of times larger than that of the

mouse and requires the cardiomyocytes to remain in the cell cycle much longer to achieve this mass. Similarly, the human heart beats nearly 10 times slower than the mouse, necessitating different systems for excitation, contraction and relaxation, and these differences likely impart different responses to external mechanical stress. It therefore seems probable that the growth responses of immature human myocardium to mechanical load and vascular ingrowth will differ in some aspects from common laboratory models.

Early growth and maturation processes have been difficult to study in humans, due in part to difficulties in obtaining sufficient human cells. Cardiomyocytes in the postnatal human heart are essentially post-mitotic,[35] precluding their expansion *in vitro*. Fetal human tissue is difficult to obtain, and endogenous adult stem cells have not, to date, shown a robust ability to generate cardiomyocytes. In contrast, pluripotent stem cells such as human embryonic stem cells (hES cells)[36] or induced pluripotent stem cells (iPS cells)[27] can now be used to generate large-scale cultures of human cardiomyocytes at purities >50%.[20, 22, 23, 37] These cardiomyocytes resemble fetal human cardiomyocytes in terms of their cardiac-specific transcription factors and contractile proteins, and they exhibit excitation-contraction coupling and synchronous contraction in culture.[38-41] This creates opportunities for studying human cardiac growth pathways.

Most *in vitro* studies of myocardial growth have relied upon cardiomyocyte monocultures and 2-dimensional culture conditions. Monolayer growth on a rigid substrate is clearly not reproducing the heart's native environment, however, and this has led us and other groups to explore tissue engineering. Tissue engineering can provide a more natural 3-D environment with appropriate stiffness, can improve intercellular organization, and can facilitate intercellular crosstalk which modulates cardiomyocyte differentiation and growth. A variety of 3-D scaffolds have been used with non-human cardiomyocytes, including various synthetic polymers,[2, 19, 42] as well as natural ones such as alginate,[4] fibrin,[5] fibronectin,[43] and collagen.[8, 44] Type I collagen is attractive for cardiac tissue engineering because it is the major endogenous constituent of the heart's extracellular matrix.[45] Furthermore, collagen is self-polymerizing and can be uniformly seeded with cells as a liquid gel, molded into desirable shapes, and subjected to mechanical forces to promote cellular organization. It has been reported that rat neonatal cardiomyocytes cultured in a 3-D collagen matrix and subjected to cyclic stress are able to align in the direction of stress,

express organized sarcomeres, and electrically couple by gap junctions.[8, 44]

In this study, we have generated 3-dimensional human cardiac tissue constructs using collagen type I and human ES cell-derived cardiomyocytes to assess cardiomyocyte proliferation, maturation, and architecture under different conditions of stress. Additionally, we have examined co-culture with vascular and stromal cells within the matrix as a means to further recreate cardiomyocyte and vascular organization within the cardiac construct.

Results

Rat Neonatal Cardiomyocyte Constructs

To establish a baseline against which to compare our human constructs, we first optimized production of engineered heart tissue using primary rat neonatal cardiomyocytes (rNC). These studies determined that 1.10-1.25 mg/mL of type I collagen is required to prevent construct failure under stress and that a density of at least 2 million cells per 100 µL of construct is necessary for adequate survival of cardiomyocytes within the collagen matrix (data not shown). Constructs generated by this process have dimensions of 20 mm in length and 0.5 mm in thickness. As the cells remodel and contract the collagen gel, nylon tabs hold the construct under static tension or allow the application of controlled cyclic stress (Figure 2.1).

Cardiomyocyte constructs subjected to uniaxial static stress or cyclic stress conditioning (4 days of 1 Hz, 5% elongation) developed cell alignment not observed in 2-D cell culture (Figure 2.2A) or unstressed 3-D gels (Figure 2.3A). Intercellular alignment was quantified from the reciprocal of the cell axis angle dispersion, where a low standard deviation of angles indicates a high degree of alignment (Figure 2.3B). We found that, in comparison to no stress (alignment value of 2.68), cardiomyocyte alignment increased by 2-fold with either cyclic or static stress conditioning (to 5.30 and 5.41, respectively; $p<0.001$ for each versus no stress). However, no significant difference was found between static and cyclic stress ($p=0.65$). While improved, this degree of cell alignment did not reach the level observed in longitudinal fibers within adult rat heart (alignment value of 9.08). Cardiomyocyte alignment within the collagen matrix developed between 1 day and 4 days of stress conditioning (Figure 2.3C); further increases in alignment were not observed between 4 and 7 days (data not shown). Addition of

endothelial cells resulted in the formation of cord structures within the constructs (Figure 2.12A), but endothelial cells did not impact cardiomyocyte alignment in either unstressed or stressed cultures (Figure 2.3B).

In addition to intercellular alignment within the construct, cells within this 3-D matrix also demonstrated signs of maturation, such as bi-nucleation (Figure 2.2C) and organized sarcomeric banding (Figure 2.2D, E) perpendicular to the direction of stress, which is similar to native cardiac tissue. Some cardiomyocytes also continued to undergo DNA replication (by BrdU incorporation, Figure 2.3A, C) and nuclear division (Figure 2.2, B). After several days in culture, these constructs beat spontaneously and synchronously. By transmission electron microscopy, rat neonatal cardiomyocytes within constructs demonstrated internal organization with active myofibrillogenesis, occasional Z-lines, numerous mitochondria, and cell-cell junctions such as desmosomes (Figure 2.3D).

Generating Human Cardiac Tissue Constructs

Cardiomyocytes derived from pluripotent human stem cells were used make 3-D tissue constructs (Figure 2.4) using conditions optimized with rNCs. When cultured under static stress, human tissue constructs generated from either ES cell-derived cardiomyocytes or iPS cell-derived cardiomyocytes began to beat synchronously and spontaneously between 1 and 4 days, indicating that these cells were capable of electromechanical coupling within the collagen matrix. Immunostaining showed that cells throughout the construct strongly expressed the cardiac contractile proteins β-myosin heavy chain (βMHC) (Figure 2.4A) and α-actinin (Figure 2.4B, C), as well as cardiac troponin T (cTnT), and the cardiomyocyte transcription factor Nkx2.5 (not shown). The human cardiomyocytes underwent frequent DNA synthesis, with 15-45% of nuclei incorporating BrdU after an overnight pulse (Figure 2.4A). Furthermore, these cells demonstrated sarcomeric banding of the contractile apparatus by α-actinin immunostaining (Figure 2.4B). Constructs generated using cardiomyocytes differentiated from iPS cells also showed strong sarcomeric binding by α-actinin immunostaining (Figure 2.4C). The iPS cell constructs appeared indistinguishable from the ES cell-derived constructs of similar conditioning. In both cases, sarcomeres appear more aligned in the static stress-conditioned constructs than in the unstressed constructs. Human ES cell-derived cardiac constructs also were examined by transmission electron

microscopy. The contractile cytoskeleton of the human cardiomyocytes was generally less well developed than that of the rat, indicating a less mature phenotype. Nevertheless, similar to rNC constructs, hCM constructs contained cardiomyocytes demonstrating ongoing myofibrillogenesis, including partially organized myofilament bundles associated with polyribosomes and nascent Z-lines (Figure 2.5C, D). The human cardiomyocytes contained numerous mitochondria, and the extracellular space contained readily identifiable collagen fibrils (not shown). Thus, spontaneously beating human myocardial tissue can be created in collagen gels using techniques similar to that for rat tissue engineering.

Human Cardiomyocyte Alignment with Stress

To test whether exogenous stress promotes human cardiomyocyte self-organization, human cardiac constructs were generated both with and without endothelial cells and subjected to no stress, static stress, and 1 Hz cyclic stress conditioning for 4 days. Constructs were immunostained for βMHC (Figure 2.5A), and cardiomyocyte alignment was quantified as described above (Figure 2.5B). Unstressed human constructs did not have significantly different cell alignment than 2-dimensional cell culture (alignment values of 1.96 versus 2.05, respectively). However, static and cyclic stress conditioning strongly increased cell alignment (4.09 for each, $p<0.005$ versus unstressed conditions). As with rat constructs, there were no significant differences in human cardiomyocyte alignment in static vs. cyclic stress ($p=1.00$).

Matrix Structure Organization with Stress

We also investigated the effect of stress conditioning on the organization of the extracellular matrix within the bioengineered constructs. To analyze the collagen fiber architecture within the cardiac constructs, we combined picrosirius red staining (to determine total collagen) and polarized light (to assess the presence of organized collagen fibers).[46-48] Circularly polarized light was utilized to avoid the orientation-dependence of birefringence associated with linearly polarized light.[46] In the absence of cells, no large collagen fibers were seen following static stress conditioning (Figure 2.11A). In human cardiac constructs, we observed large collagen fiber bundles by yellow birefringence (Figure 2.6A). The collagen fiber bundles were disarrayed in unstressed constructs, but fiber architecture was much more orderly

following static and cyclic stress conditioning (Figure 2.6A). Rat neonatal cardiomyocyte constructs in the same conditions showed even more distinct collagen fiber organization (Figure 2.11A). The absence of large collagen fibers in cell-free collagen constructs indicated that these structures require cells for their synthesis and alignment within the tissue construct. Quantitative analyses (Figure 2.6B) showed a 2-fold increase in collagen alignment when comparing no stress conditions (alignment value of 2.42) to static and cyclic stress conditioning (5.10 and 4.56, respectively, $p<0.01$). Thus, in the context of bioengineered cardiac tissue, stress facilitates the cell-driven development of matrix architecture as well as self-organization of the cardiomyocytes within the construct.

Effects of Mechanical Load on Human Cardiomyocyte Proliferation and Hypertrophy

Next, we tested the hypothesis that human cardiac constructs would proliferate in response to mechanical stress. Myocardial constructs were pulsed with BrdU for 24 hours before fixation, and cardiomyocyte DNA synthesis rates were determined by measuring βMHC and BrdU double labeling (Figure 2.7A, B). Absolute BrdU incorporation rates ranged from 15-45%, indicating high baseline rates of proliferation. Due to run-to-run variation in baseline BrdU incorporation rates, however,[49] measurements were normalized to the basal DNA synthesis rates in static stress conditions. Consistent with our hypothesis, both static and cyclic stress increased human cardiomyocyte BrdU incorporation within the ES cell-derived construct by 15-21% over conditions of no stress (85%, 100%, and 106% for no stress, static, and cyclic, respectively; Figure 2.7A). The difference between no stress and cyclic stress was highly significant ($p=0.01$). To further characterize the effect of stress on human cardiomyocyte proliferation, we analyzed the incorporation of BrdU in iPS cell-derived cardiac constructs (Figure 2.7B). In this experiment, cyclic stress conditioning increased DNA synthesis by 7.4% over a basal rate of 32.8% ($p<0.005$).

Cyclic stress conditioning also increased the spontaneous beating rate of iPS cell-derived constructs, from 0.71Hz to 0.83hz to 0.95Hz, respectively, for no stress, 1 day cyclic stress, 4 days cyclic stress ($p<0.05$ compared to no stress; Figure 2.7D), indicating changes in electromechanical structure of the cardiomyocytes within the construct in response to conditioning. To assess if mechanical stress promoted cardiomyocyte hypertrophy, we quantified the βMHC+ area within each ES cell-derived

construct and divided this by total cardiomyocyte nuclear number (Figure 2.7C). Cardiomyocyte area within the construct markedly increased with both static and cyclic stress, more than doubling in response to cyclic stress from 62% to 136% of static stress-normalized area ($p=0.05$). We assessed the effect of stress conditioning on hypertrophy in iPS cell-derived cardiac constructs by quantitative RT-PCR (Figure 2.7E). The data showed that transcripts for βMHC, cTnT, the L-type Ca^{2+} channel, the ryanodine receptor, atrial and B-type natriuretic factors, and SERCA2A increased by 2-6 fold in response to cyclic stress conditioning. Thus, mechanical stress induces both DNA synthesis and hypertrophy in human myocardial tissue constructs.

Pre-Vascularizing Human Cardiac Constructs

Myocardium is a highly vascular tissue, and the coronary circulation supports myocardial development through both perfusion and paracrine signaling pathways.[32, 33, 50] We therefore explored the effects of adding a vascular cell network to our engineered human heart tissues. In constructs generated from preparations of hES cell-derived cardiomyocytes, endothelial cells are occasionally detected by CD31 immunostaining, but they very rarely form any sort of multicellular structure (data not shown). However, when exogenous endothelial cells are added to cardiac constructs, both cord structures and structures containing lumens are observed (Figure 2.8A). The total number of endothelial structures increased markedly when support cells were added into the constructs in tri-culture with human cardiomyocytes and endothelial cells (Figure 2.8B), approximately doubling in the presence of either mouse embryonic fibroblasts (MEFs) or human marrow stromal cells (MSCs) (Figure 2.8C). Compared to cardiomyocyte + endothelial cell constructs, the addition of MEFs increased the prevalence of endothelial cord structures by 10-fold, while the presence of human adult MSCs increased these structures by 8-fold (Figure 2.8C) ($p<0.05$ for MEFs, $p<0.01$ for MSCs). The number of lumenal structures did not significantly change with either stromal cell population ($p=0.76$ for MEFs, $p=0.56$ for MSCs). Similar results were found when endothelial and stromal cells were added to neonatal rat cardiomyocyte constructs (Figure 2.12B). Thus, in both human and rodent cardiac tissue constructs, the addition of a stromal cell population strongly augmented endothelial structure formation.

Despite formation of relatively large vascular-like structures, addition of endothelial cells had no effect on cardiomyocyte or matrix alignment in constructs, regardless of stress conditioning (Figure 2.5, 2.6). Similarly, cardiomyocyte hypertrophy, although increased more than 2-fold with cyclic stress, did not change with endothelial cell co-culture (Figure 2.7B). Interestingly, addition of endothelial cells increased hES cell-derived cardiomyocyte DNA synthesis rates in all stress conditions (up to 19%, p=0.01), implying endothelial-derived mitogens were stimulating cardiomyocyte proliferation (Figure 2.7A). The mitogenic properties of co-culture with endothelial cells was also seen in human iPS cell-derived cardiomyocyte constructs (Figure 2.7B). Cyclic stress and co-culture together increased cardiomyocyte DNA synthesis by 35% (p=0.004). Thus, mitogenic pathways are induced in human cardiomyocytes by both endothelium and cyclic stress.

Frank-Starling Relation in Bioengineered Human Cardiac Tissue

We next studied contractile function in bioengineered human cardiac tissue that had been subjected to 3 weeks of static stress conditioning. Human ES cell-derived constructs were mounted between a force transducer and a post whose position was controlled by a motor, thereby varying resting tension. A representative trace and analysis is presented in Figure 2.9 (n=9). The tissue was subjected to a series of 4% length increases (Figure 2.9A) while continuously measuring force (Figure 2.9B). Active force transients (twitch force) were apparent starting from just above slack length and were increased in amplitude at higher magnitude stretches (Figure 2.9B, left and right insets, respectively). Passive force (preload) recorded 15 seconds after each stretch was normalized to cross-sectional area and graphed against change in length to determine the Young's Modulus (Figure 2.9C). This yielded a curvilinear relationship with modest increases in tension at stretches up to 45% over slack length, and higher increases thereafter. Contractility was assessed by plotting the amplitude of active force against change in construct length (Figure 2.9D). This yielded a linear relationship, in which active force increased 8-fold over the first 60% of stretch over slack length and plateaued thereafter. Linear regression over the first 25% of this curve (the most physiologically relevant) yielded an R^2 value of 0.99. This active force/length relationship is analogous to Frank-Starling curves in the intact heart and indicates our engineered tissue recapitulates a fundamental property of native cardiac muscle.

Cardiac Engraftment

Finally, we investigated the viability of human bioengineered cardiac tissue to engraft in the hearts of athymic rats. Constructs derived from hCM-only and human tri-culture constructs containing cardiomyocytes, endothelial cells, and MSCs were conditioned by static stress and engrafted onto the epicardial surfaces of uninjured athymic rat hearts (n=5 for hCM-only, n=4 for Tri-cell, n=1 for iPS cell-derived hCM-only). Hearts were harvested one week later and studied histologically. When a subset of 3 hearts were probed for the presence of human cells by in situ hybridization for human-specific centromeric repeats, the human cardiac constructs were readily identified on the epicardial surface in each heart (data not shown). Furthermore, grafts with GFP-expressing MSCs were visible by fluorescence on the surface of the heart in animals receiving tri-culture constructs (Figure 2.12D). The implanted constructs expressed the human cardiac marker βMHC in all 10 engrafted animals (Figure 2.10A, C, E) as well as the cardiac transcription factor Nkx2.5 (data not shown). These human cardiomyocytes were often in close proximity to the host myocardium (Figure 2.10A), and there was no foreign body reaction to the implanted construct. Engrafted human ES cell-derived and iPS cell-derived cardiac constructs both showed sarcomeric banding, indicative of intracellular contractile organization, as well as similar cell to cell alignment, indicating intercellular organization (Figure 2.10B, D, respectively). Furthermore, a microvascular network was present throughout the constructs, and these blood vessels were filled with host erythrocytes (Figure 2.10E, F). A subset of the host-perfused vessels stained for human-specific CD31 (Figure 2.10F) within the human tri-culture construct grafts (4 out of 4 grafts) but not in the hCM grafts (rare vessels in 1 out of 5 grafts, likely from “contaminating” endothelial cells), indicating that the endothelial network which had self-organized *in vitro* within the pre-vascularized construct could form bona fide blood vessels *in vivo*.

Discussion

During development, the heart responds to biomechanical cues as well as signals from resident cells and matrix to determine overall cardiac size and architecture.[33, 34] Cellular and mechanical factors are also important determinants of the modification that occurs when the post-natal heart has to maintain

performance while adapting to physiological change such as growth, pregnancy, exercise conditioning, or injury.[33, 51, 52] Although animal models have been critical in our understanding of the factors that modulate cardiac tissue development and homeostasis, as discussed above, these have limitations due to species-intrinsic differences in cardiac size, heart rate and so on. To our knowledge this is the first study to examine the effects of mechanical stress and vascularization on cardiomyocyte architecture, proliferation, and maturation in human cardiac tissue. Our major findings are: 1) both static and cyclic stress conditioning promote human cardiomyocyte alignment and hypertrophy within a collagen 3-D matrix, 2) mechanical stress and endothelial cell co-culture both induce human cardiomyocyte proliferation, and 3) stromal cells of various types, including human MSCs, increase vascular network formation within bioengineered human cardiac tissue. Furthermore, these optimized human cardiac tissue constructs can 4) be generated from human iPS cell-derived cells and 5) can generate active forces responsive to changes in construct length, analogous to Starling curves generated in the intact heart.

Multiple studies have shown that interactions between cardiomyocytes and endothelial cells are necessary for normal rodent and avian myocardial development.[34] For instance, endothelial-specific knockout experiments using Tie2-cre mice[53] have been used to identify a number of signaling molecules within the endothelium, including Tie2 itself[54], neurofibromin,[55] and EphrinB2,[56] which modulate myocardial development and trabecular architecture. In fact, co-culture of human endothelial cells and signaling though EphB4 receptor tyrosine kinase has been determined to be critical for high yield generation of cardiomyocytes from EphB4-null mouse ES cells,[57] although it is not yet clear if this effect is due to a direct influence on differentiation or on cardiomyocyte survival or proliferation. Similarly, production of neuregulin by endocardial cells is essential, as well as myocyte-specific expression of its cognate receptor ErbB4, for formation of ventricular trabeculae.[58-60] It is likely, but not yet shown, that many of these endothelial-cardiomyocyte interactions directly translate to the human myocardium.

Some progress has been made towards creating *in vitro* models of vascularized skeletal muscle[61] and even human cardiovascular tissue with ES cell-derived cardiomyocytes. For example, Caspi et al. seeded hES cell-derived cardiomyocytes and vascular cells onto poly-l-lactic acid scaffolds, and they also observed that endothelial cells enhance cardiomyocyte proliferation.[2] Because synthetic scaffolds may not allow normal cellular remodeling and are known to elicit foreign body reactions that may limit graft-

host integration, our group has been exploring scaffold-free[12, 62] or natural matrices for tissue engineering such as collagen type I and type III, the major components of the primate myocardial matrix.[45] We found that scaffold-free human myocardial constructs, comprised only of cardiomyocytes and the matrix they secrete, survive poorly after transplantation, but the addition of endothelial and stromal cells markedly enhances vascularization and survival.[12] Furthermore, when implanted onto the heart, they showed no foreign body reaction at the graft-host interface.

While scaffold-free approaches show promise, the cardiomyocytes in these constructs are developmentally immature, and their assembly in rotary culture via cell-cell adhesion makes it difficult to control tissue architecture. The desire to control cardiomyocyte hypertrophy and fiber alignment prior to engraftment led us to test collagen hydrogels as vehicles for tissue engineering. Previous studies reported that cyclic stress induces cardiomyocyte alignment in rat neonatal cardiomyocytes within a collagen gel.[8, 44] No reports, to our knowledge, have previously demonstrated stress-induced development of alignment in human cardiomyocytes or of alignment of myocardial matrix with stress conditioning. Because isolated type I and III fibrillar collagens can polymerize into triple helical fibrils *in vitro*, it was long thought that the process of fiber polymerization in tissue occurred via self-assembly.[63, 64] However, it has more recently been established that cell surface integrins play a role in facilitating the assembly of type I and type III collagen fibers in MEF cultures, and that this assembly is independent of collagen synthesis.[65] The data presented here suggest that cell-directed organization of collagen matrix occurs in cardiomyocyte cultures as well, and that stress increases the ability of cells to organize these fibers and align them with vectors of external force.

It has been postulated that mechanical stress modulates architecture of the developing,[66, 67] mature[68, 69] and injured myocardium.[69, 70] *In vitro*, the establishment of cardiomyocyte cellular organization due to stress has been studied thus far in rat neonatal cardiomyocytes. Optimal sarcomere length in rNCs is re-established during sudden longitudinal static stress and involves PKCε phosphorylation,[71] whereas detection of transverse static stress is accomplished through FAK and ERK1/2 phosphorylation.[72] Sensing directionality of mechanical stress has been hypothesized to be a mechanism by which cardiomyocytes may add sarcomeres in series in response to diastolic stretch or in parallel due to increased systolic stress, leading to re-establishment of homeostasis and preservation of cardiac

performance under changing physiological conditions.[73] Here we demonstrated that human cardiomyocytes within unstressed constructs show no more alignment than cells in 2-dimensional cell culture. Conversely, static and cyclic stress conditioning both promoted cell and matrix alignment much closer to that measured in native cardiac muscle (Figures 2.3, 2.5, 2.6). And, while cyclic stress conditioning promoted more cardiomyocyte hypertrophy within the construct, we were surprised that it conferred no additional benefit to cardiomyocyte alignment over static stress conditioning. It is possible that further increased exogenous cyclic stress—either greater amplitude, faster rate, or longer culture conditions than used here—may further improve alignment. However, our pilot studies showed that conditions of 10% elongation caused mechanical failure in some constructs, most often at the points of attachment to the nylon tabs, and conditions of 5% cyclic stress up to 7 days did not show an increase in alignment over 7 day static stress (data not shown). Another possible explanation for comparable alignment in static and cyclic stress conditions is the spontaneous contractions observed in both situations. The cardiomyocytes may induce their own cyclic stress conditioning under “static” external loading conditions.

One of the only other reports on human myocardial tissue engineering demonstrated an increase in both endothelial structure formation and proliferation due to co-culture with stromal cells.[2] This study found a similar significant increase in vascular structure formation; however, we observed that the presence of stromal cells actually decreases endothelial cell proliferation within the human constructs (Figure 2.12C). Several differences exist between the two studies, including the scaffold material (poly l-lactic acid versus collagen), the metric used for measurement of proliferation (Ki67 versus BrdU incorporation) and the stromal cell type, i.e. we investigated both MEFs and human MSCs. The latter are clinically more relevant due to their human origin, smooth muscle differentiation capabilities,[74] and putative cardiac function benefit upon injection following injury.[75-78] We found similar results with both stromal cell types. Furthermore, the time point of the proliferation measurement in the study by Caspi et al. is not clearly delineated, although other analyses within that study have endpoints from 1 hr to 7 days. In our study, we measured proliferation after 5 days in culture with a 1 day pulse of BrdU. At 5 days, significant vascular structure development was evident. Endothelial cells within the cardiac construct may

be involved in a high degree of proliferation followed by apoptosis as part of normal vascular pruning, and the presence of stromal cells may play a role stabilizing the nascent endothelial cell structures.

In summary, we developed a collagen-based, bioengineered human cardiac tissue construct in a self-organizing co-culture with endothelial and stromal cells and demonstrated the development of cardiomyocyte alignment, proliferation, and hypertrophy due to mechanical stress and co-culture. Furthermore, we determined that these constructs engraft into the myocardium with cardiac and endothelial contributions of human origin, and ascertained that engrafted constructs are perfused through connections to host vasculature within a week. These cardiac constructs may provide additional engraftment benefit over cell injection therapies for infarct repair due to positioning of a cardiac repair construct over and across an infarct scar rather than within it. This differential placement may increase therapeutic performance due to 1) separation of the graft from the inflammatory infarct environment and 2) positioning which may promote electrical coupling with intact myocardium on both sides of the infarct.[9] These studies validate mechanical conditioning and vascular and stromal co-culture as practical and constructive methods of affecting human cardiomyocyte organization, replication, and maturation in bioengineered human cardiac tissue.

Materials and Methods

Cell Culture

Undifferentiated human ES cells of the H7 line (James A. Thomson, U. Wisconsin-Madison) were maintained as described previously.[12, 25, 62, 79] IMR90-iPS cells (James A. Thomson, U. Wisconsin-Madison) were maintained similarly.[80] Pluripotent cells underwent directed differentiation into cardiomyocytes in monolayer culture with activin-A and BMP4 as described previously.[20] Briefly, human ES cells were grown to confluence in MEF-conditioned medium supplemented with 4 ng/mL basic FGF (Peprotech) on Matrigel (BD Biosciences). At confluence, the cells were switched into a RPMI medium and B27 supplement (Invitrogen) and 100 ng/mL activin-A (R&D) was added for 1 day followed by 10 ng/mL BMP4 (R&D) for 4 days.

Cells were cultured for an additional 15 days, after which they were spontaneously contracting and expressing cardiac markers. For further cardiomyocyte enrichment, Percoll gradient centrifugation[20]

or suspension culture (where cardiomyocytes self-aggregate and non-myocytes die off) was used.[81] Percoll was followed by at least 1 day each of recovery in suspension culture and replating on gelatin, both in Human Embryoid Body medium (80% Knockout-DMEM, Invitrogen; 20% fetal bovine serum, HyClone; 1 mmol/L L-glutamine, Gibco; 0.1 mmol/L β-mercaptoethanol; 1% nonessential amino acid stock (Gibco); penicillin G, 100 U/mL, Cellgro; and streptomycin, 100 mg/mL, Cellgro)[25, 82] before cells were used for construct generation. Preparations averaged 52% cardiomyocytes based on β-myosin heavy chain (βMHC) immunostaining of the input population at the time of construct generation. This preparation is referred to as "cardiomyocytes" through the remainder of the manuscript.

Rat cardiomyocytes were isolated from 1-3 day old Fisher-344 neonates (Charles River) as previously described[83] and maintained on gelatin for a period of no more than 4 days before use in Rat NeoCardio medium (DMEM; Invitrogen, and M199; Sigma, in a 4:1 ratio supplemented with 10% horse serum, 5% fetal bovine serum, penicillin G; 100 U/mL, and streptomycin; 100 mg/mL). Human umbilical vein endothelial cells (HUVEC, Lonza) of passage 4-8 were maintained on gelatin in EBM2 medium (Lonza). Human marrow stromal cells (MSCs) of passage 2-4 were maintained on gelatin (Sigma) in MSCGM (Lonza), and mouse embryonic fibroblasts (MEFs, Lonza) of passage 5-7 were maintained in DMEM (Invitrogen) with 10% fetal bovine serum, penicillin G (100 U/mL), and streptomycin (100 mg/mL). For the construct preparation, cells were enzymatically dispersed using TrypLE (Invitrogen).

Generation of Cardiac Constructs

Engineered heart tissue constructs were generated using collagen type I (final concentration 1.25 mg/mL, neutralized with NaOH; Gibco), 11% mouse basement membrane extract (Geltrex, Invitrogen), and 57% Human Embryoid Body medium or, when appropriate, Rat Neocardio medium, mixed together on ice with cells gently added.[8] Unless otherwise noted, each 100 μL suspension contained 2 million cardiomyocytes; in bi- and tri-culture experiments, 2 million cardiomyocytes were mixed with 1 million HUVEC and 1 million MSCs or MEFs.

A FlexCell system was used for tissue engineering and mechanical conditioning. The gel-cell mixture was pipetted into a trough of 20 mm by 3 mm formed in tissue train plates mounted over trough loader posts on a loading station set in a Bioflex base-plate under vacuum (Flexcell International Corp.).

Each end of the construct was impregnated into a nylon mesh tab attached to the deformable silicon floor of each well, providing a means to transmit tension to the construct. After one hour at room temperature, the constructs were placed in medium (for human and rNC constructs, RPMI medium with B27 supplement and Rat NeoCardio medium, respectively).

To investigate the effects of cyclic stress conditioning, constructs in tissue train plates were placed onto an Arctangle loading station connected to an FX-4000T system (Flexcell International Corp) on the day following construct generation. Uniaxial cyclic strain was applied at 1 Hz, 5% elongation for 4 days using a square sine waveform setting. Static stress was achieved by allowing cells to contract the collagen gel against the fixed ends of the construct. For culture without stress conditioning, one end of the construct was cut free of the mesh tab. For electron microscopic analysis, constructs were conditioned in static stress or no stress for 7 days. For α-actinin immunohistochemistry of iPS cell-derived constructs, static stress conditioning or no stress conditioning was applied for 14 days, and conditioning for active and passive force measurements took place for 21 days before analysis. All other experiments were conducted with 4 days of conditioning. To measure DNA synthesis rates, 10 μmol/L BrdU was added to the medium for the last 24 hours before fixation.

Cardiac Engraftment

Animal procedures used in this study were reviewed and approved by the University of Washington Institutional Animal Care and Use Committee, and conform to federal guidelines for laboratory animal care. Male Sprague Dawley athymic nude rats (Charles River, n=10) were anesthetized with 5% inhaled isofluorane (Terrell) with an O_2 flow rate of 1.5-2 liters/minute, intubated, and mechanically ventilated with 2.5% isoflurane. After intubation, each animal received a subcutaneous injection of buprenorphine hydrochloride (0.05-0.1 mg/kg, Hospira). The chest was opened and the pericardium incised to expose the anterior surface of the heart. Following 1 week of *in vitro* culture, one construct was sutured directly onto the epicardium (n=5 for ES cell-derived hCM-only, n=4 for ES cell-derived Tri-culture, n=1 for iPS cell-derived hCM-only). One week following engraftment, animals were anesthetized with isofluorane and sacrificed with a 1.5 ml intraperitoneal injection of Beuthanasia-D (390mg/mL pentobarbital sodium, 50mg/mL phenytoin sodium, Schering-Plough Animal Health) and the

hearts were removed for fixation overnight in Methyl Carnoy's fixative or 4% paraformaldehyde, followed by paraffin embedding and sectioning.

Mechanical Measurements

Constructs were carefully dissected away from the nylon mesh tab and placed in 30°C Tyrode's buffer (containing, in mmol/L: $CaCl_2$ 1.8, $MgCl_2$ 1.0, KCl 5.4, NaCl 140, HEPES 10, NaH_2PO_4 0.33, glucose 5,; pH 7.4). Constructs were further dissected into 1-2 mm long sections and then suspended on stainless steel hooks attached to a force transducer (Aurora Scientific, model 400A) and a length controller (Aurora Scientific , model 308B). The dimensions of the constructs were 1.67 ± 0.13 mm by 0.57 ± 0.03 mm (L x W) Initial length (L_o) of the preparation was standardized by stretching constructs to just-above-slack-length similar to as previously described.[84] Force of spontaneously contracting constructs (1.3 ± 0.1 Hz) was then continuously monitored as preparation length was changed by adjusting the position of the length controller arm. Length was increased in small increments with 20 sec between length changes in order to monitor several contractions at each length. Force and length signals were digitally recorded and analyzed using custom LabView software. Passive tension and the amplitude of spontaneous isometric twitch force were measured on 3 or more transients at 15 sec after each length step. Force was normalized to cross-sectional area of the preparation, calculated by measuring the diameter at non-strained length and assuming circular geometry. All measurements were acquired at 30°C.

Quantitative RT-PCR

RNA was isolated from each construct using the RNeasy Fibrous Tissue Kit (Qiagen). 1µg of RNA was used to generate cDNA using random hexamers (Promega) and Superscript II Reverse Transcriptase (Invitrogen). For each set of cDNA, one sample was duplicated in parallel without reverse transcriptase as a check for genomic contamination. cDNA was diluted 1:10 and 5µL were used per 20µL reaction, along with 0.2µM primers and 2x SensiMix SYBR reagent (Bioline), including 3mM $MgCl_2$. Samples were run in triplicate in a 96-well plate format with no template controls for each primer set on a 7900HT Fast Real Time PCR System (Applied Biosystems) with the following reaction design: Step 1:

95℃ 15min; Step 2: 95℃ 15sec, 60℃ annealing 30sec, 72℃ elongation 30sec (40 cycles); Step 3: 72℃ cleanup 5min; followed by a melting curve (Step 4) of 95℃ 15sec, 60℃ 15sec, and a 2% ramp rate to 95℃ 15sec to check for single product formation by melting curve peaks. Primers specificity was additionally verified by gel electrophoresis for amplicon size; primer specifications are listed in Table 2.2. qPCR was performed as described above with the following exceptions— for SERCA2: 62℃ annealing temperature; for RYR2: 0.6μM primer concentration and 62℃ annealing temperature; for NPPB: 0.1μM primers, 4mM $MgCl_2$, and 58℃ annealing temperature. For qPCR analysis, Cts were determined automatically using SDS 2.2.1 software (Applied Biosystems), and mRNA expression was normalized to levels of HPRT transcripts.

Immunostaining

For immunohistochemistry, constructs were fixed for 30 minutes in cold methanol or 4% paraformaldehyde and embedded in paraffin. 5 μm sections were cut, and primary antibody staining was performed overnight, followed by one hour of secondary antibody incubation. For light microscopy, biotinylated secondaries were used followed by a thirty-minute incubation in the enzyme-based ABC reagent (Vector Labs); the binding was visualized by DAB (Sigma) when horseradish peroxidase (Vector Labs) was used and by Vector Red (Vector Labs) when alkaline phosphatase (Vector Labs) was used, all followed by hematoxylin nuclear counterstain. For immunofluorescence, Alexa fluorphore-conjugated secondary antibodies were employed; Hoechst (Sigma) counterstain was used to visualize the nuclei. The following primary antibodies were used with methanol-fixed constructs and tissue: mouse monoclonal anti-β-myosin heavy chain clone A4.951 (ATCC,1:10 dilution of hybridoma supernatant), mouse monoclonal anti-desmin (Dako, 1:5), mouse monoclonal anti-human CD31 (Dako, 1:15), mouse monoclonal anti-cardiac troponin T (Developmental Studies Hybridoma Bank, 1:1000), mouse monoclonal anti-cardiac troponin I (AbCam, 1:800), and mouse monoclonal anti-BrdU-POD (Roche, 1:40). Mouse monoclonal anti-α-actinin (1:800, Sigma) was used with paraformaldehyde-fixed constructs and tissue with proteinase K digest (Roche). Light microscopy secondary antibodies used were biotinylated goat anti-mouse IgG (Jackson Labs, 1:500) and biotinylated horse anti-goat IgG (Jackson Labs, 1:500). Immunofluorescent secondaries included Alexa 488- or 594-conjugated goat anti-mouse or

horse anti-goat (Invitrogen, 1:100). For collagen matrix visualization, slides were stained with Sirius Red (1%, Sigma) and counterstained with FastGreen (1%, Sigma) made up together in saturated picric acid (1.3% in water, Sigma). Permount (Fisher) and Vectashield (Vector Labs) media were used to mount #1 glass coverslips (Corning) onto light microscopy and immunofluorescent slides correspondingly.

Transmission Electron Microscopy

Entire constructs were fixed in half-strength Karnovsky's fixative (2.0% paraformaldehyde, 2.5% glutaraldehyde, 0.1mol/L cacodylate buffer, 3mmol/L $CaCl_2$, pH 7.3) overnight. They were washed in 0.1mol/L cacodylate buffer for 1h and then either stored in 0.1mol/L cacodylate buffer or immediately post-fixed in 1.0% OsO_4, rinsed and dehydrated through a graded series of alcohols and propylene oxide. Before embedding into Eponate resin (Ted Pella), each construct was subdivided into three longitudinal segments. In this study, only middle segments were visualized. Sections for light and transmission electron microscopy were cut using a Reichert Ultracut E microtome. Sections were mounted on 0.25% formvar coated rhodium/copper grids and stained with uranyl acetate and lead citrate.

Microscopy and Image Preparation

Light micrographs were taken at room temperature using Nikon Eclipse 80i microscope fitted with dry 10x- and 60x-Nikon objective with lenses of 0.30 and 0.95 NA correspondingly. The images were captured by Olympus Qcolor 3MB camera operated by Qcapture Pro software. Circularly polarized light microscopy was conducted as described previously[46] at room temperature using a Nikon E800 microscope with a 10x/0.45 objective. Images were collected with a Photometrics Coolsnap camera in color mode (Roper Scientific) and METAMORPH software (Molecular Devices). Circular polarization was used and adjusted to obtain a deep uniform dark background. Illumination intensity, condenser aperture and exposure time were maintained uniformly for all images.

All immunofluorescent images were collected by a Nikon A1 Confocal System attached to a Nikon Ti-E inverted microscope platform and using water-immersion Nikon 60x CFI Plan Apo objective lens with 1.2 NA. Image acquisition was performed at room temperature using Nikon NIS Elements 3.1 software to capture 12-bit raw files that were then rescaled to 16-bit images for further processing. All

images were collected as a single scan with the pinhole adjusted to 1 Airy unit at 1024x1024 pixel density. For electron microscopy, samples were examined using a JEM 1200EX II transmission electron microscope (JEOL Ltd, Tokyo). Operating conditions for the instrument included an accelerating voltage of 80kV, a 300u condenser aperture, a 50u objective aperture and a spot size setting of 3. Images were collected with Olympus Morada digital camera using iTEM image acquisition and analysis software. For figure preparation, images were exported into Photoshop 7.0 (Adobe). If necessary, brightness and contrast were adjusted for the entire image and the image was cropped.

Histological and Statistical Analysis

To quantify cardiomyocyte axis alignment within constructs, we analyzed 100x micrographs of slides stained for desmin (rNC constructs) or βMHC (hCM constructs) using a custom fiber orientation analysis program (developed by Dr. Michael Regnier's lab, University of Washington). Briefly, this Matlab program divides a user-defined region of interest into small subimages and, by edge detection, obtains the major axis angle of each subimage. For the whole image, an average angle and the angle dispersion (standard deviation of angles of cell edges) is determined. Cellular alignment is quantified by magnitude of angle dispersion, such that low angle dispersion (low standard deviation of cell axis angles) indicates a high degree of alignment, which is graphed as the inverse of angle dispersion, expressed as a percentage of the mean (i.e. the reciprocal of the coefficient of variance). Adult rat cardiac tissue was used as a positive control for cardiomyocyte alignment: sections were stained for desmin and quantification was performed only on regions with linear, longitudinal fiber orientation without fibers in cross-section, large vascular structures, or intersecting fiber planes.

To assess cardiomyocyte proliferation, slides double stained for BrdU and βMHC were counted in a blinded fashion, with 500 cardiomyocyte nuclei counted per section as either BrdU positive or negative. Cardiomyocyte area within the construct was assessed by quantifying βMHC positive area within each construct as described previously.[62, 85] The number of red pixels in 100x micrographs were counted in Photoshop and expressed as a percentage of total pixel area. This area was then normalized by the number of cardiomyocyte nuclei per micrograph. To quantify vascular structure within the constructs, slides were analyzed in a blinded fashion for multicellular CD31 positive formations that were scored as

either cord structures or structures with lumens and normalized per area counted, over 4 fields per section.

N=3-6 for each experiment unless otherwise noted. Error bars represent standard error of the mean (SEM), significance was determined using single factor ANOVA followed by Student's t-test with 95% or greater confidence level.

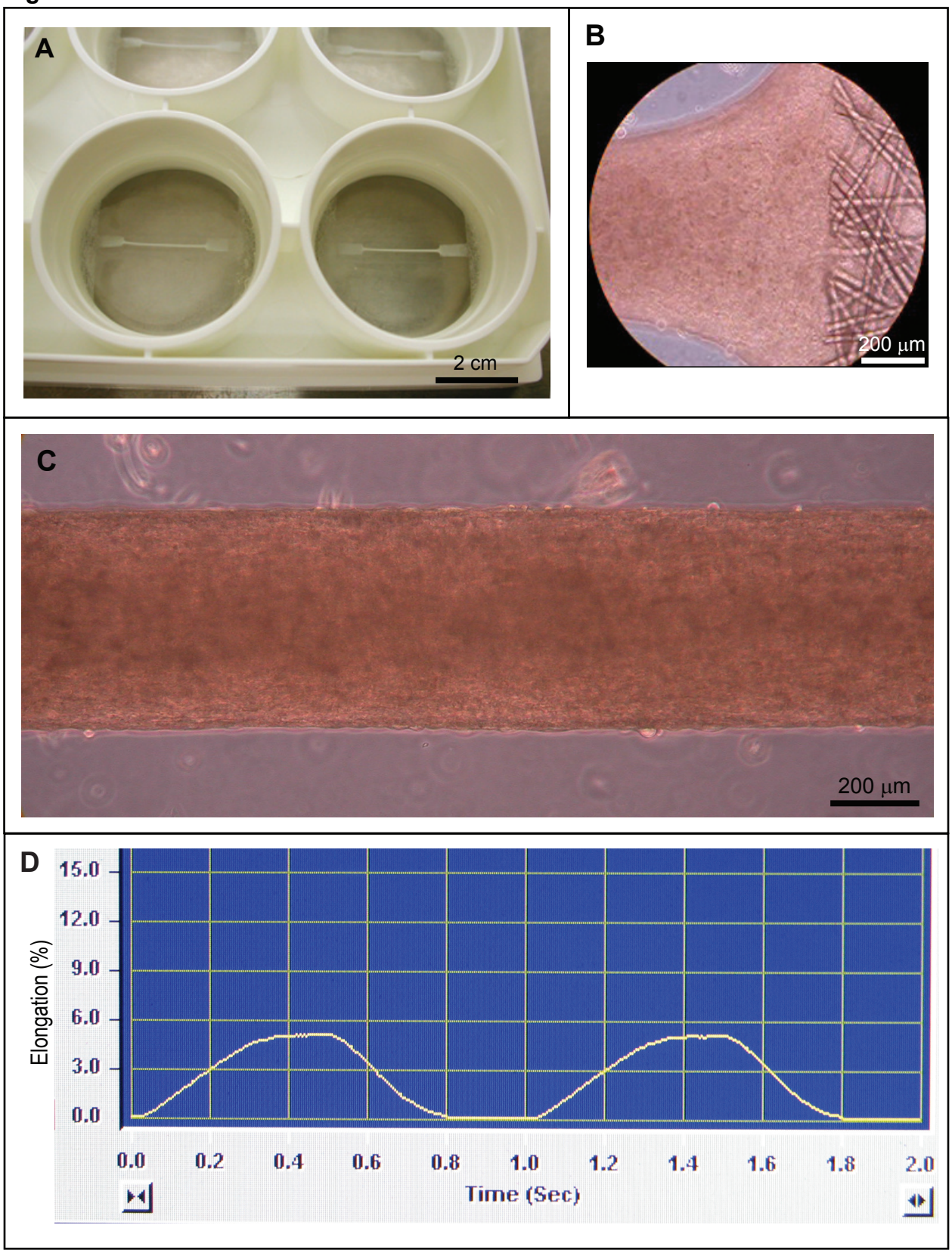

Figure 2.1. Cardiac construct manufacture and conditioning. A, Constructs under low magnification in 6-well plate. **B,** Closeup view of construct end enmeshed in nylon tab with 20x objective. **C,** 10x objective view of length of contractile cardiac construct. **D,** Program of cyclic stress conditioning: 5% elongation, 1Hz, square sine wave generated with the FX-4000T system (Flexcell International Corp).

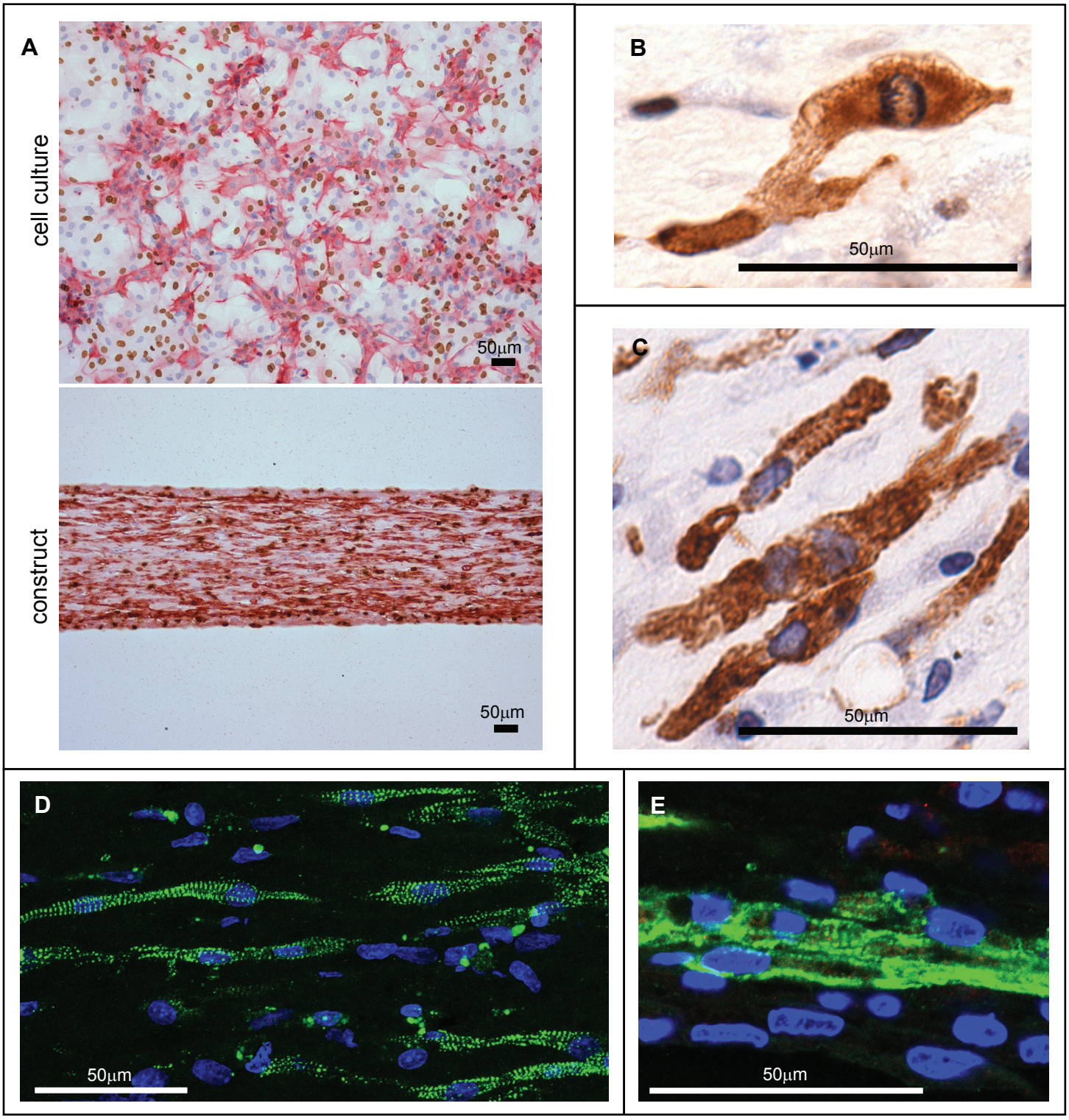

Figure 2.2. Alignment and protein expression within rat neonatal constructs. **A,** Desmin and BrdU staining (red and brown, respectively). Cardiomyocytes cultured under normal 2-D culture conditions did not align with each other, whereas those in the 3-D collagen matrix under static stress conditioning became aligned in parallel with the direction of stress. **B,** Cardiomyocytes within the construct express cardiac troponin I and can undergo nuclear division. **C, D,** and **E,** Desmin, α-actinin, and cardiac troponin T staining, respectively. Cardiomyocytes within the construct demonstrate internal alignment and signs of maturation including sarcomeres and binucleated cardiomyocytes, similar to native cardiac tissue.

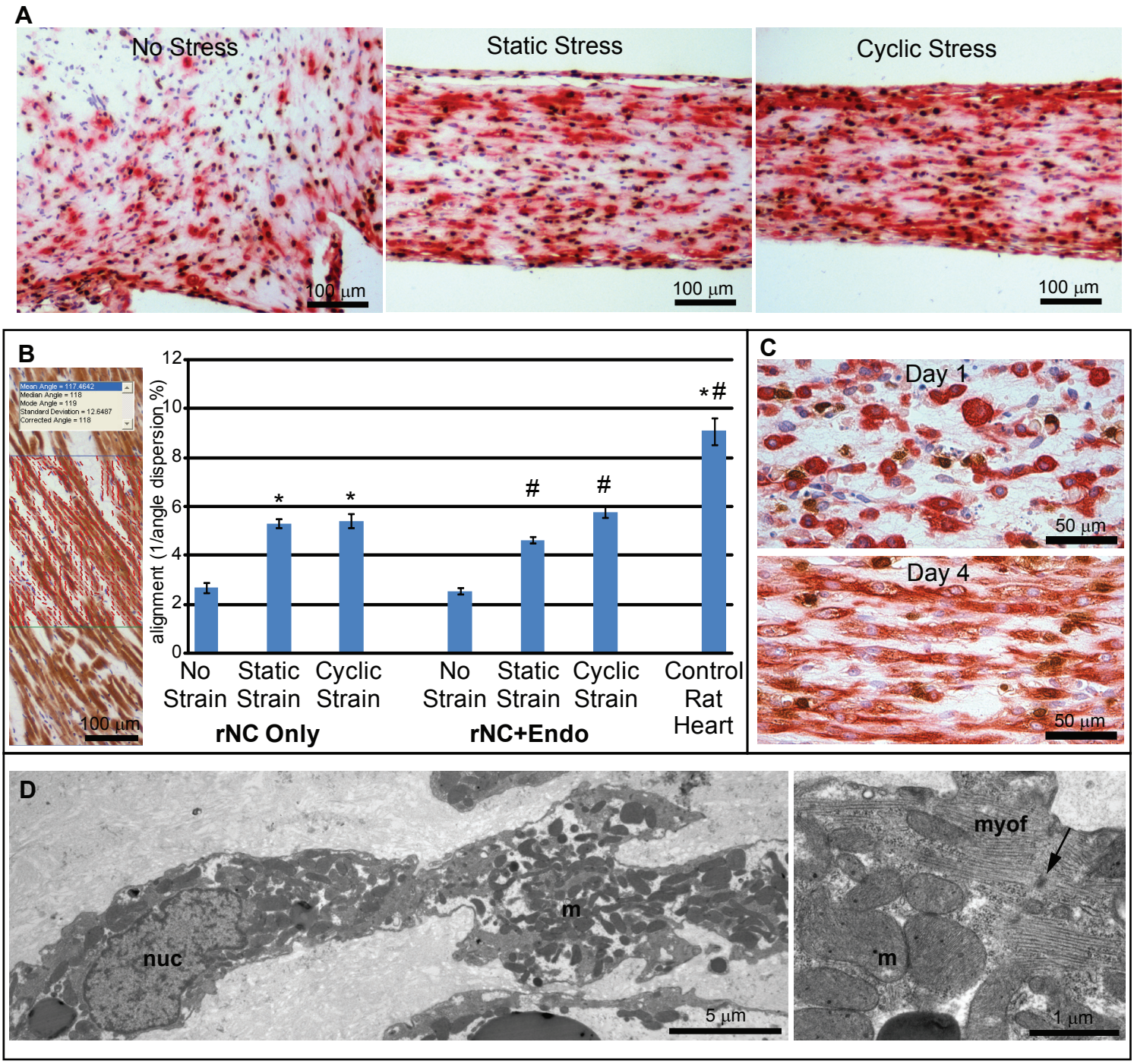

Figure 2.3. Rat cardiac tissue constructs organize under strain. Desmin (red) and BrdU (brown) immunostain. **A,** Rat neonatal cardiomyocyte (rNC) constructs conditioned under static or cyclic stress contained elongated, aligned cardiomyocytes, in comparison to constructs under no stress. **B,** Increased alignment was noted in static and cyclic stress groups, and co-culture of endothelial cells did not inhibit the development of cardiomyocyte alignment. Error bars = SEM; * = $p<0.001$ compared to rNC Only, No Stress; # = $p<0.001$ compared to rNC+Endo, No Stress. Inset, alignment analysis vectors depicted on micrograph of rat heart with desmin staining. **C,** Cardiomyocyte alignment within the constructs developed between 1 and 4 days of static stress conditioning. **D,** Transmission electron microscopy of cardiac constructs revealed elongated cardiomyocytes within the collagen matrix, with nuclei (nuc), numerous mitochondria (m), and contractile filaments. Higher magnification revealed mitochondria among myofibrils (myof) with scattered nascent Z-disks (arrow). n=3-7.

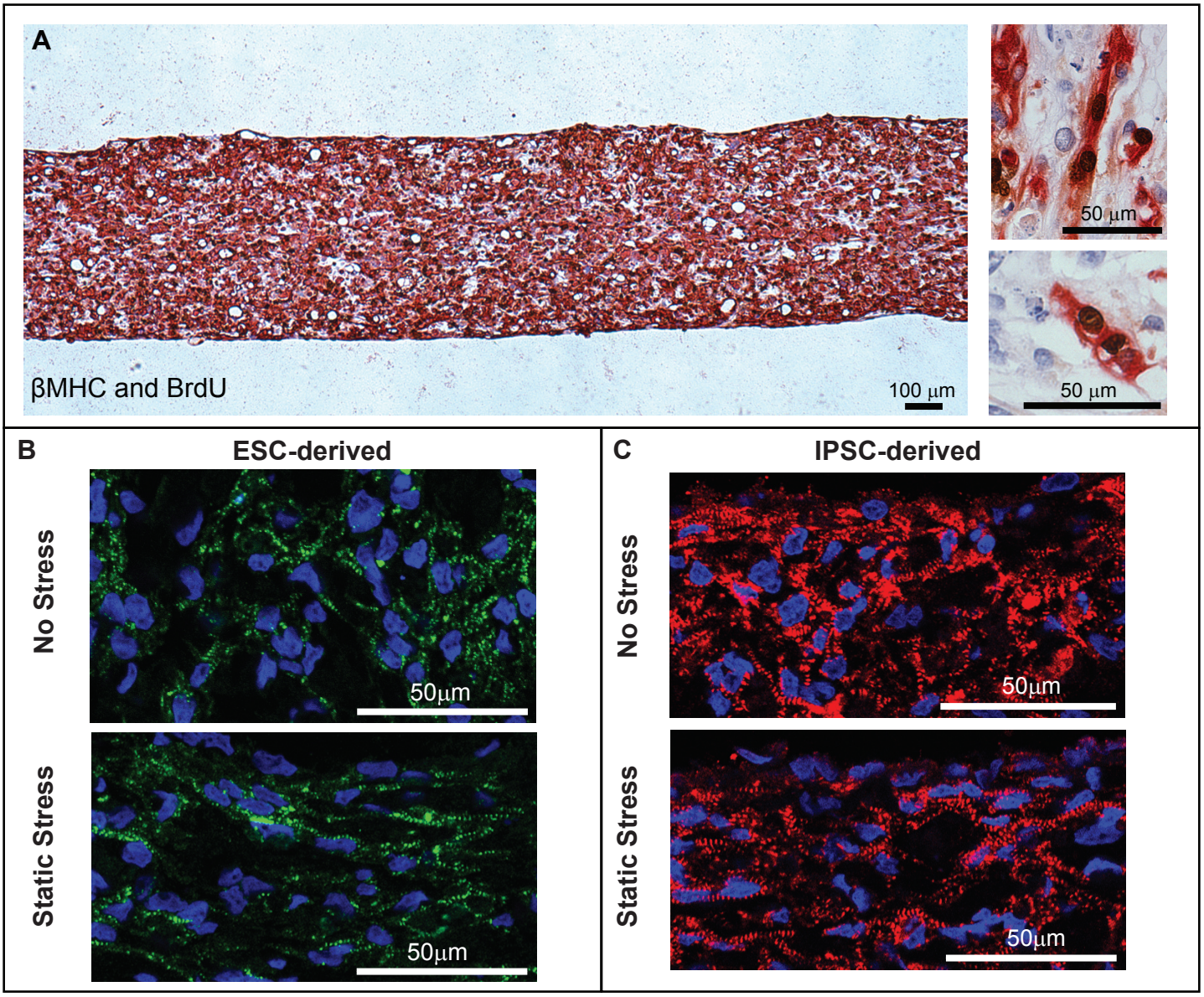

Figure 2.4. Characterization of ES and iPS cell-derived human cardiac tissue constructs. A, Constructs generated from human ES cell-derived cardiomyocytes stained strongly for the cardiomyocyte marker βMHC (red) and the proliferation marker BrdU (brown). High magnification (right): human cardiomyocytes were observed undergoing nuclear division within the collagen matrix. **B,** Constructs generated from ES cell-derived cardiomyocytes subjected to static stress conditioning (lower) or no stress conditioning (upper) stained strongly for the sarcomeric protein α-actinin (green). **C,** Constructs generated from iPS cell-derived cardiomyocytes also stained strongly for α-actinin (red). As in B, the construct edges and vector of stress conditioning are horizontal. These constructs appeared indistinguishable from the ESC-derived constructs of similar conditioning. In both cases, myofibrils appear more aligned in the static stress conditioned constructs. n=4-6.

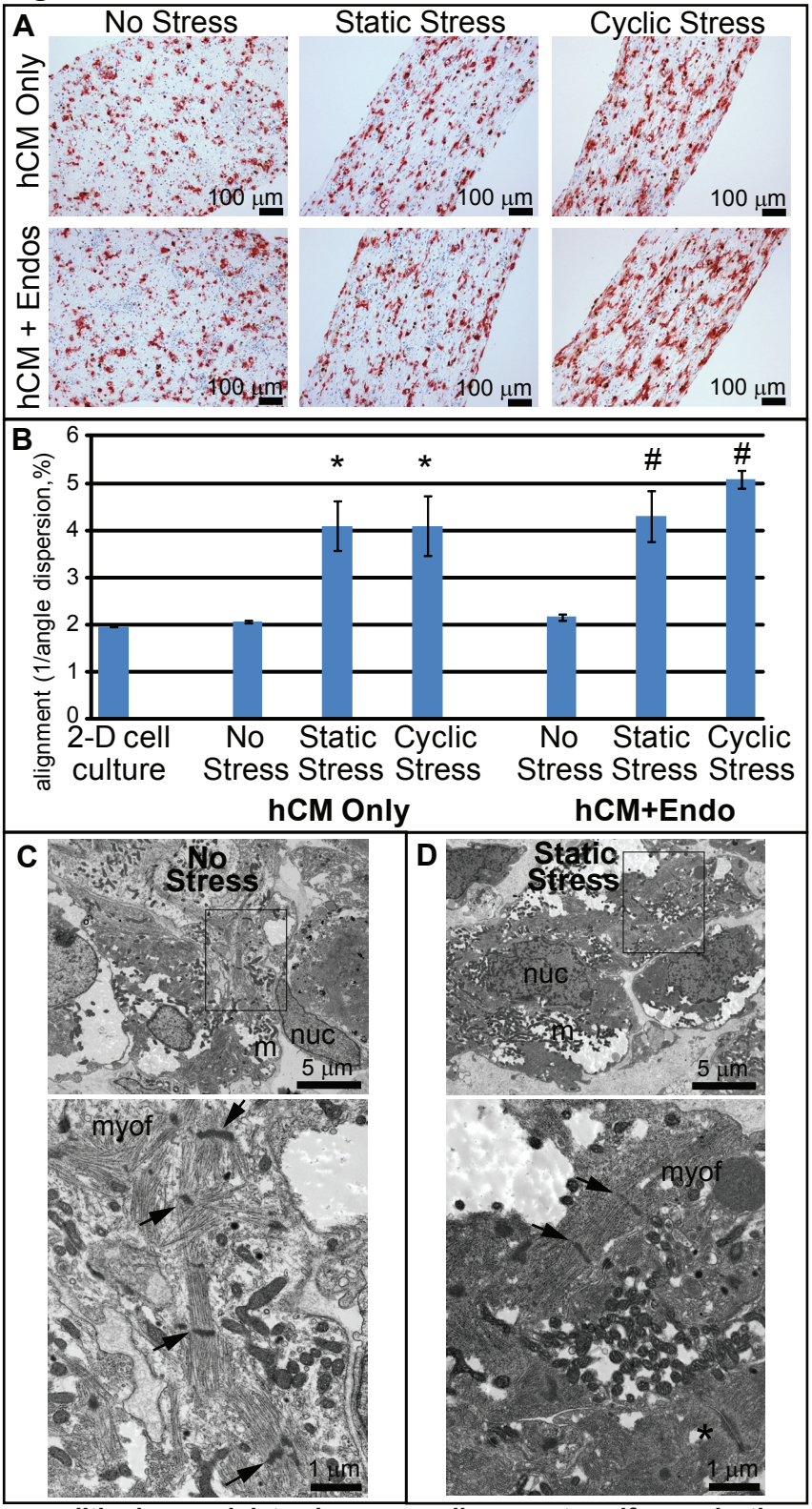

Figure 2.5. Stress conditioning modulates human cardiomyocyte self-organization. **A,** hCM constructs derived from hES cells with or without endothelial cells were placed under conditions of no stress, static stress or cyclic stress and stained for βMHC (red) and BrdU (brown). Under static and cyclic stress conditions, cardiomyocytes aligned with each other in parallel to the direction of stress. **B,** Quantitative alignment assessment. Unstressed constructs did not have significantly different cell alignment versus 2-D cell culture. Static and cyclic stress significantly increased cell axis alignment (* = $p<0.005$ versus hCM only, No Stress). Co-culture of endothelial cells within the construct did not inhibit development of cardiomyocyte alignment (# = $p<0.005$ versus hCM+Endo, No Stress). **C,** By electron microscopy, human cardiac constructs with no stess conditioning contained, cardiomyocytes with numerous mitochondria (m). Nucleus, nuc. Higher magnification (below): showed relatively disorganized nascent myofibrillar bundles (myof) in the cytoplasm and scattered Z-disks (arrows) associated. D) Static stress conditioned constructs had more regular contractile filaments with interspersed Z-disks. Occasional desmosomal juctions were observed (lower right, *). n=3-7.

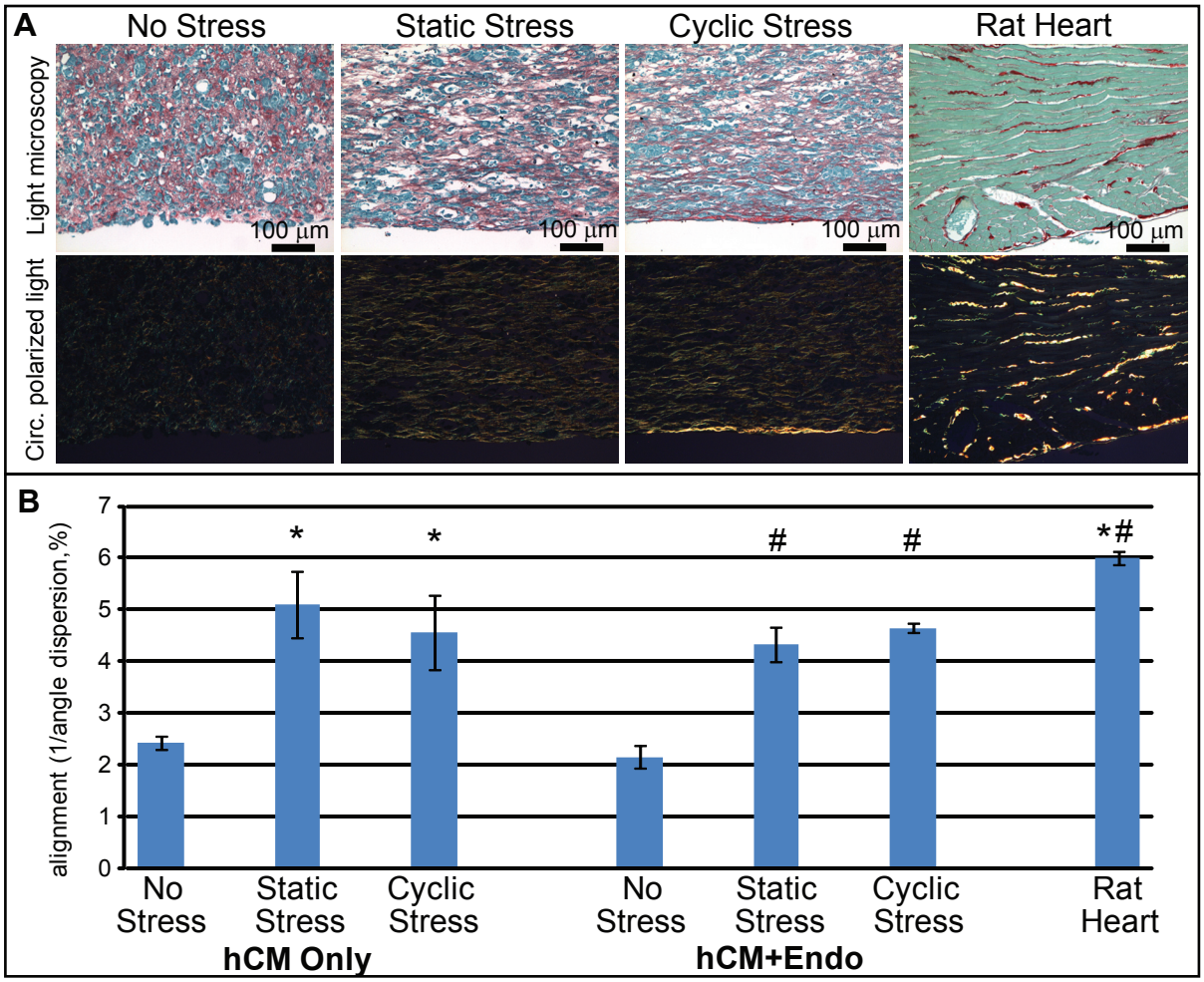

Figure 2.6. Stress conditioning facilitates the cell-driven development of matrix architecture. **A,** Assessment of collagen fiber bundle organization using picrosirius red and polarized light. Large bundle collagen fibers fluoresced yellow in the interstitium of rat myocardium and between cells in constructs generated from human ESC-derived cardiomyocytes. These fibers appeared disarrayed in no stress conditions but closely aligned under stress conditioning. **B,** Quantitative alignment assessment of extracellular matrix in human cardiac constructs indicated a 2-fold increase with stress conditioning. The presence or absence of human endothelium in co-culture did not affect matrix organization. n=3-5; * = $p<0.01$ versus hCM only, No Stress, # = $p<0.005$ versus hCM+Endo, No Stress.

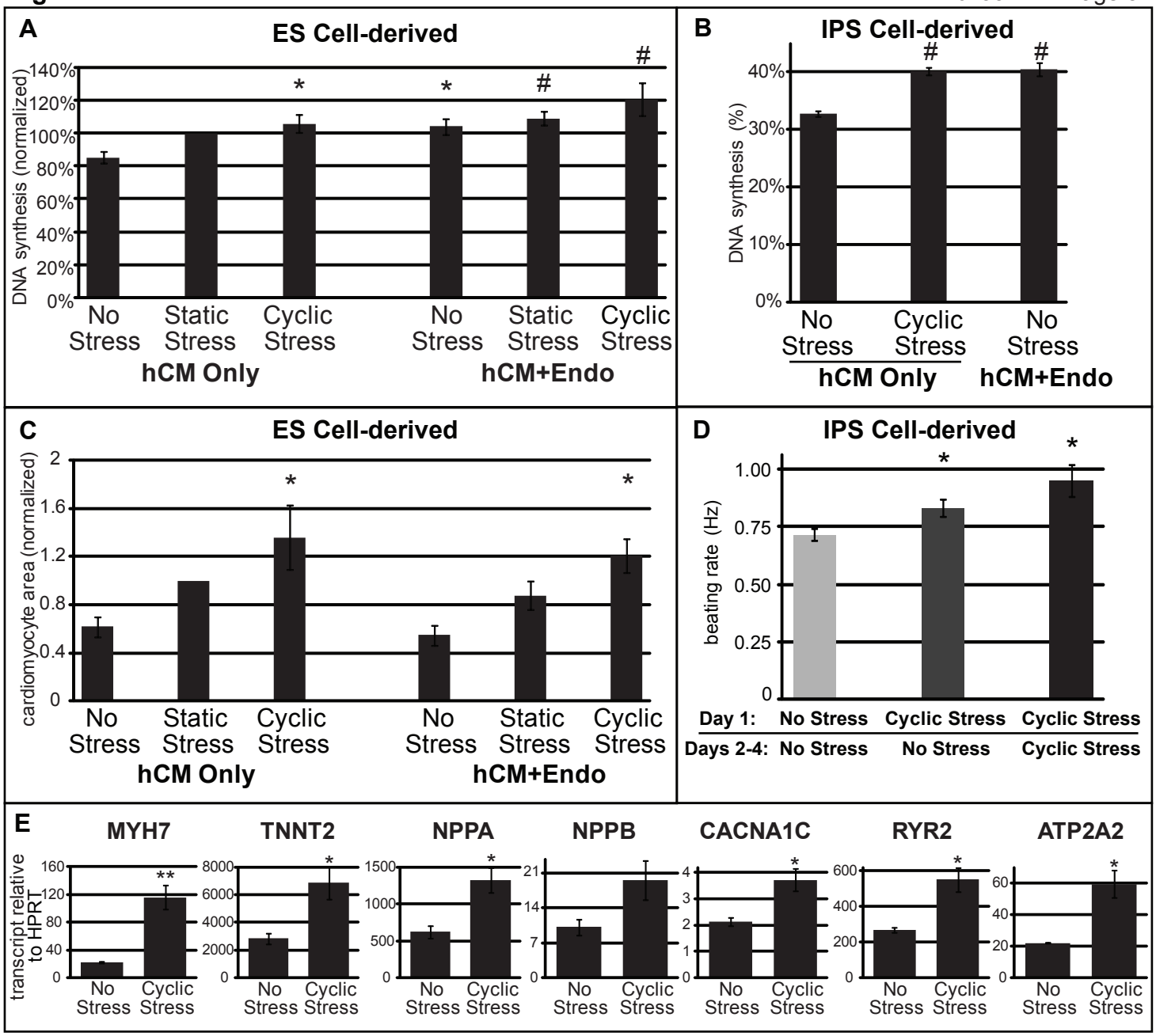

Figure 2.7. Stress and co-culture modulate human cardiomyocyte proliferation and hypertrophy. A, Cardiomyocyte DNA synthesis was measured by βMHC and BrdU double staining in hES cell-derived cardiac constructs. Data are given as fold over basal rate in the hCM-only, static stress condition. Static and cyclic stress markedly increased hES cell-derived cardiomyocyte BrdU incorporation over no stress (15% and 21% increases, respectively) as did the addition of endothelial cells (19%). **B,** Cardiomyocyte DNA synthesis within a single experiment (n=4 per group) of iPS cell-derived cardiac constructs. Co-culture and cyclic stress conditioning both significantly increase iPS cell-derived cardiomyocyte DNA synthesis. **C,** Cardiomyocyte hypertrophy within hES cell-derived cardiac constructs was assessed by βMHC immunostaining, measuring stained area within each construct, and normalizing to number of cardiomyocyte nuclei. Due to variability in input purity, data are given as fold over the hCM only, static stress condition. Cardiomyocyte area increased 2.2-fold in response to cyclic stress conditioning. **D,** Spontaneous beating frequency with stress conditioning in iPS cell-derived cardiac constructs. The following experimetal conditions were used: no stress for 4 days, 1Hz, 5% elongation cyclic stress for 1 day followed by 3 days of no stress, or 4 days under the cyclic stress condition. Afterward, beating rate was visually assessed and a time-dependent effect due to stress conditioning was observed. **E,** Quantitative RT-PCR was performed on iPS cell-derived cardiac constructs conditioned with no or cyclic stress for 4 days to determine the mRNA transcript levels of the following contractile and hypertrophy related genes: MYH7 (βMHC), TNNT2 (cTnT), NPPA (ANP), NPPB (BNP), CACNA1C (L-type calcium channel subunit 1Cα), RYR2 (sarcoplasmic calcium channel/ryanodine receptor) and ATP2A2 (SERCA2, sarcoplasmic calcium transporter). Significance was determined by Single Factor Anova followed by Student's t-test in comparision to the hCM only, no stress condition. n=3-6; * = $p<0.05$; ** = $p<0.01$; # = $p<0.005$ compared to the hCM Only, No Stress condition; error bars represent standard error.

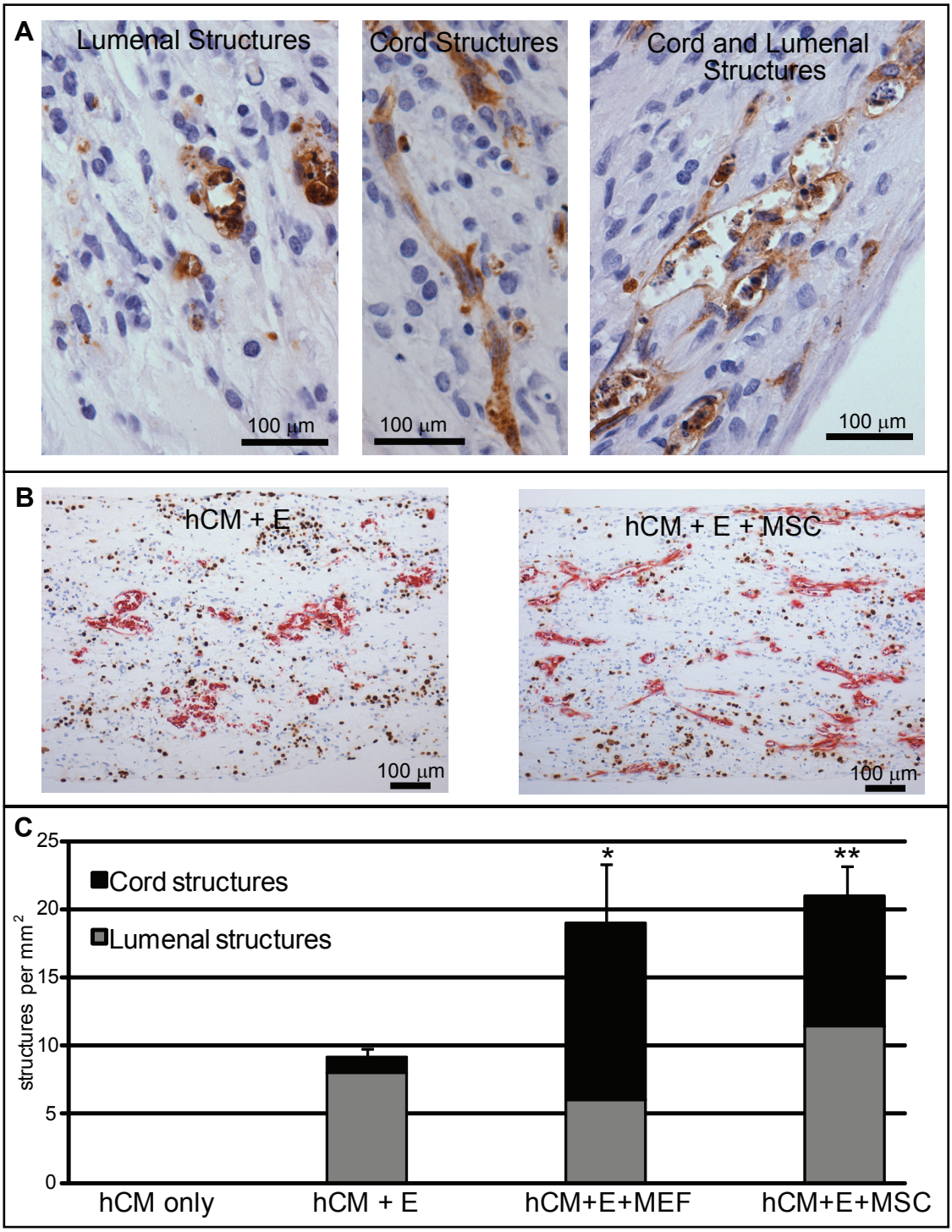

Figure 2.8. Stromal cells affect vascular organization within the human cardiac construct. **A,** ES cell-derived cardiac constructs were generated by co-culture with endothelial cells with and without stromal cells and immunostained for the endothelial marker CD31. Shown at high magnification, endothelial cells organized into cord networks, structures with lumens, or structures with characteristics of both (left, hCM+Endo; middle, hCM+Endo+MEF; right hCM+Endo+MSC). **B,** Shown at low magnification, the prevalence of endothelial structures (CD31, red, and BrdU, brown) in the constructs increased with the addition of stromal cells (left, without MSCs; right, with MSCs). **C,** Quantitation of endothelial structures. The total number of structures (cord and lumenal) doubled with either MSC or MEF co-culture. The number of cord structures increased by approximately 10-fold. *, $p<0.05$; **, $p<0.01$ for cord structures compared to hCM+Endo, n=3.

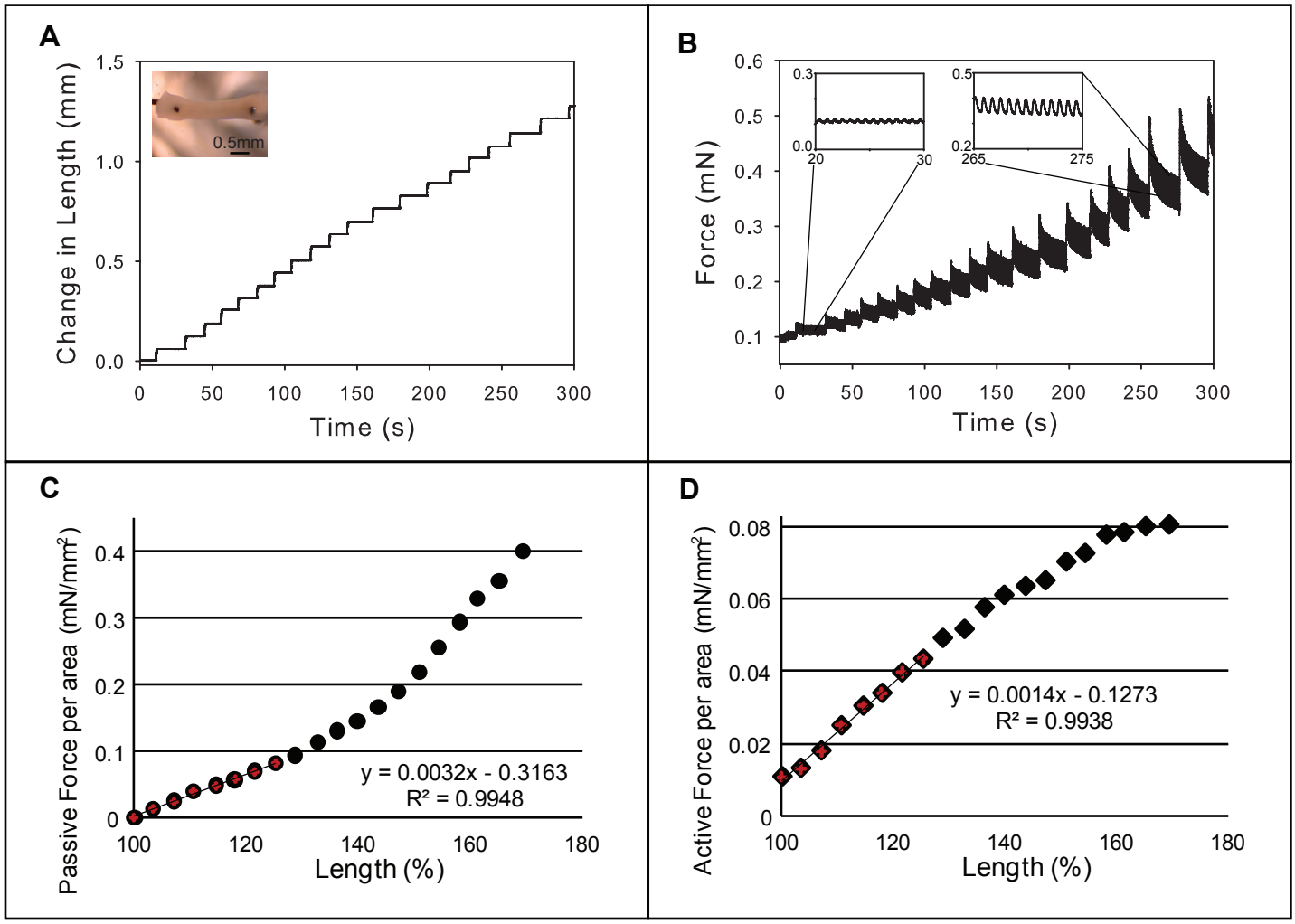

Figure 2.9. Force/length dependence in bioengineered cardiac constructs. Constructs generated from human ES cell-derived cardiomyocytes were subjected to static stress conditioning for three weeks before assement of active force development at different lengths with a force transducer and a high speed length controller. **A,** Steps of 4% length increase were made starting from the slack length of the bioengineered cardiac tissue construct. **B,** Force was continuously measured, and an increase in magnitude (insets) occurred at greater lengths. **C,** Passive force (baseline) recorded 15 seconds after each acute stretch was normalized to cross-sectional area, graphed against change in length, and the slope of the first 25% length change (Young's Modulus) was determined. **D,** Active force twitch height at 15 seconds was graphed against construct length. The magnitude of active force increased 8-fold in a linear manner over increasing preparation lengths before leveling off at large magnitude stretches, and the slope of the first 25% length change was calculated with an R^2 value of 0.9938. This Force/Length Relationship is analogous to Starling curves generated in the intact heart. n=9, 1 representative shown.

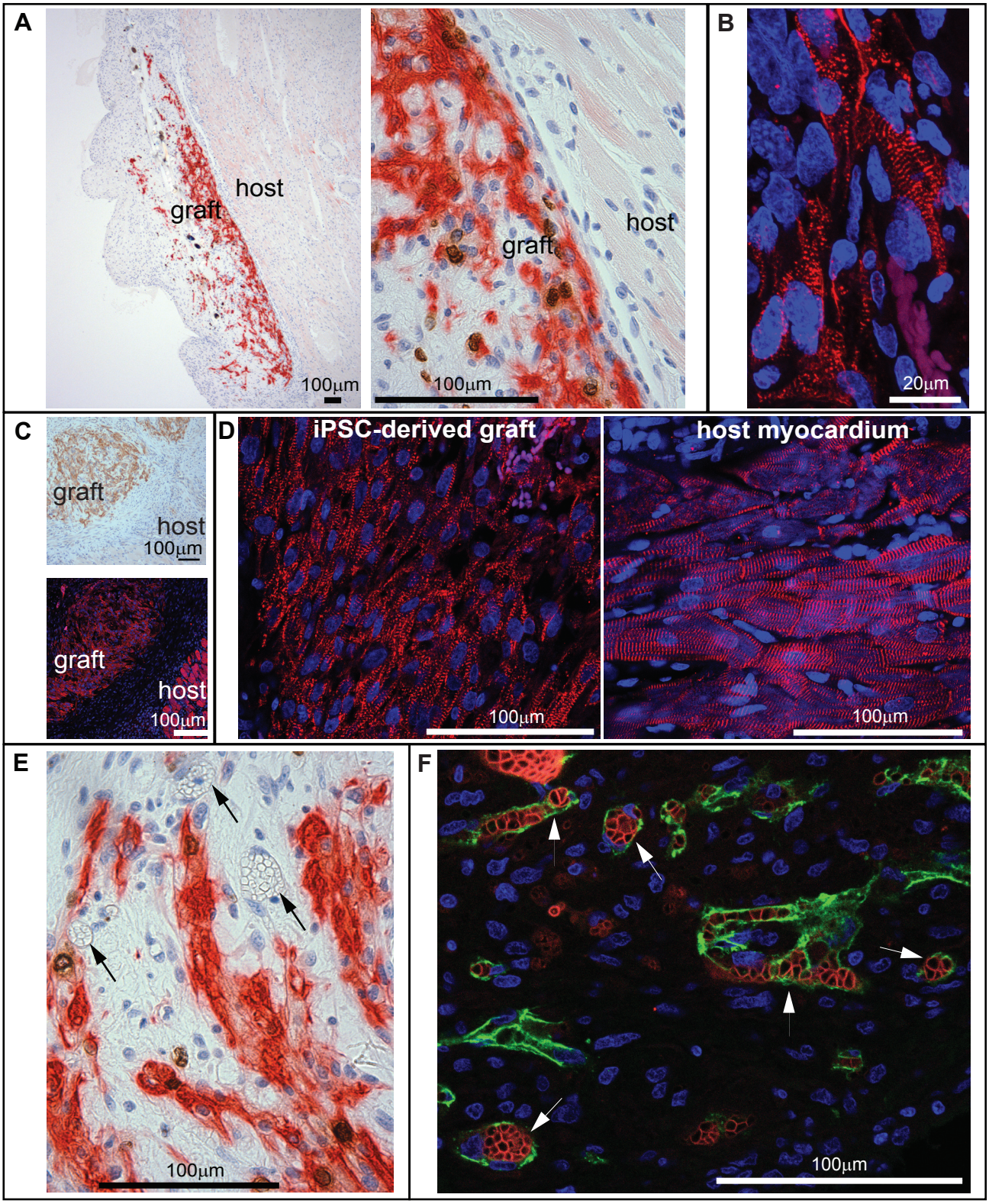

Figure 2.10. Cardiac engraftment. Human cardiac tissue constructs were pulsed for 1 day with BrdU and sutured onto myocardium of athymic rats. After 1 week in vivo, the hearts were excised, sectioned, and immunostained. **A,** βMHC and BrdU double immunostain of hES cell-derived, hCM only cardiac tissue construct. Left, graft overview, right, close apposition at graft-host interface in the myocardium. **B,** α-actinin immunofluorescence showed sarcomeric organization of engrafted human cardiomyocytes from the hES cell-derived, hCM only cardiac tissue construct. **C,** IPS cell-derived cardiac tissue construct engrafted onto the myocardium. Top, βMHC, bottom, α-actinin, showing the graft-host interface. **D,** Left, closeup of the engrafted iPS cell-derived cardiac constuct, right, closeup of the native myocardium (red, α-actinin). **E,** Within the βMHC positive area of engrafted hES cell-derived constructs, patent blood vessels were filled with erythrocytes (arrowheads), indicating host perfusion of the graft. **F,** In engrafted hES cell-derived Tri-cell human cardiac tissue constructs, human CD31 immunostaining (green) was used to mark human vessels and Ter119 (red) to mark erythrocytes. Endothelial structures of human origin containing red blood cells are indicated with arrows. n=5 for hCM only, ES cell-derived; n=4 for Tri-cell, ES cell-derived; n=1 for hCM only, iPS cell-derived.

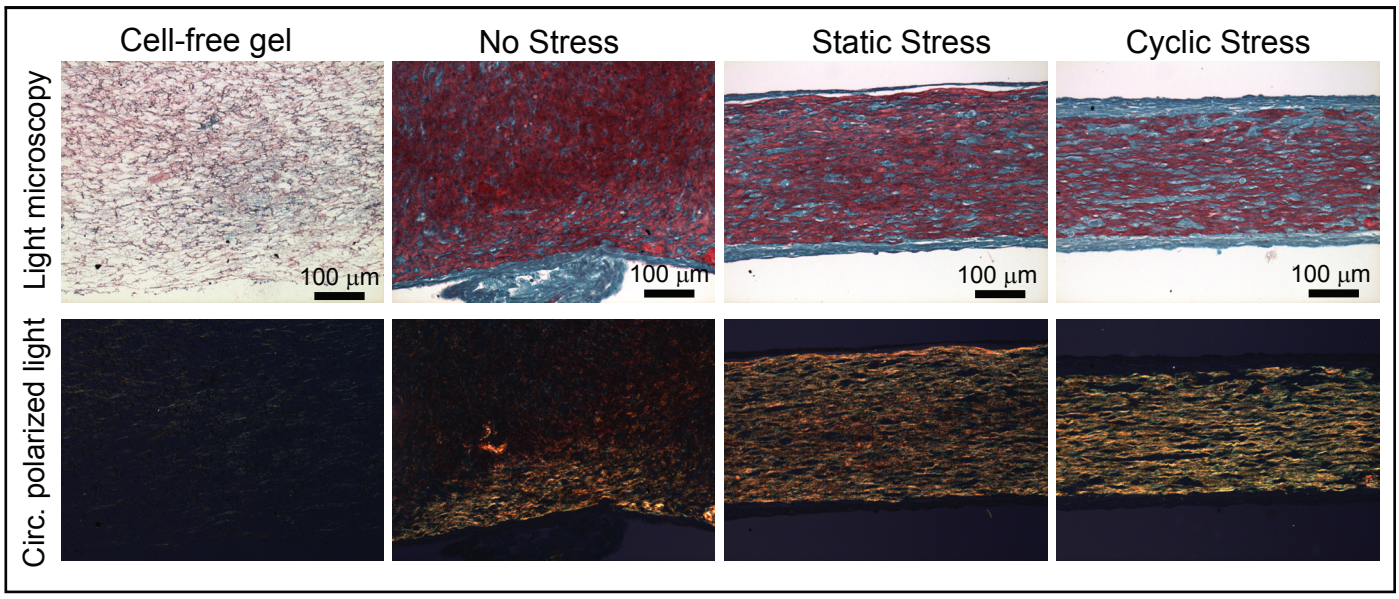

Figure 2.11. Collagen alignment in rat neonatal cardiac constructs. Staining was performed using picrosirius red for assessment of collagen fiber bundle organization by birefringence under circularly polarized light. Large bundle collagen fibers fluoresced yellow in rNC constructs in contrast to cell-free collagen constructs, demonstrating an absence of large collagen fibers in the starting material. These fibers appeared disarrayed in the unstressed condition but closely aligned with conditioning, indicating that that collagen fiber architecture was also greatly improved by static and cyclic stress.

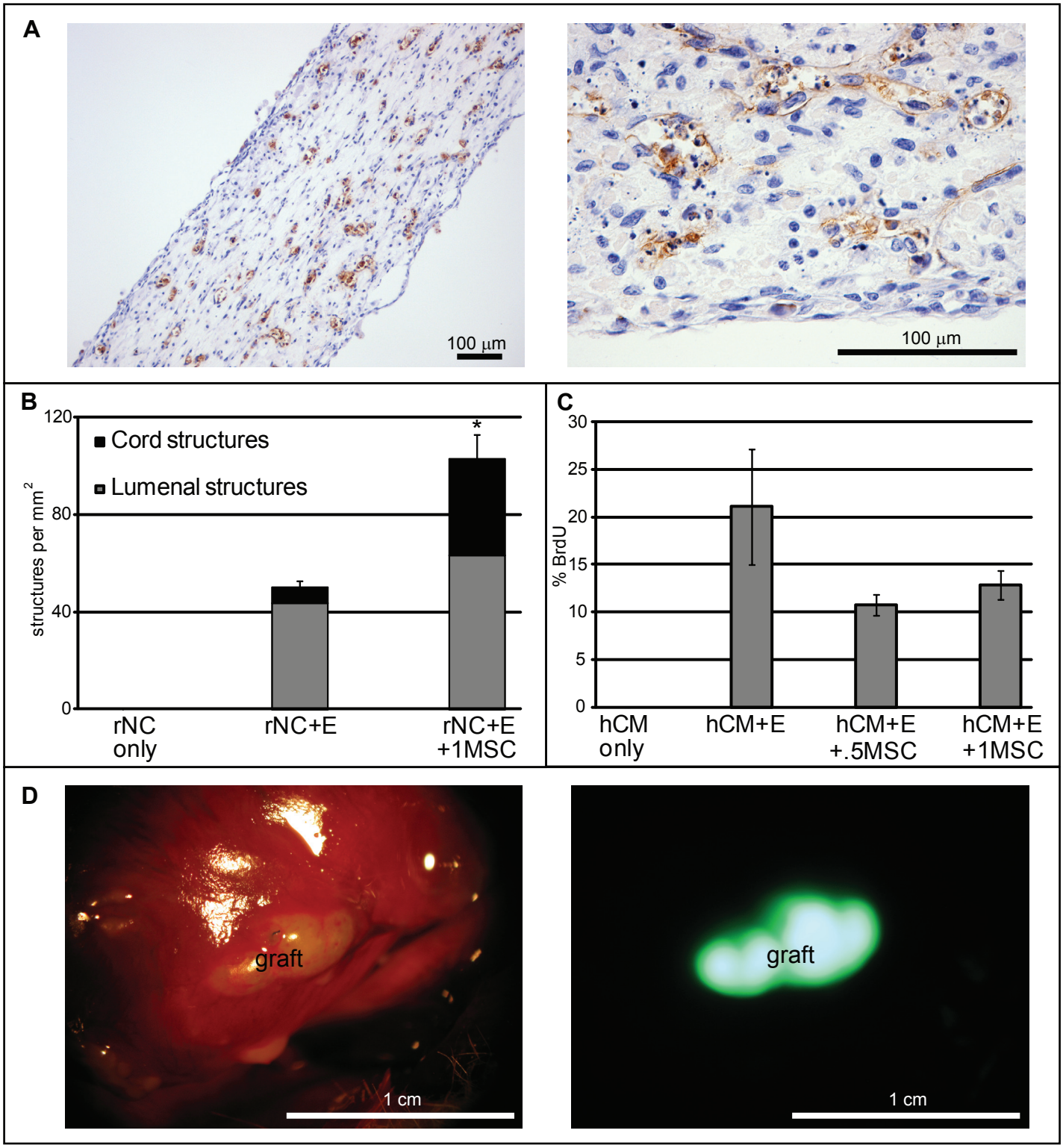

Figure 2.12. Vascularization and implantation of rat and human cardiac constructs. A, CD31 immunohistochemistry (brown). Constructs generated with rat cardiomyocytes and human endothelial cells contain endothelial structures dispersed throughout. Right, closeup of endothelial structures. **B,** In rat neonatal cardiac constructs under static strain, endothelial structure formation was increased by the addition of human MSCs. *, $p<0.05$ for cord structures compared to rNC+Endo. **C,** Endothelial proliferation was measured in statically strained human cardiac constructs pulsed with BrdU on day 4 and fixed on day 5. Slides were double stained for BrdU and CD31 and the ratio of BrdU-positive to BrdU-negative endothelial cells was quantified. Addition of a 1:1 ratio of MSCs to Endos (+1MSC) or half has many MSCs (0.5MSC) decreased endothelial proliferation rate between day 4 and day 5 (n=3 for hCM only, hCM+Endos, hCM+Endos+1MSC, n=2 for hCM+Endos+0.5MSC). **D,** Human triculture cardiac constructs were generated with MSCs expressing GFP, conditioned with static strain for 7 days, and grafted into the myocardium of an athymic rat. After an additional seven days, the construct is brightly visible on the epicardial surface under fluorescent light.

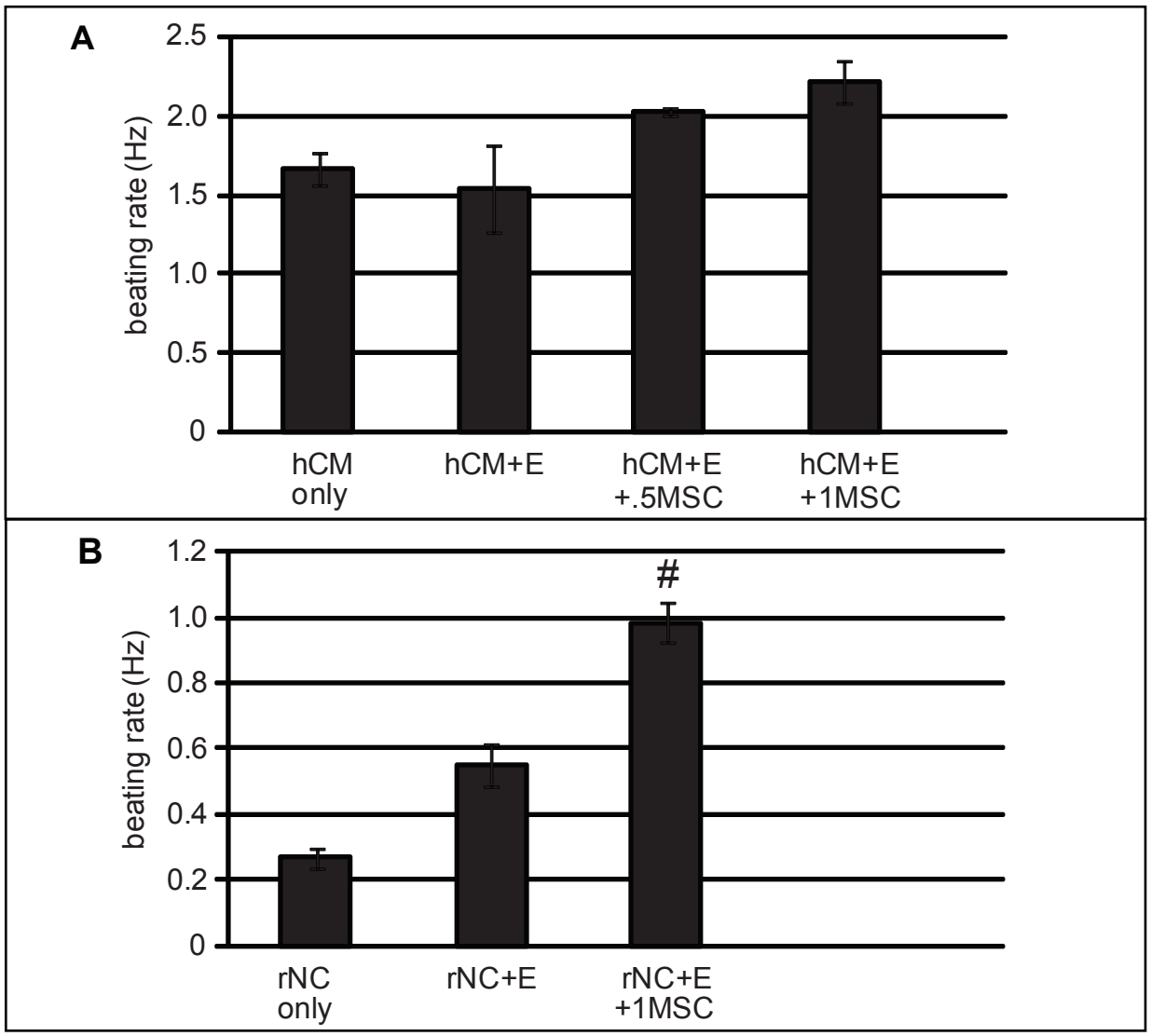

Figure 2.13. Contractility of human and rat cardiac constructs with tri-culture. A, Human ES cell-derived constructs generated with or without 1 million human endothelial cells, 1 million human MSCs (+1MSC), or 0.5 million MSCs (+.5MSC) were conditioned with static strain for 5 days before beating rate was assessed visually (n=2). **B,** rNC constructs generated with or without 1 million human endothelial cells (rNC+E) and 1million human MSCs (+1MSC) were conditioned with static strain for 3 days before spontaneous beating rate was assessed visually (# = $p < 0.005$).

Figure 2.14

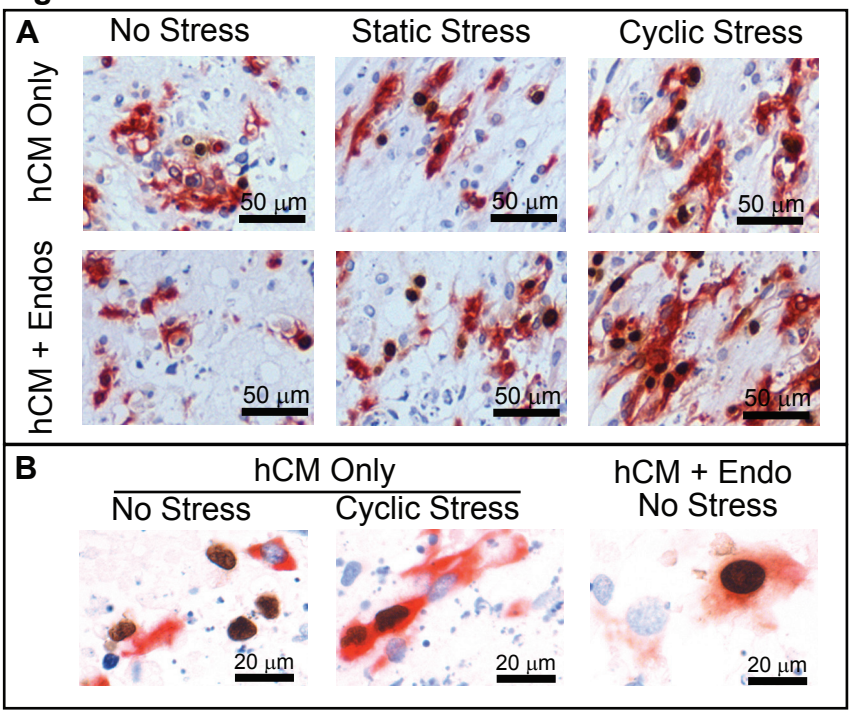

Figure 2.14. BrdU labeling of proliferating ESC-derived and iPSC-derived human cardiac constructs. **A,** hCM constructs derived from hES cells with or without endothelial cells were placed under conditions of no stress, static stress or cyclic stress and immunostained for βMHC (red) and BrdU (brown). Cardiomyocytes undergoing DNA synthesis were double-labeled with brown nuclei and red cytoplasm. Levels of DNA synthesis in cardiomyocytes were quantified in Figure 2.5A. **B,** hCM constructs derived from iPS cells with or without endothelial cell were placed under conditions of no stress or cyclic stress and immunostained for βMHC (red) and BrdU (brown). Representative double-labeled cells within the construct are shown. Levels of DNA synthesis were quantified in Figure 2.5B. N=4.

Table 2.1

Immunostain	ESC Undiff	Cardio **Ave** (**%** ± SEM)
Oct4	71.0%	**0.0** ± 0.0%
βMHC	0.0%	**52.8%** ± 18.6%
CD31	0.0%	**0.1** ± 0.1%
Smooth muscle actin	0.0%	**36.3** ± 32.0%
Cytokeratin	0.0%	**3.8** ± 3.1%
α-fetoprotein	0.0%	**6.2** ± 6.2%
β3-tubulin	0.0%	**0.1** ± 0.1%

Table 2.1. Characterization of differentiated cells. The hESC-derived input cardiomyocyte population was stained and quantified using lineage markers for cardiovascular and support cell types (βMHC, CD31, SMA) as well as for endodermal, ectodermal, and pluripotent cell types (α-fetoprotein, β3-tubulin, and oct4, respectively). Undifferentiated hESCs (n=1) were analyzed as well.

Table 2.2

Gene	Sequences, 5'-3'	Tm	Size
MYH7	GGGCAACAGGAAAGTTGGC ACGGTGGTCTCTCCTTGGG	60°C	202bp
TNNT2	TTCACCAAAGATCTGCTCCTCGCT TTATTACTGGTGTGGAGTGGGTGTGG	60°C	175bp
NPPA	ACAGACGTAGGCCAAGAGAG GTCTGACCTAGGAGCTGGAA	60°C	158bp
NPPB	CACCGCAAAATGGTCCTCTA GTCCATCTTCCTCCCAAAGC	58°C	87bp
CACNA1C	CAGAGGCTACGATTTGAGGA GCTTCACAAAGAGGTCGTGT	58°C	220bp
RYR2	AGAACTTACACACGCGACCTG CATCTCTAACCGGACCATACTGC	62°C	199bp
ATP2A2	TTT CCT ACA GTG TAA AGA GGA CAA CC TTC CAG GTA GTT GCG GGC CAC AAA	62°C	364bp
HPRT1	TGACACTGGCAAAACAATGCA GGTCCTTTTCACCAGCAAGCT	60°C	94bp

Table 2.2. Characteristics of primers used for quantitative RT-PCR.

Chapter 3: Mechanical Strain Promotes Maturation of Human Myocardium from Embryonic Stem Cell-Derived Progenitors

Summary

Recent advances in pluripotent stem cell biology have identified a population of human cardiovascular progenitors that give rise to cardiomyocytes, smooth muscle cells and endothelial cells. Because the heart develops in 3-D under constant mechanical load, we sought to test the effects of a 3-D microenvironment and mechanical stress on differentiation and maturation of cardiovascular progenitors into myocardial tissue. Progenitors were derived from embryonic stem cells, cast into collagen hydrogels, and left unstressed or subjected to static or cyclic mechanical stress. Compared to 2-D culture, the unstressed 3-D environment increased cardiomyocyte numbers by 34% and decreased smooth muscle numbers by 68%. Similarly, 3-D culture increased cardiomyocyte maturation (>100% per-cell by expression of contractile proteins) while suppressing smooth muscle cell maturation by >40%. Mechanical stress conditioning further improved cardiomyocyte maturation by >50%,with no effect on cardiomyocyte or smooth muscle specification. Endothelial cells formed vessel-like networks with lumens under 3-D conditions, and their numbers increased by >100% with cyclic stress conditioning. Cyclic stress-conditioning increased expression of β-myosin transcript by 550%, and the tissue showed enhanced calcium dynamics, with >100% increases in the rate and magnitude of calcium transients. Thus, 3-D growth conditions favor cardiac differentiation and maturation of cardiovascular progenitors, whereas 2-D conditions promote smooth muscle differentiation. Furthermore, mechanical loading promotes maturation of these cardiomyocytes and enhances the differentiation of progenitors into endothelial cells. This 3-D system may facilitate understanding how cues such as mechanical stress affect the differentiation and morphogenesis of distinct cardiovascular cell populations into organized, functional human cardiovascular tissue.

Introduction

The development of functional human myocardium for basic research and regenerative therapy would be greatly enhanced by an ability to generate the several differentiated cell types found in mature cardiac tissue within a single tissue construct. This could theoretically be done by subjecting a single line

of pluripotent cells to several specific differentiation protocols, for example, differentiating vascular endothelium using endothelial specific differentiation protocol[25] and cardiomyocytes using a cardiogenic protocol,[20] and then mixing the resulting cell types in the context of a 3-dimensional (3-D) matrix. The discovery of a tri-potential cardiovascular progenitor population[22] – existing partway between the pluripotent cell state and the differentiated cardiac and vascular fates – provides an attractive alternative for creating differentiated cardiovascular tissues. These KDR and PDGFRα-expressing progenitor cells could potentially provide the basis for bioengineered tissues consisting of working myocardium pre-set with its own genotype-specific vasculature, useful for both the paracrine induction of cardiomyocyte proliferation[86] within the tissue and the "plug and play" vasculature that facilitates *in vivo* engraftment.

The idea of creating a tissue with intentionally mixed cell types is relatively novel, with most attempts prior to 2007[2] using only a single, often rodent, cardiac cell type or an unpurified neonatal heart preparation.[8-10, 14] However, several studies have demonstrated that admixture of other cell types improves the viability and function of cardiomyocyte themselves.[2, 15, 19] Our own recent work has demonstrated that co-culture with endothelial cells significantly increases cardiomyocyte proliferation, whereas the further addition of a stromal cell type in turn increases vascular structure formation.[86] While in retrospect such cross-talk may have been predictable, given that natural tissues are composed of many cell types, the tools to replicate and study such interactions in relevant, human-based model systems have been limited.

Previous studies in cardiac tissue engineering using mixed cell populations have tended to use cells from different sources, even from different species.[2, 12] Our goals were, first, to create human cardiac tissue from a single genetic background, with cells differentiating and self-organizing together; and second, to see whether specific manipulations, such as 3-D scaffolding versus 2-D culture, or mechanical stress conditioning compared to unstressed conditions, differentially affected fate choice and maturation among the resulting cell types. Understanding how particular manipulations can affect distinct but interacting cell populations is essential to building organized, functional cardiovascular tissue *in vitro*.

Results

Bioengineered Progenitor Constructs Mature into Cardiovascular Tissue

Human ESCs of the H7 line were differentiated into tri-potential cardiovascular progenitor cells using BMP4, activin A, basic FGF, VEGF and Dkk-1 in 3 sequential stages as previously reported.[22] The large majority of cells collected at day 5 after the onset of differentiation co-express the lineage markers KDR and PDGFRα (Figure 3.1A), signifying a tri-potential population capable of differentiating along cardiac and vascular fates.[22, 87] Other than this majority population of double-positive, KDR-low expressing progenitors, there was a minority subset which was KDR-high expressing. These are noted to be hemangioblast progenitors with endothelial and hematopoetic potential.[22, 88] However, the cardiogenic potential the sorted majority KDR+low/PDGRFα+ population versus the cardiogenic potential of the unsorted cells has been found to be virtually identical.[87] In light of these published studies, we employed the unsorted progenitors following 5 days of CVP differentiation as our input population for the generation of cardiovascular tissue within a 3-dimensional (3-D) collagen-based scaffold. Preparations averaged 76±2% cardiovascular progenitors and 9±2% hemangioblasts based on flow cytometry of the input population at the time of construct generation. This preparation is referred to as “progenitors” through the remainder of the manuscript.

Over the course of two weeks of differentiation within this 3-D matrix, these tri-potential progenitor-derived constructs mature into contractile cardiovascular tissue (see Figure 3.1B-F composed of cells expressing the myocyte marker desmin, the cardiac transcription factor Nkx2.5, the contractile protein cardiac troponin T (cTnT), the endothelial marker CD31, or the smooth muscle marker α-SM actin (SMA). Some cTnT+ cardiomyocytes and CD31+ endothelial cells continue to proliferate as noted by 24 hour BrdU incorporation.

Progenitor Fate-Choice and Maturation in 2-D versus 3-D Bioengineered Tissue

By flow cytometric analysis, tri-potential cardiovascular progenitor cells cultured within 3-D engineered tissue differentiated into cardiomyocytes at 34% higher purity in than progenitors plated in 2-dimensional (2-D) culture (Figure 3.2A; 62.6% versus 46.6%, respectively $p<0.05$). Smooth muscle cells, on the other hand, differentiate at 3-fold lower purity in constructs (Figure 3.2B; 3.3% versus 11.4%

respectively, p=0.0001), and endothelial cell differentiation remained unchanged (Figure 3.2C; 9.1% versus 7.5%).

In addition to differences in fate choice, cardiomyocyte, endothelial, and smooth muscle cell maturation was differentially affected by culture in 3-D engineered tissue versus 2-D culture conditions. When normalized on a per cell basis, cardiomyocytes cultured in 3-D tissue had an over 2-fold increased average cTnT intensity per cTnT+ event over those cultured in plated conditions (Figure 3.2D; intensity values of 386 and 810 for plated culture and engineered tissue, respectively). Similarly, endothelial cells had an over 2-fold higher CD31 content per cell in engineered tissue (Figure 3.2F; intensity values of 543 versus 1164 for plated culture and engineered tissue, respectively). Conversely, smooth muscle cells in 3-D engineered tissues had a 1.7-fold decrease in per-cell SMA intensity compared to 2-D culture (Figure 3.2E; SMA intensity of 635 and 365, for plated and engineered tissue, respectively).

Progenitor Fate-Choice and Maturation with Mechanical Stress Conditioning

To investigate the effects on fate choice and maturation of stress conditioning, cardiovascular progenitor constructs were subjected to 2 weeks of no stress, static stress, or exogenous 1Hz, 5% elongation, cyclic stress conditioning before quantification by flow cytometry. Cyclic stress conditioning markedly increased endothelial differentiation (Figure 3.2C). On the other hand, none of the 3 conditioning regimes had any significant effect on cardiomyocyte or smooth muscle fate choice (Figure 3.2A, B). The finding that stress conditioning does not seem to differentially affect cardiomyocyte differentiation was independently verified by cell counts in histological sections (data not shown). However, 2 weeks of cyclic stress conditioning increased cTnT intensity per cell by more than 1.5-fold over static or no stress conditioning (cTnT intensities of 1265, 823, and 810 for cyclic, static, and no stress, $p<0.05$), indicating that cyclic stress conditioning has a distinct effect on cardiomyocyte maturation (Figure 3.2D). In contrast, smooth muscle maturation as measured by per cell SMA intensity was not at all affected by the conditioning regimes tested (Figure 3.2E).

Cell Maturation and Cell Fate by Quantitative RT-PCR

Following 2 weeks of stress conditioning, whole cardiovascular progenitor construct lysates were analyzed by quantitative RT-PCR for expression of cardiomyocyte contractile gene β-myosin heavy chain (βMHC). Cyclic stress conditioning very significantly increased the expression of βMHC — by 550% to 800% — over no stress and static stress conditions (Figure 3.3A). Concurrently, αMHC gene expression significantly decreased with cyclic stress conditioning, to 62% or 50% of no stress or static stress condtions (Figure 3.3B). Interestingly, analysis of individual tissue constructs showed that β-MHC and α-MHC transcripts exhibit inverse proportionality (Figure 3.5), with α-MHC declining rapidly as β-MHC increased with maturation. On the other hand, expression of the cardiomyocyte fate marker Nkx2.5 remained unchanged over the different conditioning regimes (Figure 3.3C), indicative of a cardiomyocyte maturation effect rather than a promotion of cardiogenic fate-choice.

For further validation that the changes noted with cyclic stress conditioning were specific to cardiac gene subsets rather than changes in housekeeping gene expression, a second, unrelated, normalization gene was analyzed. Both HPRT1, involved in purine biosynthesis, and GAPDH, essential in glycolysis, show similar relative expression under all stress conditions (Figure 3.3D).

Calcium Dynamics of Stress-Conditioned Bioengineered Cardiovascular Tissue

Calcium transients were visualized using the ratiometric calcium flurophore Fura-2AM and an IonOptix setup and were recorded in 30˚C medium under low magnification with a 10x objective. Representative spontaneous calcium transients from human cardiovascular tissue conditioned with 2 weeks of no stress, static stress, or cyclic stress are shown in Figure 3.4A; colors correspond to regions of interest further quantified (Figure 3.4B). Calcium dynamics were markedly increased in cyclic strain-conditioned constructs by measurement of a number of different parameters. Peak calcium flux was increased by over 100% (peak height of 0.18, 0.16, and 0.37 for no strain, static strain, and cyclic strain, respectively, $p<0.005$). When adjusted for any potential differences in baseline calcium intensity (bl%peak h), cyclic stress-conditioned peak height remained over 100% increased ($p<0.005$). Additionally, departing velocity was increased by 120% to130% with cyclic stress conditioning (no stress: 0.38, static stress: 0.37, cyclic stress: 0.84, $p<0.0005$). This increased calcium influx in cyclic stress-conditioned

constructs was reflected not only in peak height and departing velocity kinetics, but also in a 3-fold increase in area under the departing curve (area dep a) and 3 to 9-fold increase in the area under the return curve (data not shown). However, the time to peak (peak t), was not noticeably changed between conditions, indicating a similar calcium influx time-frame between all groups, and the return velocity of the transient was comparable among groups.

Discussion

In this study, we demonstrate the development of human cardiovascular progenitors in a 3-D bioengineered tissue environment into differentiated human cardiovascular tissue composed of multiple cell types and that the 3-D environment altered fate significantly compared to 2-D culture. Furthermore, this study reveals that mechanical stress conditioning in a 3-D bioengineered tissue environment differentially affected specification and maturation of cardiac, endothelial, and smooth muscle subsets. Finally, we demonstrate that the calcium handling of this engineered cardiovascular tissue is markedly increased with cyclic stress conditioning, in comparison to static stress or no stress conditioned counterparts.

Our initial findings that differentiation from the initial KDR+ progenitor population into the cardiac, endothelial, and smooth muscle fates was possible within the 3-dimensional tissue construct environment (Figure 3.1) were promising. We next sought to examine differences in fate choice between the standard 2-D culture environment and the 3-D scaffold. We devised a construct disassociation procedure which allowed us to quantitatively analyze whole constructs on a single-cell basis by flow cytometry, and found that cardiomyocyte differentiation was markedly increased in the 3-D environment while the smooth muscle fate was strongly diminished (Figure 3.2). We next looked at maturation of each subset, by mean intensity per cell of the cardiomyocyte, smooth muscle, or endothelial cell marker, finding that cardiomyocytes and endothelial cells differentiated in 3-D tissue conditions had a significantly increased amount of the contractile protein cTnT or endothelial protein CD31 per cell, respectively, whereas smooth muscle cells differentiated within the 3-D scaffold had a much lower SMA protein content than those plated in 2-D.

We next looked at the effect of mechanical stress conditioning on progenitor fate choice. Progenitor constructs subjected to 2 weeks of cyclic or static stress conditioning did not, surprisingly to us, have an increased percentage of cardiomyocytes or smooth muscle cells than constructs maintained in unstressed conditions (Figure 3.2). In addition, expression of the cardiomyocyte fate marker Nkx2.5 remained unchanged in the different conditioning groups (Figure 3.3). However, the endothelial cell proportion increased significantly with cyclic stress conditioning (Figure 3.2).

Stress conditioning affected maturation of the cardiovascular subsets differently. Smooth muscle content of SMA protein did not change at all with stress conditioning, nor did CD31 intensity in the endothelial subset. However, cardiomyocyte expression of the sarcomeric protein cTnT was markedly increased by cyclic stress conditioning, specifically, over static or no stress conditioning (Figure 3.2D). Quantitative PCR analysis of a second contractile gene, β-myosin (βMHC), corroborated this finding, revealing a striking increase in βMHC transcript specifically in cyclic stress-conditioned constructs (Figure 3.3A). These data are strongly indicative of a cardiomyocyte maturation effect due to cyclic stress conditioning rather than a promotion of cardiogenic fate-choice, especially as the cardiomyocyte-specifying transcription factor Nkx2.5 did not change in expression with conditioning (Figure 3.3C).

Intriguingly, expression of α-myosin (αMHC) was down-regulated by stress conditioning (Figure 3.3B). These two genes, αMHC and βMHC, lie adjacent to each other in human and rodent genomes, and are known to be coordinately regulated in a negative reciprocal manner in the developing rat myocardium through a fascinating antisense-based inhibition of mRNA transcript levels.[89] Indeed, there is a noticeable inverse correlation between α and β-MHC expression in these conditioned human cardiovascular tissue constructs on a per-construct basis (Figure 3.5). We propose that there may be a cooperative mechanism at play in human cardiac developmental maturation that is analogous to that described in the rat, which merits further study. Alternately, atrial and ventricular cardiomyocytes differ in their relative α and β-MHC expression, with α -MHC generally higher in the former and β-MHC higher in the latter, so we cannot rule out differential cardiomyocyte subtype specification, rather than maturation of a single cardiomyocyte subtype.

Finally, we examined the calcium transient dynamics of these cardiovascular constructs. Cyclic stress conditioning markedly increased both departing velocity and calcium transient peak height (Figure

3.4) indicating that rate and magnitude of calcium influx was markedly increased by 2 weeks of cyclic stress conditioning. Taken together, these changes in contractile gene expression, protein levels, and calcium flux all indicated that cyclic stress conditioning, and not static or no stress conditioning, increased maturation of the cardiac subset of this engineered human cardiovascular tissue.

In conclusion, we were able to create a complex engineered cardiovascular tissue with multiple cell types arising from a single genetic background, with cells differentiating together within the tissue matrix. We also examined how 3-D scaffold versus 2-D culture affected both fate-specification between the cardiac and vascular subsets and maturation of the resulting differentiated cells. Finally, we determined that exposure to cyclic stress conditioning affects maturation in the cardiac but not smooth muscle or endothelial compartments, as well as markedly increasing the contractility of the resulting cardiovascular tissue. We believe that understanding how particular manipulations, such as mechanical stress conditioning, can affect the differentiation and maturation of developing cell populations is essential to building complex, functional human cardiovascular tissue.

Materials and Methods

Cell Culture

Undifferentiated human ESCs of the H7 line were maintained as described previously.[25, 79, 86] Briefly, human ESCs were maintained on Matrigel (BD Biosciences) in MEF-conditioned medium supplemented with 8 ng/mL basic FGF (Stemgent) and passaged with collagenase IV (200 U/mL, Invitrogen) and 0.05% trypsin-EDTA (Invitrogen). Differentiation of cardiovascular progenitor cells and progenitor constructs took place in a “Backbone” medium made daily containing Stempro Base medium, Supplement 34 (Invitrogen), penicillin G (100 U/mL, Cellgro), streptomycin (100 mg/mL, Cellgro); L-glutamine (1 mmol/L, Invitrogen), ascorbic acid 2-phosphate (50ug/mL, Sigma), transferrin (150ug/mL, Roche), and monothioglycerol (0.039 µL/mL, Sigma), with the further addition of various stage-specific cytokines as previously described.[22] Maintenance of differentiated constructs and cultures containing, in various proportion, cardiomyocyte, endothelial and smooth muscle cells was managed with Backbone medium supplemented with VEGF (10 ng/mL, R&D Systems).

Cardiovascular Differentiation

For differentiation of cardiovascular progenitor cells, plates of H7 hESCs at 80% confluence were pre-incubated for 1 hour in 10μM ROCK inhibitor Y27632 (Tocris Bioscience), washed 2 times with phosphate buffered saline (PBS) and incubated for 5 minutes with collagenase IV followed by 15 seconds of 0.05% trypsin-EDTA. Following aspiration of trypsin, Stop solution containing 50% DMEM/F12 (Invitrogen), 50% fetal bovine serum (FBS, Hyclone), Matrigel (1:800), and DNAse (200 U/mL, Calbiochem) was added to each plate and the colonies were gently detached using a cell lifter (Corning) and pelletted for 5 minutes at 800rpm. The colonies were resuspended in Backbone medium with low dose BMP4 (0.5 ng/mL, R&D Systems) and ROCK inhibitor (10μM) and cultured as embryoid bodies (EBs) in ultra-low attachment 10-cm plates (Corning) at a density of 6 million cells per plate for 24 hours in relative hypoxia (5% oxygen).

On day 1 of differentiation, EBs were gravity-settled and resuspended in a Mesoderm Induction medium (Backbone medium supplemented with a cocktail of 10 ng/mL BMP4, 6 ng/mL activin A, R&D, and 5 ng/mL basic FGF) and placed back into hypoxia. On day 4 of differentiation, the EBs were gravity settled for 20 minutes in hypoxia, resuspended in IMDM (Invitrogen) to rinse off any remaining activin A and BMP4, and pelletted for 5 minutes at 800 rpm. The EBs were then resuspended in Backbone medium supplemented with VEGF (10 ng/mL) and Dkk1 (150 ng/mL, R&D Systems) in order to promote cardiovascular progenitor differentiation, and placed back in hypoxia. After an additional 24 hours, the EBs we pre-incubated for 1 hour in ROCK inhibitor before pelletting and digestion with trypsin solution. This procedure consisted of a 1-2 minute incubation at 37˚C with occasional light vortexing followed by disruption with a 20-gauge needle (BD Biosciences) and the addition of Stop solution. Cells were counted, pelletted, and resuspended in Backbone medium. An aliquot was taken for live cell KDR/PDGFRα staining and flow cytometry, and the remaining cells were used to generate cardiovascular progenitor constructs (described below) or plated at a density of 1 million cells per well in Matrigel-coated 6-well plates; both constructs and plated progenitors were kept in Backbone medium with VEGF (10ng/mL) and Dkk1 (150ng/mL) in normoxic (20% oxygen) conditions. On day 9 of differentiation, plated cells and constructs were again fed with Backbone medium supplemented with VEGF and Dkk1; however, all subsequent feeds were in Backbone medium supplemented solely with VEGF. Based on

double labeling with antibodies to KDR and PDGFRα, preparations at day 5 averaged 76±2% cardiovascular progenitors and 9±2% hemangioblasts (Figure 3.1). This preparation is referred to as "progenitors" through the remainder of the manuscript.

Generation of Cardiovascular Progenitor Constructs

At 5 days post-differentiation induction, the KDR+/PDGFRα tri-potential cardiovascular progenitors were encapsulated in a collagen-based 3-dimensional scaffold as previously described.[86] Briefly, cardiovascular progenitor tissue constructs were generated using collagen type I (final concentration 1.25 mg/mL, neutralized with NaOH; Invitrogen), 11% mouse basement membrane extract (Geltrex, Invitrogen), and 57% Backbone medium mixed together on ice with cells gently added. Bioengineered tissue constructs were cast in a 20 mm by 3 mm trough at a density of 1 million cells per 50 μL of gel mixture. These troughs were formed in Tissue Train 6-well plates (Flexcell International Corp.) mounted over Trough Loader posts set in a Bioflex baseplate under vacuum (Flexcell). At opposing ends of each trough, the cell-gel mixture saturated nylon mesh tabs affixed to the periphery of the well, securing the construct at a fixed length and providing means to transmit uniaxial tension to the construct. After 1 hour at room temperature for matrix solidification, the baseplate vacuum was released and the resulting cardiovascular progenitor constructs were placed into Backbone medium with VEGF and Dkk1. To investigate the effects of exogenous cyclic stress conditioning, Tissue Train plates containing constructs were placed onto an Arctangle loading posts in a baseplate connected to an FX-4000T system (Flexcell) on the day following construct fabrication. Uniaxial cyclic strain was applied at a 1 Hz, 5% elongation using a square sine waveform setting. Static stress conditioning was achieved by maintaining constructs at a fixed static length, whereas no-stress conditions were achieved with one end of the construct cut free of the nylon tab. Constructs were maintained in a regimen of no stress, static stress, or cyclic stress conditioning for a period of 2 weeks (through day 19 of differentiation) before analysis.

Flow Cytometry

KDR / PDGFRα dual staining for flow cytometry was conducted on live cells at day 5 of differentiation to assess the presence and extent of double-positive cardiovascular progenitors in the input population at the time of progenitor construct fabrication. Briefly, cells were resuspended in IMDM with 5% FBS containing the directly conjugated antibodies hKDR-PE (mouse IgG1, R&D Clone 89106) at a 15:100 dilution and hPDGFRα-APC (mouse IgG1, R&D Clone PRa292) at a 10:100 dilution. Isotype controls used for flow cytometry gating were made with mouse IgG1-PE (eBioscience Clone P3.6.2.8.1) and mouse IgG1-APC (eBioscience Clone P3.6.2.8.1) at appropriate dilutions for similar antibody concentration to KDR and PDGFRα-stained samples. After a 30 minute incubation at 4° C in the dark, samples were washed 3 times with PBS with 5% FBS, fixed in 1.3% paraformaldehyde (PF, Sigma), and analyzed by flow cytometry within 7 days.

For disruption of cardiovascular tissue constructs for flow cytometry, the 3-D constructs were dispersed to single cells using a trypsin-based technique. Briefly, each was washed 2 times in the calcium-chelating solution versene (0.5 mM EDTA and 1.1 mM glucose in PBS) containing 2,3 butanedione monoxime (30μM, BDM, Sigma) and ROCK inhibitor Y27632 (10μM). These compounds were used to promote matrix detachment, to stop actomyosin interaction, and to prevent detachment-related anoikis, respectively. The construct was then dissected into several pieces with a scalpel and placed in a 0.05% trypsin solution also containing 30 mM BDM and 10 μM Rock inhibitor. After 2 rounds of 5 minute 37° C incubation and light vortex, the remaining pieces were subjected to disruption with 20-gauge needle before an equal volume of Stop solution was added. Further trituration with a P1000 pipette was performed if necessary before the single cells were pelletted. Following dispersion, the cells were fixed for 10 minutes in cold 4% PF and resuspended in PBS with 5% FBS.

For analysis of cardiovascular fate choice by flow cytometry, cells from conditioned constructs or from plated progenitors were resuspended with 0.75% saponin (Sigma) in PBS with 5% FBS and stained with cardiac troponin T (cTnT, mouse IgG1, ThermoScientific Clone13-11, 1:100 dilution), smooth muscle α-actin (SMA, rabbit IgG, Abcam Clone E184, 1:200 dilution) or hCD31-PE (mouse IgG1, eBioscience Clone WM59, 1:5 dilution). Samples were incubated for 30 minutes at room temperature and washed twice with 0.75% saponin in PBS with 5% FBS. Secondaries used for cTnT staining and SMA staining

were goat anti-mouse-IgG-PE (GαM-PE, Jackson Cat# 115-116-072, 1:200) and donkey anti-rabbit-IgG-APC (DαR-APC, Jackson Cat# 711-136-152, 1:500), respectively, with a 30 minute room temperature incubation in the dark. The CD31 antibody was directly conjugated and did not require a secondary antibody. Isotype control primary antibodies used for cTnT and SMA staining were mouse IgG1 (eBioscience Cat# 14-4714, 1:100) and rabbit IgG (Cell Signaling Cat# 2729, 1:1000) used in conjunction with the secondary antibodies listed above; whereas mouse IgG1-PE (eBioscience Cat# 12-4714, 1:100) was used as isotype control for CD31 staining. After the final incubations, each sample was washed once with 0.75% saponin in PBS with 5% FBS and 2 times with PBS with 5% FBS before fixation of antibody to epitope in 1.3% PF and analyzed by flow cytometry within 7 days on a BD FACS Canto II machine (BD Biosciences) or on a BD FACS Aria II (BD Biosciences). Samples were gated against isotype controls, human umbilical vein endothelial cells were used as positive controls for CD31 in each run, and results were analyzed using FlowJo version 9.3.1 software.

Unless otherwise specified, data are a summary of 3-6 biological replicates, each with groups of 2-6 constructs. However, due to high basal variability in endothelial differentiation from run to run (from 1% to 8% for no stress, 4% to 18% for cyclic stress) a representative biological replicate out of 3 is depicted here. For measurements of protein intensity per cell, events gated as cTnT+, SMA+, or CD31+ were analyzed for averaged mean PE (cTnT, CD31) or APC (SMA) fluorescence. For graphical purposes, the lower gated threshold is set as 0 and results were normalized to the whole experiment average to account for differences in flow collection voltages or fluorophore intensity between replicate experiments.

Quantitative RT-PCR

RNA was isolated from whole constructs using the RNeasy Fibrous Tissue Kit (Qiagen) with the following minor modifications. Each construct was disrupted in RLT buffer with 1% β-mercaptoethanol (Sigma) and homogenized with a 20-gauge needle (BD Biosciences); additionally the RNAse-free DNAse Set (Qiagen) was used to clear genomic DNA from the sample. RNA concentration and quality was quantified using a NanoDrop 1000 Spectrophotometer (Thermo Scientific), and 1ug of RNA was used to generate cDNA using random hexamers (Promega) and Superscript II Reverse Transcriptase (Invitrogen). For each set of cDNA, one sample was duplicated in parallel without reverse transcriptase as

a check for genomic contamination. cDNA was diluted 1:10 and 5μL were used per 20μL reaction for quantitative PCR, along with 0.2μM primers and 2x SensiMix SYBR reagent (Bioline), including 3mM MgCl2. Samples were run in triplicate in a 96-well-plate format with no template controls for each primer set on a 7900HT Fast Real Time PCR System (Applied Biosystems), using the following reaction design: Step 1: 95℃, 15min; Step 2: 95℃ 15sec, 60℃ annealing 30sec, 72℃ elongation 30sec (40 cycles); Step 3: 72℃ cleanup 5min; followed by a melting curve (Step 4) of 95℃ 15sec, 60℃ 15sec, and a 2% ramp rate to 95℃, 15sec to check for single product formation by melting curve peak. Primer specificity was additionally verified by gel electrophoresis for amplicon size; primer sequences are as follows: βMHC: GGGCAACAGGAAAGTTGGC, ACGGTGGTCTCTCCTTGGG; αMHC: GTCATTGCTGAAACCGAGAATG, GCAAAGTACTGGATGACACGCT; Nkx2.5: CCAAGGACCCTAGAGCCGAA, ATAGGCGGGGTAGGCGTTAT; GAPDH: CATCCATGACAACTTTGGTATC, CACCCTGTTGCTGTAGCCAA; and HPRT: TGACACTGGCAAAACAATGCA, GGTCCTTTTCACCAGCAAGCT. For qPCR analysis, sample Ct were determined using SDS 2.2.1 software (Applied Biosystems), and mRNA expression was normalized to levels of GAPDH transcripts. For verification of normalization, a second housekeeping gene not involved in basic metabolism, HPRT, was verified against GAPDH expression. N=3-6 constructs per experiment, in 2 biological replicates.

Calcium Transient Analysis

Calcium transient traces were collected from spontaneously beating cardiac tissue constructs using the ratiometric calcium fluorophore Fura2-AM (Invitrogen) in medium at 30℃ under low magnification using a 10x objective. Calcium transients were measured in Fura2-loaded cells using IonOptix system video microscopy (IonOptix LLC) as described previously.[90, 91] Fura-2 fluorescence was measured with an IonOptix spectrophotometer (Stepper Switch) which was attached to a fluorescence microscope. Emitted Fura2 fluorescence passed through the objective, through a 510 nm filter, and was detected by a photomultiplier tube. In each experiment, 6-10 construct traces were recorded per group, and 15-30 consecutive transients from each trace were analyzed to produce average transient values per

trace. Traces were analyzed using IonOptix software and over 250 transients were analyzed per conditioning group, with over 800 transients analyzed total.

Immunostaining

For immunohistochemistry, constructs were fixed for 20 minutes in 4% PF and embedded in paraffin. 5 μm sections were cut, and primary antibody staining was performed overnight, followed by one hour of secondary antibody incubation. For light microscopy, biotinylated secondary antibodies were used followed by a thirty-minute incubation in the enzyme-based ABC reagent (Vector Labs); the binding was visualized by DAB (Sigma) when horseradish peroxidase (Vector Labs) was used and by Vector Red (Vector Labs) when alkaline phosphatase (Vector Labs) was used, all followed by hematoxylin nuclear counterstain. For immunofluorescence, Alexa fluorophore-conjugated secondary antibodies were employed; Hoechst (Sigma) counterstain was used to visualize the nuclei.

The following primary antibodies were used for light microscopy: mouse monoclonal anti-cardiac troponin T (Developmental Studies Hybridoma Bank, 1:1000), mouse monoclonal anti-desmin (Dako, 1:5), goat polyclonal anti-human Nkx2.5 (R&D Systems, 1:400), mouse monoclonal anti-human CD31 (Dako, 1:15), mouse monoclonal anti-SMA (DAKO, 1:200), and mouse monoclonal anti-BrdU-POD (Roche, 1:40). Mouse monoclonal anti-α-actinin (Sigma, 1:800) and rabbit polyclonal anti-connexin 43 (Abcam, 1:500) were used with fresh-frozen constructs and tissue after treatment with proteinase K digest (Roche). Light microscopy secondary antibodies used were biotinylated goat anti-mouse IgG (Jackson Labs, 1:500) and biotinylated horse anti-goat IgG (Jackson Labs, 1:500). Immunofluorescent secondaries included Alexa 488- or 594-conjugated goat anti-mouse or horse anti-goat (Invitrogen, 1:100). Permount (Fisher) and Vectashield (Vector Labs) media were used to mount #1 glass coverslips (Corning) onto light microscopy and immunofluorescent slides correspondingly.

Microscopy and Image Preparation

Light micrographs were taken at room temperature using Nikon Eclipse 80i microscope fitted with dry 10x- 20x-, and 60x-Nikon objective with lenses of 0.30 and 0.95 NA correspondingly. The images were captured by Olympus Qcolor 3MB camera operated by Qcapture Pro software. All

immunofluorescent images were collected by a Nikon A1 Confocal System attached to a Nikon Ti-E inverted microscope platform and using water-immersion Nikon 60x CFI Plan Apo objective lens with 1.2 NA. Image acquisition was performed at room temperature using Nikon NIS Elements 3.1 software to capture 12-bit raw files that were then rescaled to 16-bit images for further processing. All images were collected as a single scan with the pinhole adjusted to 1 Airy unit at 1024x1024 pixel density. For figure preparation, images were exported into Photoshop 7.0 (Adobe). If necessary, brightness and contrast were adjusted for the entire image and the image was cropped.

Statistical Analysis

Results are depicted as average value ± standard error of the mean (SEM). Significance was determined using single factor ANOVA followed by Student's t-test with 95% or greater confidence level. To test for significance of values from subsequent stretches or stretches with and without BDM or isoproterenol, Student's paired t-test was used.

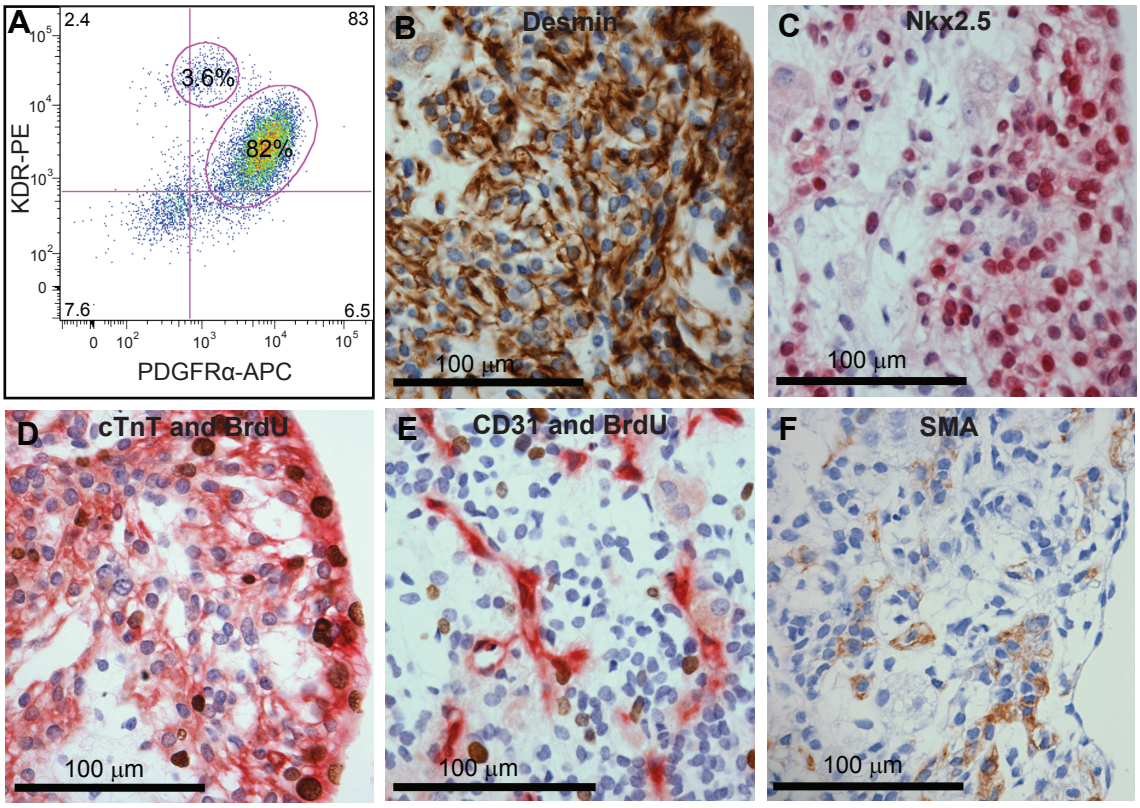

Figure 3.1. Bioengineered cardiovascular progenitor tissue constructs mature into cardiovascular tissue. **A**, Human ES cell-derived cardiovascular progenitors at the KDR+/PDGFRα+ tri-potential stage 5 days post induction of differentiation were introduced into the collagen gel-based scaffold. A minor population of this input population is KDR-high expressing, hemangioblast progenitors. **B**, These progenitors mature over two weeks into contractile cardiac tissue, expressing the myocyte marker desmin, **C**, the cardiac transcription factor Nkx2.5, **D**, the contractile protein cardiac troponin T (cTnT), **E**, the endothelial marker CD31, and **F**, the smooth muscle marker SMA. A proportion of both the cardiomyocyte and endothelial populations continue to proliferate (BrdU, brown).

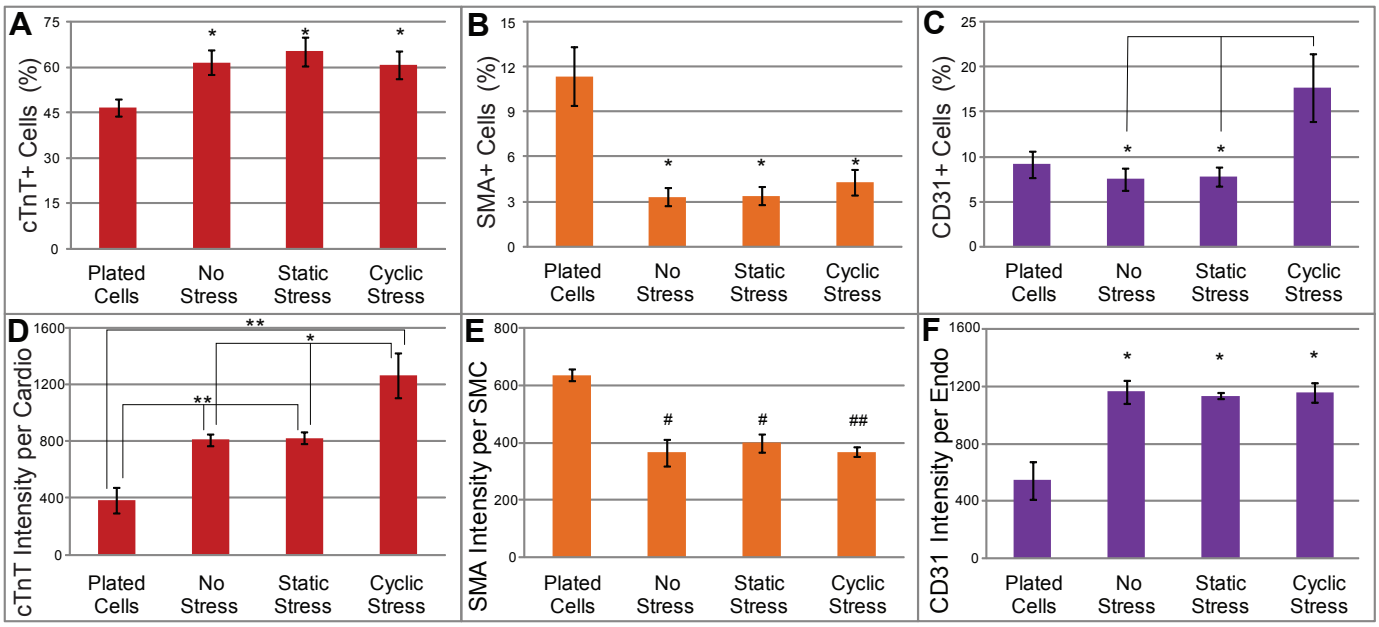

Figure 3.2. Quantification of progenitor fate and maturation by flow cytometry. **A**, Cardiomyocytes differentiate at 34% higher purity in constructs versus 2-dimensional plated culture conditions (62.6% versus 46.6%, respectively). **B**, Smooth muscle cells differentiate at 3-fold lower purity (3.7% versus 11.4% respectively). However, neither static nor cyclic stress conditioning for 2 weeks significantly changes the ratio of differentiation into definitive cardiac or smooth muscle cell types. **C**, However, cyclic stress conditioning did markedly increase endothelial differentiation. **D**, Constructs have significantly higher average cTnT intensity per cTnT+ event than plated cells. Additionally, 2 weeks of cyclic stress conditioning markedly increased cTnT intensity over static or no stress conditioning, indicating an effect on cardiomyocyte maturation due to stress conditioning. **E**, Conversely, plated smooth muscle cells had a 1.7-fold increased SMA intensity over SMA+ cells derived in 3-D engineered tissue, but no increase in smooth muscle maturation with different conditioning regimes. **F**, In contrast, CD31 is down-regulated in plated CD31+ cells versus those grown in 3-D tissue. Error bars represent standard error. * = $p<0.05$; ** = $p<0.01$; # = $p<0.005$; ## = $p<0.001$, with respect to plated unless otherwise specified.

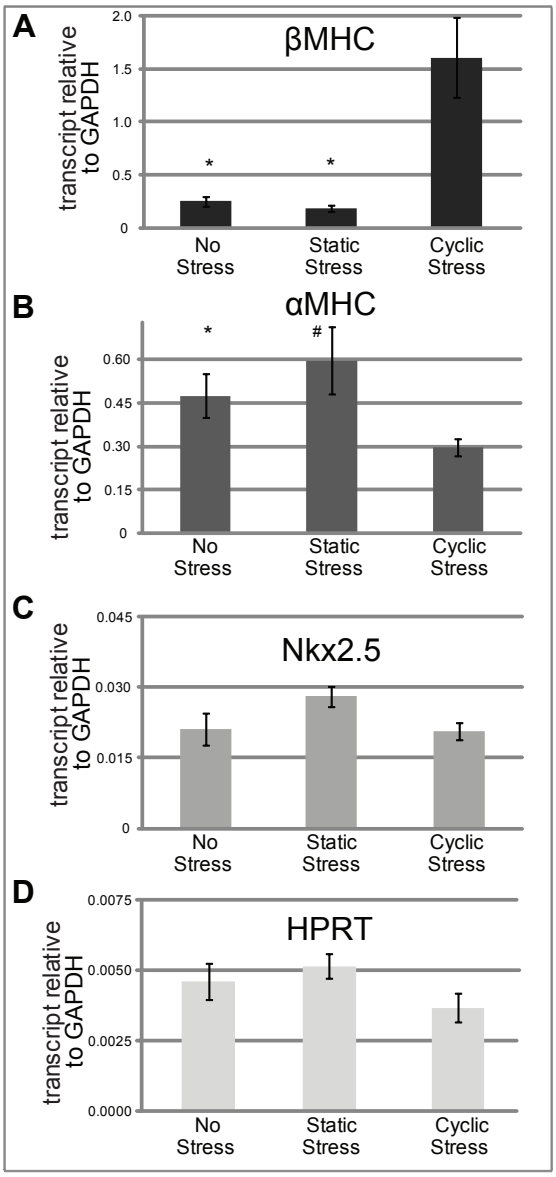

Figure 3.3. Cell maturation and cell fate by quantitative RT-PCR. A, Following 2 weeks of conditioning, whole cardiovascular progenitor construct lysates were analyzed by qPCR. Cyclic stress conditioning very significantly increased the expression of βMHC. **B,** Concurrently, αMHC gene expression significantly decreases with cyclic stress. **C,** Expression of the cardiomyocyte fate marker Nkx2.5 remained unchanged over the different conditioning regimes, indicative of a cardiomyocyte maturation effect rather than a promotion of cardiogenic fate-choice. **D,** Expression of a second normalization control gene, HPRT1, does not change with stress conditioning.

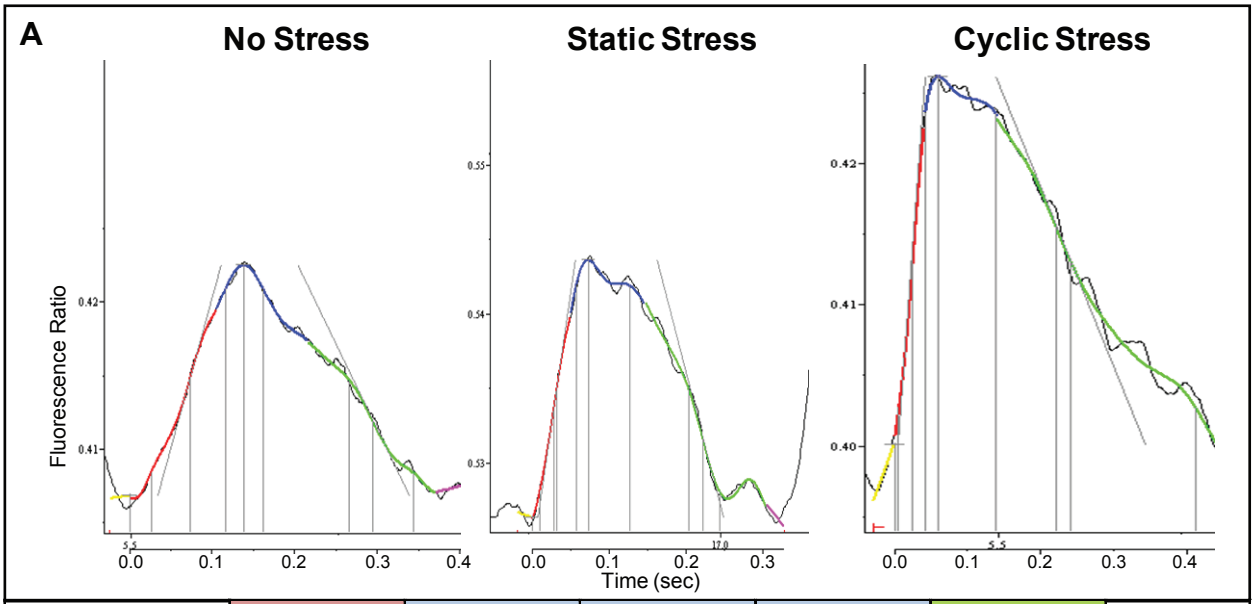

B	dep v	peak t, sec	peak h	bl%peak h	ret v	Rate, Hz
No Stress	**0.38** ±0.04 #	**0.116** ±0.013	**0.018** ±0.002 *	**3.8** ±0.3 *	**-0.21** ±0.01	**1.5** ±0.4
Static Stress	**0.37** ±0.04 #	**0.097** ±0.007	**0.016** ±0.002 *	**3.2** ±0.5 *	**-0.28** ±0.01	**3.1** ±0.4 *
Cyclic Stress	**0.84** ±0.07	**0.127** ±0.017	**0.037** ±0.004	**7.9** ±0.8	**-0.18** ±0.02	**1.0** ±0.1

* = significant difference to CS with $p < 0.005$

\# = significant difference to CS with $p < 0.0005$

Figure 3.4. Calcium transient maturation of cyclic stress-conditioned engineered tissue. A, Representative calcium transients from engineered human cardiovascular tissue conditioned with two weeks of no stress, static stress, or cyclic stress conditioning. Colors correspond to regions of interest parameterized in B. **B,** Maximum rate of calcium signal increase (departing velocity, dep v) was over 2-fold increased in cyclic stress-conditioned constructs compared to no stress or static stress-conditioned constructs. Similarly, the amplitude of the calcium transient (peak h) increased in the cyclic stress-conditioned constructs by greater than 2-fold. When adjusted for potential differences in baseline calcium intensity (bl%peak h), cyclic stress-conditioned peak height remained over 2-fold greater. Time to peak (peak t) was not significantly different between the groups, indicating that the differences in departing velocity and calcium transient height are due to increased calcium flux occurring over the same depolarization time-frame. Return velocity and contraction rate was not significantly different between cyclic stress and no stress groups, but was moderately faster in the static stress group. Spontaneous contraction rate was closely tied to the cyclic stress conditioning rate of 1Hz in the cyclic stress group, but more variable in the unpaced groups. Values are shown as average ± SEM.

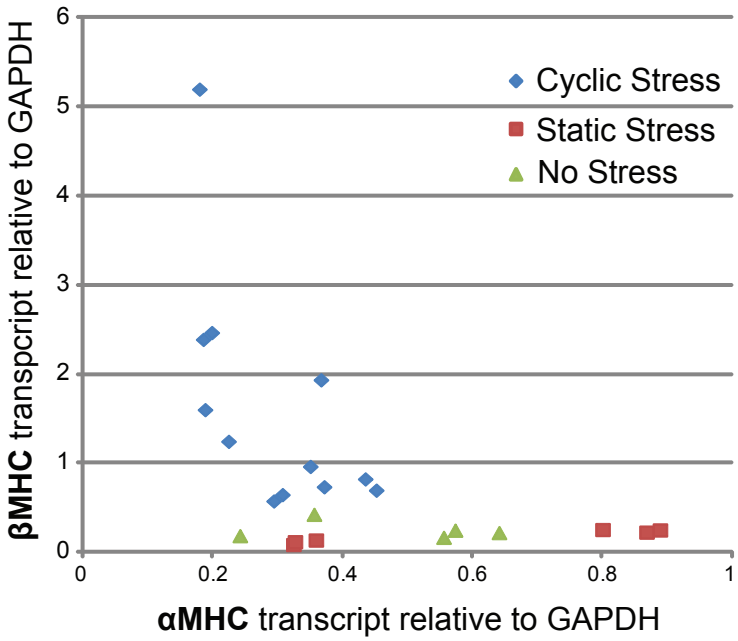

Figure 3.5. Negative relationship between αMHC and βMHC expression. αMHC transcript levels were graphed against βMHC transcript levels, on a per-construct basis. There is a noticeable inverse correlation between αMHC and βMHC expression within the conditioned human cardiovascular tissue constructs.

Chapter 4: Cardiovascular Potential of Skin-Derived iPS Cells

Summary

The reprogramming of adult cells to a pluripotent state resembling embryonic stem (ES) cells is one of the most exciting advances in stem cell biology in the last decade. These induced pluripotent stem cells (iPS cells) offer the potential for autologous regenerative therapies, new models to understand disease, and systems for drug discovery. Little is known, however, about the ability of iPS cells to generate cell types of relevance to the cardiovascular system. Two recent papers[92, 93] indicate that cardiomyocytes, smooth muscle cells and multiple types of endothelium can be derived from mouse iPS cells, encouraging efforts toward developing patient-matched cells for cardiovascular disorders.

Creating Pluripotent Non-ES Cells

The cloning of Dolly the sheep [94] involved reprogramming of an udder cell to a totipotent state by fusion with an enucleated sheep oocyte. While this breakthrough demonstrated that all mammalian tissues could arise from a single differentiated nucleus, the factors required remained enigmatic. The mechanistic breakthrough came when Yamanaka's group[95] over-expressed a battery of candidate genes in mouse dermal fibroblasts and then grew the cells under conditions favoring expansion of ES cells. They found that ES-like cells emerged, and they systematically winnowed the required list down to four transcription factors: oct4, sox2, c-myc and klf4 (Figure 4.1). Oct4 and sox2 are part of the core transcriptional network required for pluripotency. C-myc is a proto-oncogene required for cell cycle progression. Klf4 is a cell cycle regulator that may control self-renewal of ES cells and block apoptotic pathways induced by c-myc. Recently, reprogramming of human dermal fibroblasts was achieved with the same four factors [27, 96] or with a slightly different cocktail of oct4, sox2, nanog and lin28.[80] Fortuitously, retrovirally expressed genes are typically silenced in pluripotent cells, meaning, once established, pluripotency is maintained by endogenous genes subject to normal regulation after differentiation.

Mouse iPS cells generate teratomas (tumors comprised of ectoderm, mesoderm and endoderm derivatives) when injected into adult mice and form chimeric mice after blastocyst injection.[27, 80, 95] The chimeras transmitted the iPS genome to offspring, indicating germline transmission. These properties

indicate that mouse iPS cells are as potent as ES cells. Human iPS cells similarly generate teratomas after transplantation, and differentiation to neural progenitors and cardiomyocytes [27] suggest human iPS cells may be as potent as their mouse counterparts.

Although iPS cells can generate all mammalian cell types, many intriguing questions remain. For instance, are the yields for generating the cells of interest from iPS cells comparable to that of ES cells? Can different cardiovascular cell subtypes be generated? Are the cells generated from iPS and ES cells functionally equivalent? Do the different iPS lines have distinct differentiation properties? The two iPS cell articles[92, 93] critically reviewed in this chapter characterize more comprehensively the cardiovascular differentiation capabilities of independently derived iPS lines with respect to ES cells.

Generation of IPS Cell-Derived Cardiovascular Cells

Both of these groups use iPS cells generated with the original 4-factor cocktail including c-myc. While Mauritz et al. used a single line of iPS cells selected using the oct4 promoter, [92] Narazaki et al. utilized 3 independent iPS cell lines selected by the nanog promoter (Figure 4.1).[93] The differentiation protocols also differ between the two groups. Mauritz' group induced differentiation by forming 3-dimensional aggregates (embryoid bodies; EBs) and treating the cells with serum.[92] Narazaki et al. differentiated in monolayer using serum and selected by FACS for mesodermal cells expressing the VEGF receptor, flk1.[93] They then obtained endothelial and mural cells by the addition of VEGF plus serum and cardiomyocytes by coculture with OP9 cells.

The results of the two studies disagree slightly regarding several aspects of differentiation. Mauritz et al. report delayed iPS cell-cardiomyocyte differentiation in comparison to ES cells, measured both by percentage of spontaneously contracting EBs and by expression of cardiomyocyte-specific mRNA for troponin (3-5 fold lower in iPS cell-derived EBs).[92] In this regard it is important to note that their line of ES cells showed unusually efficient differentiation into cardiomyocytes (100% of EBs beating by day 8), while cardiogenesis in iPS cells was comparable to published reports with other ES cell lines.[97] Along these lines, Narazaki and colleagues found that cardiac differentiation of iPS cells was within the range of the different lines of ES cells they studied, both in terms of beating activity and cardiac gene expression.[93] Given that cardiac differentiation efficiency and yield varies significantly between ES cell

lines, it seems reasonable to conclude that cardiogenesis from mouse iPS cells is in the same ballpark as mouse ES cells. It would be interesting to systematically evaluate various iPS cell lines to assess their variability in differentiation.

Both groups found that iPS cell-derived cardiomyocytes are structurally and functionally similar to ES cell-derived cardiomyocytes. IPS cell-derived cardiomyocytes exhibit regular sarcomeric organization and express myocyte markers including troponin T, connexin 43, sarcomeric α-actinin and titin. Furthermore, both groups show that these cells spontaneous beat at frequencies similar to cardiomyocytes derived from ES cells. Mauritz et al. performed additional characterization of the functional properties of iPS cell-derived cardiomyocytes.[92] They found synchronous calcium transients among groups of cells, indicating electrical connection through gap junctions, and calcium release following caffeine treatment suggested similar stores of calcium in the sarcoplasmic reticulum for both cell types. Furthermore, beating rates in iPS cell-derived cardiomyocytes increased with isoproterenol and decreased with carbachol, indicating functional beta-adrenergic and muscarinic signaling pathways.

Narazaki and colleagues also demonstrate iPS cell differentiation into several other mesodermal derivatives.[93] They show that flk1+ cells from iPS cells can be induced along vascular lineages with VEGF, expressing either endothelial markers CD31 and VE-cadherin or smooth muscle markers α-actin, SM22α and calponin. These cells formed tube structures in 3-dimensional gels of type I collagen. While the endothelium induced by VEGF exhibited a venous phenotype, they further showed that differentiation with VEGF and a cAMP analogue could induce expression of arterial markers such as CXCR4 and ephrinB2. This group also demonstrated that iPS cell-derived flk1+ progenitors differentiate in co-culture with the OP9 stromal line into cells expressing lymphatic markers LYVE-1 and prox1 or the hematopoietic marker CD45. These results suggest iPS cells are comparable to ES cells in their vascular, lymphatic, and hematopoietic potential.

These studies are complemented by a study from Schenke-Layland et al.,[98] whose paper was published electronically after these two manuscripts were accepted. Schenke-Layland compared mouse ES and iPS cells for their ability to differentiate into cardiovascular cells. Using EB differentiation or isolated flk1+ cells grown on collagen IV or with OP9 cells, they found that induction of cardiomyocytes, smooth muscle and endothelial cells occurred at comparable efficiency in ES cells and iPS cells.

Limitations and Improvements

The reprogramming of adult cells to ES cell-like pluripotent states provides far-reaching possibilities. However, multiple issues have to be addressed before this technology can be utilized in patients. Perhaps most pressing is the need to develop techniques to generate iPS cells without integrating viruses, thereby lowering the risk of malignant transformation. Furthermore, silencing of virally encoded genes in iPS cells is not always complete. C-myc-expressing tumors develop in 15-20% of iPS cell-derived chimeric mice and their offspring.[99, 100] Along these lines, Narasaki and colleagues found incomplete silencing of klf4 and c-myc as late as two months after differentiation.[93] Recent progress indicates that c-myc is not essential for iPS cell generation[99] and that iPS cells can be selected based on morphology rather than using virally encoded antibiotic resistance genes.[101] This eliminates 2 of the 5 transgenes from the original system, and the absence of c-myc markedly reduced tumor incidence in iPS cell-derived mice.[99] Work is underway in multiple laboratories to identify alternate reprogramming techniques such as cell-permeant protein reagents, non-integrating viruses and small molecules. In the meantime it is essential that investigators using iPS cells screen for expression of the virally encoded reprogramming factors.

It is important to assess how fully pluripotent cells differentiate because residual undifferentiated pluripotent cells could form teratomas.[102] In this regard, Mauritz and colleagues show incomplete down-regulation of endogenous pluripotency markers oct4 and nanog in iPS cell EBs.[92] The sustained expression of these transcripts might be intrinsic to the cell lines used in this study. Alternatively, the heterogeneous nature of EB differentiation might result in slower differentiation (although silencing of oct4 is commonly seen in EB differentiation systems[103]). In contrast, the guided approach utilized by Narazaki et al. resulted in a progenitor population in which neither nanog nor oct4 were significantly expressed after four days of differentiation.[93] Thus, iPS cells intended for therapeutic purposes should be screened for their ability to appropriately down-regulate endogenous pluripotency factors. We think that directing differentiation toward the desired cell type maximizes yield and reduces chances of tumor formation. In this regard, use of undefined components such as serum and cell co-cultures to guide differentiation can be a roadblock to therapy. Optimized methods with fully defined components are needed for eventual use in patients.

Future Applications: Cell Therapy, Disease Models and Drug Screens

The feasibility of ES cell-derived therapies has been already demonstrated in animal models. Engraftment of human ES cell-derived cardiomyocytes in the infarcted hearts of immuno-compromised rats[20, 104] or mice[22, 105] attenuates ventricular dilation and improves contractile function. Additionally, human ES cells have been differentiated into pancreatic islet cells,[106] oligodendrocyte precursors,[107] and dopaminergic neurons[108] and shown to benefit function in models of diabetes, spinal cord injury and Parkinson disease, respectively.

The potential for iPS cell-derived therapies was recently demonstrated in murine sickle cell anemia.[109] IPS cells were generated from humanized sickle cell mouse fibroblasts with the original 4-factor reprogramming cocktail. Next, c-myc was removed by a cre-lox system to prevent its reactivation and the sickle beta-hemoglobin allele was repaired by homologous recombination. Finally, the modified iPS cells were differentiated into hematopoietic cells and transplanted into irradiated sickle cell mice to correct the disease. After the limitations mentioned earlier have been addressed, it is fairly straightforward to see how this process could be translated into a human therapy (Figure 4.2A). Even though many human applications would not require the step of repairing a genetic defect, with our current understanding the process still would be complicated, time consuming and expensive. (Note that this is true to a lesser extent for most autologous cell therapies requiring *in vitro* expansion.) Thus, therapies with patient-specific iPS cells may not be widely available for quite some time and may never be available in an acute setting. By analogy to bone marrow banking, it may be more feasible to bank iPS lines that match the population's HLA diversity, offering cell therapies for off the shelf use (Figure 4.2B).

Beyond cell replacement therapy, iPS cells may prove useful for understanding disease pathogenesis and treatment. For example, it should be possible to obtain iPS cells from patients with familial cardiomyopathy and generate cardiomyocytes that perfectly match the patient's genetics. The diseased cardiomyocytes could be studied to better understand the pathophysiology, thereby improving genotype-phenotype correlations. In addition, the ability to grow large numbers of patient-specific human cardiomyocytes may facilitate high throughput screening of small molecules for drug development. Similar

strategies could be performed for other genetically based diseases, e.g. neurodegenerative diseases, storage diseases, metabolic disorders etc.

Conclusions

Despite some variability from line to line, these two studies demonstrate that murine iPS cells are able to differentiate into cardiomyocytes and other vascular cells with comparable ease to murine ES cells.[92, 93] Furthermore, ES and iPS cell-derived cardiomyocytes have similar functional properties. Although there are limitations in current reprogramming techniques, iPS cells provide exciting possibilities for clinically applicable cellular therapies, disease research and drug discovery.

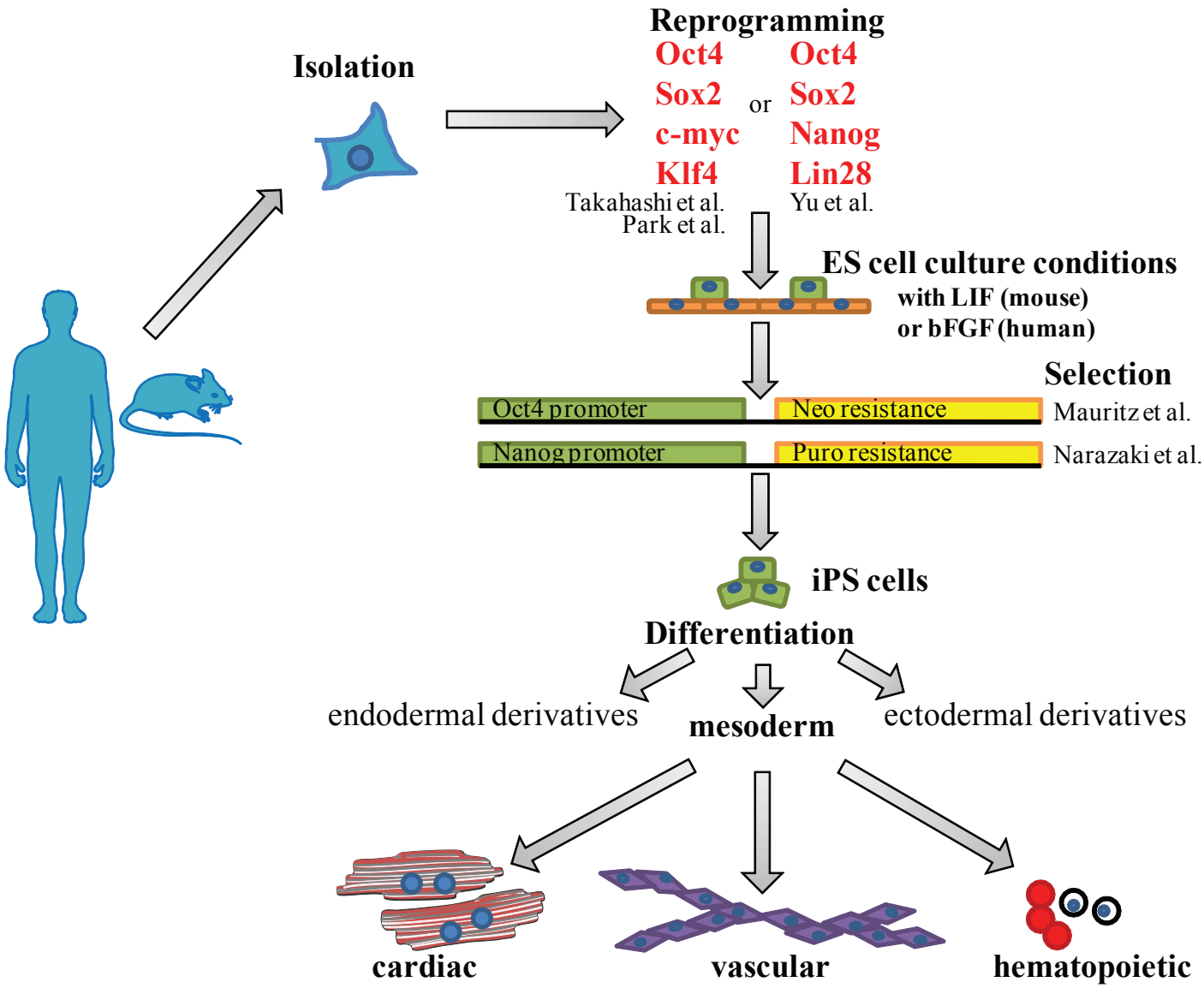

Figure 4.1. Generation of iPS cells. Mouse or human somatic cells (e.g. dermal fibroblasts) are isolated and reprogrammed with viral constructs encoding 4 transcription factors found in ES cells. These cells are grown in ES cell culture conditions (on a MEF feeder layer supplemented with LIF for mouse or basic FGF for human) and selected with an antibiotic resistance gene driven by the endogenous oct4 or nanog promoter. IPS cells grow clonally and can be differentiated into tissues from all three germ layers. The studies reviewed in this chapter focus on mesodermal derivatives including cardiac, vascular, and hematopoietic cells.

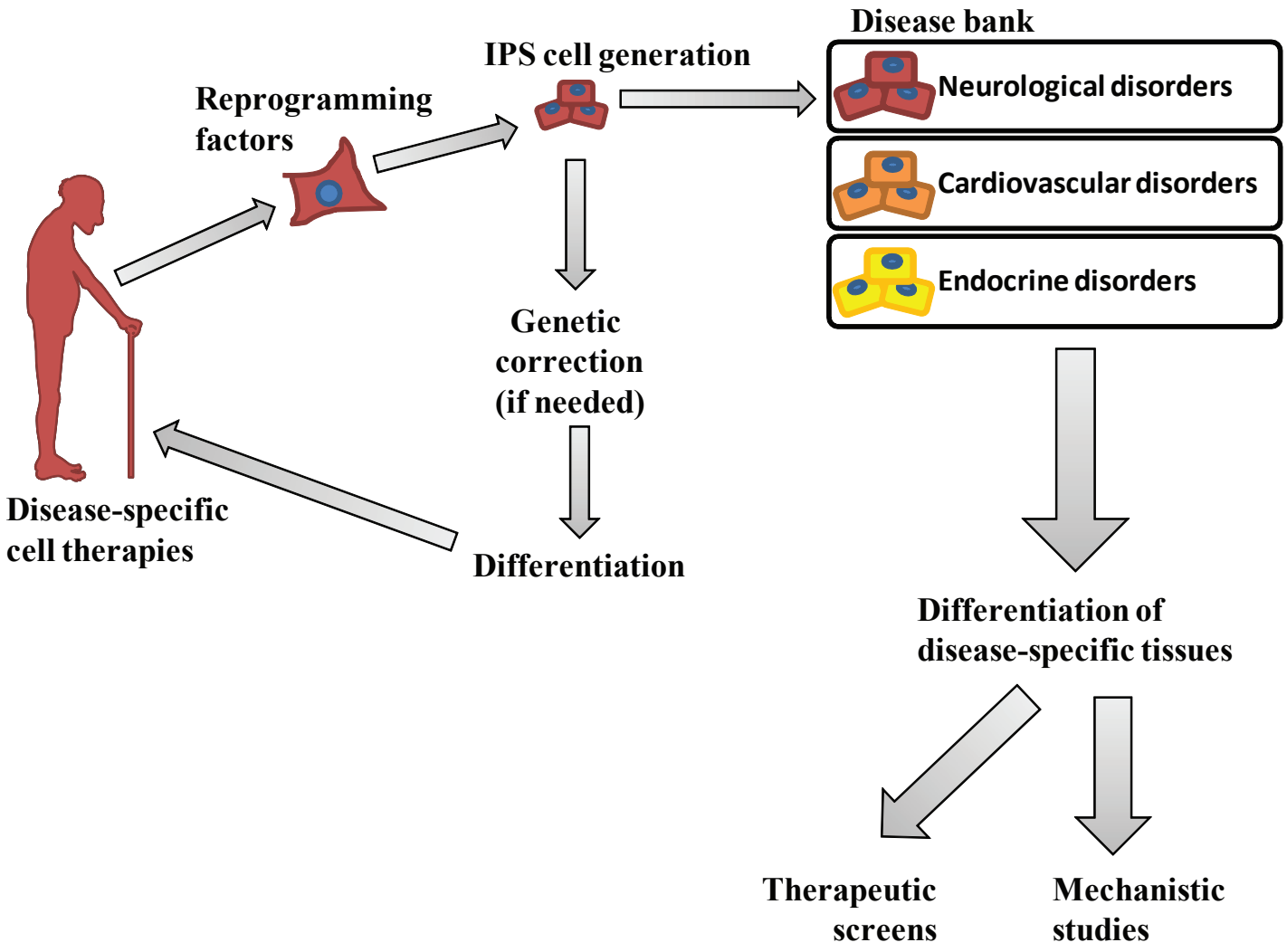

Figure 4.2. Uses of disease-specific iPS cells. IPS cells can be generated from patients, subjected to genetic correction (if necessary) via in vitro homologous recombination and selection, and differentiated into cells and tissues for autologous therapeutic use. Additionally, these same cell lines can be differentiated and used for therapeutic screens of small molecules as well as for basic mechanistic studies of disease pathologenesis.

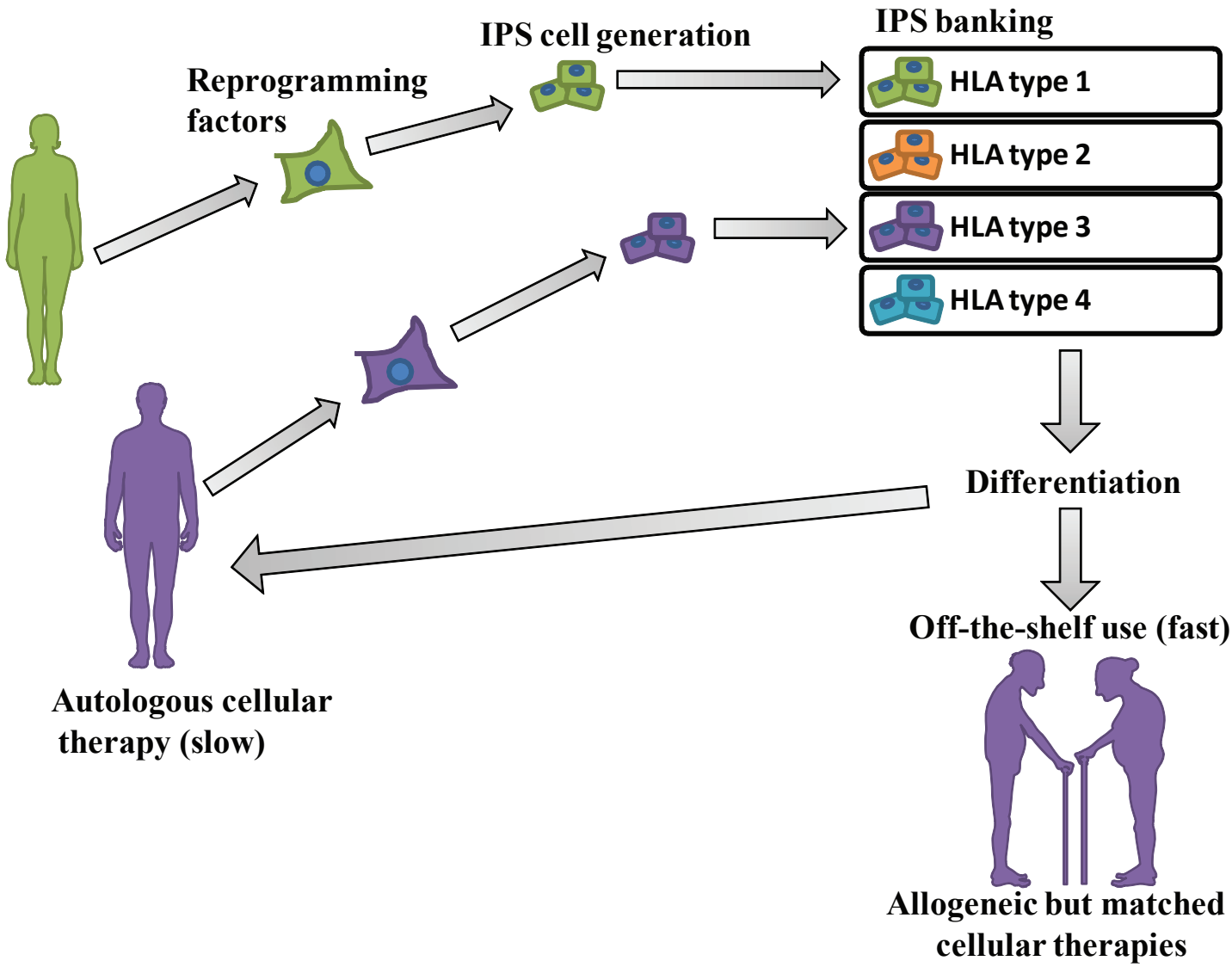

Figure 4.3. IPS cell banking for standard therapies. IPS cells can be generated from people who collectively HLA-match a large portion of the population. These cells can be banked and differentiated for off-the-shelf use, providing allogeneic but HLA-matched cellular therapies much more quickly than therapies from autologous iPS cells generated on a case-by-case basis.

Chapter 5: Mechanical Stress Conditioning Promotes Contractility and Force Development of IPS Cell-Derived Human Cardiac Tissue

Summary

Human induced pluripotent stem cells (iPS cells) can generate cardiomyocytes, but to model adult diseases or repair the heart it will be necessary for them to mature physiologically. Using engineered iPS cell-derived human myocardium, we sought to build a bioengineering toolbox to develop and study more clinically relevant cardiac tissue and then assess its functional maturation in response to mechanical conditioning. We optimized human iPS cell differentiation procedures to yield large scale cardiomyocyte preparations of >50% purity without additional enrichment steps and then generated bioengineered human cardiac tissue via collagen-based scaffolding techniques. This engineered human myocardium exhibits Frank-Starling curve-type force-length relationships, an essential feature of native myocardium. After 2 weeks of static stress conditioning, the engineered myocardium demonstrates a 2.5-fold increase in slope of the force-length relationship and a 2-fold increase in the departing velocity of the calcium transient. Furthermore, stress conditioning increases the stiffness of engineered myocardium 2-fold, yielding passive mechanics more similar to native myocardium. These studies demonstrate 1) that human cardiomyocytes can be generated from iPS cells at high purity using a monolayer-based directed differentiation protocol, 2) that iPS cell-derived human cardiac tissue is functionally contractile and demonstrates characteristic tissue-level responses such as the Frank-Starling mechanism, and 3) that this tissue is highly responsive to static stress conditioning, showing substantial maturation of active force production, calcium transient dynamics, and tissue compliance.

Introduction

The goal of replicating functional human myocardium *in vitro* has been an aim of science and medicine at least since the first heart transplant was performed in 1967. While the target of recreating a heart *in vitro* remains elusive, large strides have been made towards creating contractile human cardiomyocytes and building 3-dimensional tissues that may eventually form the basis for whole organ development. Several tissue engineering approaches have recently shown promise, using scaffold free

systems,[11, 12] engineered synthetic scaffolds,[1-3] natural non-protein scaffolds,[4] and natural protein polymers such as fibrin[5-7] and collagen I,[8-10, 86] the latter of which makes up a majority of the matrix of the native myocardium.

A major complication until recently has been a lack of suitable human cardiomyocytes for study, and much early important work was done with the P19 mouse embryonal carcinoma cell line,[110, 111] mouse ES cell-derived cardiomyocytes,[6, 13] and rat neonatal cardiomyocytes.[3, 8-10, 86, 112] Our own previous work demonstrates that lessons for creating organized rodent myocardium with rat neonatal cardiomyocytes do translate to some extent for engineering human tissue,[86] but in general the applicability of studies in these models to understanding how conditional cues direct development of human cardiac tissue is limited, because human hearts take much longer to develop, grow much larger, and beat much slower.

The publication of several protocols for the efficient differentiation of human embryonic stem cells (hES cells) into cardiomyocytes[20, 22, 24] has now made possible the direct study of human cardiomyocyte development and, importantly, attempts to engineer organized human cardiac tissue. A further recent breakthrough in stem cell biology has now made possible the reprogramming of adult, terminally differentiated cells into induced pluripotent stem cells (iPS cells),[27, 80, 96] with attributes similar to ES cells, including a highly unrestricted differentiation potential. This novel type of pluripotent stem cell has been used to generate cells of the different germ layers, including into neuronal[27, 113] and cardiac derivatives.[27, 37] Proving their differentiation versatility, mouse iPS cells have been used to generate chimeric whole animals.[114] This opens yet another window of opportunity for the creation of functional human myocardium through the application and translation of the techniques already defined for high yield cardiac differentiation from human ES cells directly to human iPS cells. Additionally, iPS cells can be derived from patients with genetic diseases such as familial hypertrophic cardiomyopathy and provide a system for disease modeling *in vitro*. In standard culture conditions, however, these stem cell-derived cardiomyocytes remain at an immature stage resembling early fetal cells. In order to functionally repair the heart or to model adult-onset diseases with fidelity, it will be important to mature them toward an adult phenotype.

In this study we used a published and widely available line of human iPS cells derived from lung fibroblasts[80] and generated contractile cardiomyoctyes at high yield and purity. We used these cells to create engineered cardiac tissue by casting them in hydrogels of type I collagen and employed static mechanical stress as a conditioning tool. We report that mechanical conditioning promotes maturation of contractility, calcium transients, and passive mechanical properties.

Results

Generation of Human Cardiac Tissue Using IPS Cell-Derived Cardiomyocytes

In order to generate the large numbers of iPS cell-derived cardiomyocytes required for these experiments, we modified the published directed differentiation procedure previously adapted for cardiomyocyte production from hES cells.[20, 86] With some adjustments, we were able to achieve runs of cardiomyocyte differentiation that were up to 70% pure for cells expressing the contractile protein cardiac troponin T (cTnT) by flow cytometric analysis (Figure 5.1A), without having to resort to post-differentiation enrichment methods such as the use of suspension culture,[81] Percoll gradient centrifugation,[20] or manual dissection.[2] The main modifications necessary for generating a high yield of cardiomyocytes from this iPS cell line were a more continued maintenance of iPS cells directly on MEFs (cells were maintained in feeder-free conditions for only 2-4 passages before differentiation) and the removal of insulin from the differentiation medium. These resulting cells displayed widespread filamentous actin networks, nuclear expression of the cardiomyocyte transcription factor Nkx2.5, and robust sarcomeric organization visualized by α-actinin immunostaining (Figure 5.1). Cardiomyocyte preparations were used for generation of cardiac constructs between day 15 and day 25 from onset of differentiation, and at the time of construct generation, moved into medium containing insulin. Cardiac tissue constructs were created using a collagen-based scaffold as described previously[8, 86] using iPS cell-derived cardiomyocytes. After 2 weeks of growth and remodeling under static stress conditions, these constructs demonstrated cardiomyocyte density and myofibrillar alignment by α-actinin immunostaining (Figure 5.2) that are qualitatively similar to human fetal heart tissue.

Stress Conditioning Modulates Stiffness of Human Heart Tissue

We measured passive force from human cardiac constructs conditioned for two weeks of static stress, or no-stress controls, by using a series of short increasing length steps and simultaneously recording tension. From the initial slack length, 4% stretches were taken to a final length of 125% initial length. Passive force (preload) recorded 15 seconds after each stretch was normalized to cross-sectional area and graphed against change in length (Figure 5.3A) to determine the Young's Modulus. The passive force increased over this length range with linear R^2 values of 0.94, 0.92, and 0.88, respectively, for cardiac constructs subjected to static stress conditioning, constructs with no stress conditioning, and collagen-only (cell-free) scaffolds (n=12-17). The Young's Modulus of static stress-conditioned constructs was almost 2-fold increased over no stress-conditioned constructs (0.78kPa and 0.40kPa, respectively; $p<0.005$, Figure 5.3B). Additionally, both static and no stress-conditioned constructs were markedly stiffer than collagen-only (cell-free) constructs (0.20kPa; $p<0.005$), indicating that cardiomyocytes increase the stiffness of engineered tissue scaffolds and that stress conditioning increases this effect.

Contractility of Human Cardiac Tissue Constructs

We examined active twitch force recorded over the same lengthening stretch routine (Figure 5.4A). As can be observed in the force trace illustrated in Figure 5.4B, active twitch force transients, undistinguishable at slack length, appeared and increased in amplitude over a series of 4% lengthening stretches, in accordance with the Frank-Starling mechanism. These spontaneous twitch force transients disappear upon incubation with 2,3-butanedione monoxime (BDM, 30 mM), a reversible inhibitor of actin-myosin interaction (Figures 5.4C, D) but reappear upon washout (Figure 5.4E). In contrast, incubation with the β-adrenergic agonist isoproterenol markedly increased the rate of spontaneous contractions.

Stress Conditioning Increases Starling Effect in Human Engineered Cardiac Tissue

Starling curves were generated by plotting the amplitude of twitch force, normalized to cross-sectional area, versus length increase. This yielded a positive linear relationship with R^2 values of 0.81 and 0.92 for static stress and no stress conditioning, respectively (Figure 5.5). A comparison of the slopes of the conditioned vs. the control constructs shows the effects of mechanical conditioning on contractility.

Interestingly, 2 weeks of static stress conditioning increased active twitch force slope by 2.5-fold over no stress conditioning (active force slope values of 0.38 mN/mm^2 and 0.15 mN/mm^2, respectively; $p<0.0001$).

We also assessed the integrity of the construct over multiple stretch routines (Tables 5.1 and 5.2). Subsequent stretches up to 25% of length increase did not decrease the slope of active force amplitude (Static Stress 1st stretch 0.388 mN/mm^2, 2nd stretch 0.390 mN/mm^2, p=0.96; No Stress 1st stretch 0.1400 mN/mm^2, 2nd stretch 0.1400 mN/mm^2, p=1.00) or the Young's Modulus (Static Stress 1st stretch 0.755 kPa, 2nd stretch 1.18 kPa, p=0.96; No Stress 1st stretch 0.4200 kPa, 2nd stretch 0.4467 kPa, p=0.075). Although BDM completely eliminated active force (Figure 5.4D), it had little or no effect on passive stiffness (0.58 kPa to 0.50 kPa in the subsequent stretch with BDM, p=0.38), indicating that acto-myosin interaction is not a major component of passive stiffness in cardiac tissue constructs with cells, despite stiffnesses 2- to 4-fold higher than collagen-only scaffolds without cells (see above and Figure 5.3).

Calcium Handling Dynamics of Bioengineered Cardiac Tissue

We hypothesized that mechanical conditioning would promote maturation of excitation-contraction coupling. To assess Ca^{2+} dynamics, we used a ratiometric calcium fluorophore to visualize calcium transients in the bioengineered cardiac tissue (Figure 5.6A). We quantified the characteristics of spontaneous and induced transients from constructs subjected to 2 weeks of static stress conditioning or no stress conditioning (Figure 5.6B). Maximum rate of Ca^{2+} signal increase (departing velocity) was over 2-fold increased in stress-conditioned constructs compared to unstressed constructs, and this relationship held true for both spontaneous transients ($p < 0.009$) and transients elicited at 0.5 Hz pacing ($p < 0.002$). Time to peak was moderately but not significantly shorter in the static stress conditioned constructs, although time to 50% peak and 90% peak was significantly shorter (data not shown). Peak height and return velocity, however, were not substantially different between the two groups, indicating that rate of calcium release was the main adaptation to stress conditioning.

Discussion

In this study, we derived human cardiac tissue from iPS cells and demonstrated increased force development and contractility of this bioengineered tissue when subjected to 2 weeks of stress conditioning. Furthermore, these experiments demonstrated that the presence of cardiomyocytes markedly increased engineered tissue stiffness, and that stress conditioning potentiates this effect. Although active twitch force in human cardiac tissue constructs has recently been observed by our group and one other,[7, 86] to our knowledge this is the first work that shows force measurements in iPS cell-derived human cardiac tissue. Furthermore, it is the first demonstration that any type of *in vitro* conditioning is able to mature the active and passive force dynamics of the tissue.

Optimization of Cardiac Differentiation

The types of bioengineering experiments described here require the derivation of human cardiomyocytes efficiently and with high purity. Thus as a first step in the process, we screened a number of human iPS cell lines to assess their cardiac differentiation efficiency. The application of our standard, published monolayer cardiac differentiation protocol which works well for H7 hES cells[20, 22] did not directly result in high yield differentiation of cardiomyocytes for the iPS cell lines tested. Our attempts included lines generated with the Yamanaka 4-factor reprogramming cocktail[27] (OCT4, SOX2, C-MYC, and KLF4) as well as with the Thomson cocktail (OCT4, SOX2, NANOG and LIN28) used to generate IMR90 iPS cells,[80] indicating that the specific cocktail or the presence or absence of c-myc in the generation of the original iPS cell line does not correlate with relative tractability for cardiac differentiation. This should not be interpreted to mean that iPS cell lines are intrinsically more difficult to differentiate than ES cell lines, however. Indeed, we and others have observed that individual mouse and human lines require line-specific protocol optimization for efficient production of mesodermal progenitors and cardiomyocytes through an analogous differentiation protocol.[87] This suggests that there is a fair bit of latitude in our current definitions of “pluripotency”, such that the conditions of initial isolation or subsequent propagation may yield cells at earlier or later stages of development, and consequently, different requirements for directed differentiation. In any case, 2 specific modifications to the directed differentiation protocol drastically increased the yield of human cardiomyocytes from the IMR90 iPS cell line. First, standard

maintenance on Matrigel in MEF-conditioned medium supplemented with basic FGF, sufficient for high yield (50-80%) differentiation from the H7 hES cell line, was not sufficient for differentiation with these iPS cells. In fact, when iPS cells were more than 4 passages removed from direct growth on a MEF feeder layer, their cardiomyocyte differentiation was minimal. The second change was based on work from the Mummery lab, which showed that the presence of insulin inhibited cardiac differentiation.[115, 116] In our hands, directed differentiation conducted in the absence of insulin produced substantially more cardiomyocytes from IMR90-iPS cells compared to medium with standard insulin levels. Spontaneously contracting cardiomyocytes were observed beginning day 8 to day 12 from the onset of differentiation (2-3 days earlier than is standard for the H7 hES cell line). Cardiomyocyte preparations were used for generation of cardiac constructs between day 15 and day 25 from onset of differentiation and, at the time of construct generation, moved into RPMI medium made with standard B27 supplement containing insulin; from this point on culture and conditioning was conducted as previously described[86] without further modification. Based on work in the neuroretinal literature[117] we speculate that exposure to insulin induces ectoderm differentiation of pluripotent IMR90 iPS cells, rather than the mesoderm differentiation required for cardiogenesis.

Matrix Remodeling by Resident Cells is Potentiated by Conditioning

The engineered human cardiac tissue generated through this process is microscopically similar to early stage human fetal heart tissue (Figure 5.2), and it also resembles hES cell-derived cardiac constructs produced by our group.[86] We measured the stiffness of the cardiac tissue constructs and found them to be markedly stiffer than the cell-free collagen scaffold itself (Figure 5.3). Furthermore, 2 weeks of mechanical stress conditioning potentiated this effect, increasing the stiffness by another factor of 2. We used BDM, a small molecule that binds to myosin and reversibly inhibits the interaction between the thick and thin filaments of the contractile apparatus itself, to examine any potential contribution of acto-myosin cross-bridges to construct stiffness. Although BDM completely eliminated active twitch force (Figure 5.4C, 4D), it had little to no effect on stiffness (Table 5.1), eliminating the possibility that acto-myosin interaction is a major component of increased stiffness observed in cardiac tissue constructs with cells. Therefore we conclude that the difference in stiffness between constructs with and without cells (and with and without

stress conditioning) is likely due to cardiomyocyte remodeling of the matrix itself, although a role for titin or other intracellular proteins cannot be ruled out completely.

This hypothesis is in agreement with our previous results using human ES cell-derived cardiac tissue constructs and rat neonatal cardiomyocyte-derived constructs with collagen birefringence visualization by circularly polarized light microscopy. In those studies, we found that organized collagen fiber bundles were markedly more apparent in the engineered cardiac tissue than in collagen cell-free scaffold and, furthermore, that stress conditioning significantly increased collagen fiber alignment of the matrix itself.[86]

Maturation of Twitch Force and Calcium Transient Dynamics

We also observed spontaneous active force production in this engineered tissue, with twitch force transients increasing in magnitude in tandem with length increases (Figure 5.4) in accordance with the Frank-Starling mechanism. We have demonstrated similar results anecdotally in human ES cell-derived tissue,[86] but in this current study, we verified this effect in human iPS cell-derived bioengineered cardiac tissue and, further, demonstrated that force production of the engineered tissue matures with 2 weeks of static stress conditioning. In fact, contractility, as measured by average slope of twitch force over the change in length, was increased 2.5-fold in the stress-conditioned group compared to the no stress-conditioned constructs. Our previous study demonstrated that mechanical stress conditioning stimulated cardiomyocyte alignment and hypertrophy in association with increased transcription of the genes encoding β-myosin heavy chain (MYH7) and cardiac troponin T (TNNT2).[86] These adaptations may in part underlie the enhanced contractile performance observed in the current study.

This increase in active force production was paired with an improved calcium transient profile in stress-conditioned constructs, as recorded in this engineered cardiac tissue in both spontaneous and stimulated transients using a ratiometric calcium fluorophore. Static stress-conditioned constructs had a 2-fold higher calcium wave departing velocity compared to no stress-conditioned constructs, indicating a more rapid influx of calcium in response to spontaneous or induced depolarization. Mechanistically, enhanced calcium release could result from increased activity of the L-type calcium channel and/or the

ryanodine receptor. We previously reported that cyclic stress conditioning in iPS cell-derived cardiac tissue increases mRNA expression for the genes encoding these two proteins (CACNA1C and RYR2).[86]

In conclusion, our findings demonstrate 1) that human cardiomyocytes can be generated from iPS cells at high purity using a modified directed differentiation protocol, 2) that iPS cell-derived human cardiac tissue is functionally contractile and demonstrates tissue-level responses such as a steep length-tension relationship that is the basis of the Frank-Starling mechanism, and 3) that static stress conditioning is sufficient to moderately improve maturity of this engineered cardiac tissue along parameters of active force production, calcium transient dynamics, and matrix remodeling. Through these studies, we are beginning to determine relationships between conditional cues and functional responses in the developing human myocardium. The implications of these results are two-fold: we begin to be able to assess and understand maturation in the developing human heart, and we also begin to build a bioengineering toolbox for the development of more clinically relevant tissues. In fact, we now can work towards the complementary objectives of generating even more mature patient-derived iPS cell-based tissue for eventual clinical cardiac therapy and of comparing engineered human cardiac tissue from normal and myopathic iPS cell lines to determine the relationships between calcium handling and force production in, for example, the pathogenesis of human cardiomyopathies.

Materials and Methods

Pluripotent Cell Culture

Undifferentiated human IMR90-iPS cells[80] (James A. Thomson, U. Wisconsin-Madison) were cultured as described previously for maintenance of pluripotency.[25, 79, 86] These cells were routinely passaged with dispase (Invitrogen) on irradiated mouse embryonic fibroblasts (MEFs) on 10cm tissue culture plates (Corning) coated with 0.1% gelatin (Sigma) with 5 ng/mL basic FGF (Stemgent) in standard Human Pluripotent Cell Medium: DMEM/F12 with 20% Knockout Serum Replacer, 1% MEM non-essential amino acids, 1% sodium pyruvate solution, 100 U/mL penicillin G, 100 mg/mL streptomycin, and 120μM β-mercaptoethanol (all Invitrogen).

Cardiac Directed Differentiation

Cardiomyocytes were generated using a modified version of the monolayer-based differentiation protocol described by Laflamme et al.[20] To prepare for differentiation into cardiomyocytes, iPS cells were weaned off of MEFs for 2-4 passages on Matrigel (BD Biosciences) in MEF-conditioned medium with 5 ng/mL basic FGF. In our hands, the differentiation quality diminished markedly with IMR90 cells more than 4 passages removed from MEFs. To set up for differentiation, cells were passaged by release with versene solution (0.5 mM EDTA and 1.1 mM glucose in PBS) and scraping with a cell lifter (Corning), followed by mild trituration with a P1000 pipette to attain a mostly single cell suspension for even replating. Cells were then plated into Matrigel-coated 24-well plates (Corning) at a density of 300,000 cells per well in 1mL of MEF-conditioned medium with 5 ng/mL basic FGF. Medium was changed daily until the plates had attained confluence with a packed in morphology (48-72 hours from plating), at which time differentiation was initiated with 0.5 mL of RPMI medium (Invitrogen) with B27 supplement without insulin (Invitrogen), 100 U/mL penicillin G, 100 mg/mL streptomycin, and 100 ng/mL activin A (R&D Systems). In our hands, directed differentiation conducted in the absence of insulin produces a more pure cardiomyocyte population from IMR90-iPS cells compared to differentiation in medium prepared with the standard B27 supplement. After 24 hours, medium was carefully changed to 1mL of the same medium supplemented with 10 ng/mL BMP4 (R&D Systems) and left for a duration of 4 days. From day 5 of differentiation on, plates were fed every other day with 1mL of the same medium without either activin A or BMP-4. Spontaneously contracting cardiomyocytes were observed beginning day 8 to day 12 from the onset of differentiation. Cardiomyocyte preparations were used for generation of cardiac constructs between day 15 and day 25 from onset of differentiation, and at the time of construct generation, moved into RPMI medium made with standard B27 supplement containing insulin. Preparations contained on average 58±5% (n=6) cardiomyocytes based on cardiac troponin T (cTnT) flow cytometry of the input population at the time of construct generation. This preparation is referred to as “cardiomyocytes” through the remainder of the manuscript.

Generation of Cardiac Constructs

IPS cell-derived cardiomyocytes were encapsulated in a collagen-based 3-dimensional scaffold as previously described.[86] Briefly, cardiac tissue constructs were generated using collagen type I (final concentration 1.25 mg/mL, neutralized with NaOH; Invitrogen), 11% vol/vol mouse basement membrane extract (Geltrex, Invitrogen), and 57% medium mixed together on ice with cells gently added. Bioengineered tissue constructs were cast in a 20 mm by 3 mm by 3 mm trough at a density of 2 million cells per 100µL of gel mixture. These troughs were formed in Tissue Train 6-well plates (Flexcell International Corp.) mounted over Trough Loader posts set in a Bioflex base-plate under vacuum (Flexcell). At opposing ends of each trough, the cell-gel mixture impregnated nylon mesh tabs affixed to the periphery of the well, securing the construct at a fixed length and providing means to transmit uniaxial tension to the construct. After 1 hour at room temperature for matrix solidification, the base-plate vacuum was released and the resulting cardiac tissue constructs were placed into RPMI medium with standard B27 supplement containing insulin. Static stress conditioning was achieved by maintaining constructs at a fixed static length, whereas no stress conditions were achieved with one end of the construct cut free of the nylon tab. Constructs were maintained in a regimen of no stress or static stress conditioning for a period of 2 weeks before analysis.

Flow Cytometry

For analysis of cardiomyocyte input purity, a subset of cells used for construct generation were quantified by flow cytometry for cardiac troponin T (cTnT). Following dispersion, cells were fixed for 10 minutes in cold 4% paraformaldehyde (PF, Sigma) and resuspended in PBS with 5% FBS with 0.75% saponin (Sigma) for staining with cTnT antibody (mouse IgG1, ThermoScientific Clone13-11, 1:100 dilution). Samples were incubated for 30 minutes at room temperature and washed twice with 0.75% saponin in PBS with 5% FBS. The secondary antibody used was goat anti-mouse-IgG-PE (GαM-PE, 1:200 dilution) with a 30 minute room temperature incubation in the dark. Each sample was washed 3 times with PBS with 5% FBS before being re-fixed in 1.3% PF, and analyzed within 7 days on a BD FACS Canto II machine (BD Biosciences). A mouse IgG1 isotype control antibody (eBioscience, 1:100 dilution), in conjunction with the same secondary, was used to gate samples with FlowJo version 9.3.1 software.

Mechanical Measurements

Constructs were carefully dissected into 1 mm-long sections and then suspended on stainless steel hooks attached to a force transducer (Aurora Scientific, model 400A) and a length controller (Aurora Scientific , model 308B). The dimensions of construct tissue tested were 0.94 ± 0.07 mm by 0.57 ± 0.04 mm (L x W). Slack length was determined as the length step before a positive amplitude twitch transient was observed on the force trace (and often a step after one where negative amplitude beating was observed). Force of spontaneously contracting constructs was then continuously monitored as preparation length was changed by adjusting the position of the length controller arm. For non-beating preparations (ex.: collagen only), slack length was set to the length at which a 4% stretch step resulted in an immediate increase in measured passive force. From the initial slack length, 4% stretches were taken at intervals of 30 seconds each to a final length of 125% initial length. Force and length signals were digitally recorded and analyzed using custom LabView software. Passive tension and the amplitude of spontaneous isometric twitch force were measured on 4 transients at 15 seconds after each length step. Force was normalized to cross-sectional area of the preparation, calculated by measuring the diameter at non-strained length and assuming circular cross-sectional geometry. All measurements were acquired in medium at 30°C. For static stress n=14, no stress n=17, collagen only n=12.

Calcium Transient Analysis

Calcium transient traces were collected from cardiac tissue constructs that were spontaneously contracting or stimulated at 0.5 Hz using the ratiometric calcium fluorophore Fura2-AM (Invitrogen) in medium at room temperature under no tension and visualized under low magnification using a 40x objective. Calcium transients were measured in Fura2-loaded cells using IonOptix system video microscopy (IonOptix LLC) as described previously.[90, 91] Fura-2 fluorescence was measured with an IonOptix spectrophotometer (Stepper Switch) which was attached to a fluorescence microscope. Emitted Fura2 fluorescence passed through the objective, through a 510 nm filter, and was detected by a photomultiplier tube. For spontaneous transient traces analyzed, n=12-16 traces per group, with at least 4 transients analyzed per trace; for transients elicited at 0.5 Hz stimulation, n=20-29 traces per group with 10 transients averaged per trace.

Immunostaining

For immunohistochemistry, constructs were fixed for 20 minutes in 4% PF and embedded in paraffin. 5 μm sections were cut, and primary antibody staining was performed overnight, followed by one hour of secondary antibody incubation. For immunofluorescence, Alexa fluorophore-conjugated secondary antibodies were employed; Hoechst (Sigma) counterstain was used to visualize the nuclei.

The following primary antibodies were used: goat polyclonal anti-human Nkx2.5 (R&D Systems, 1:400 dilution), FITC-conjugated phalloidin (Invitrogen, 1:40 dilution), as well as mouse monoclonal anti-α-actinin (Sigma, 1:800 dilution), which was used after after proteinase K digestion (20 μg/mL in 0.01 M TrisHCl buffer, pH 7.3, at 37℃ for 30 min, Roche). Immunofluorescent secondary antibodies included Alexa 488- or 594-conjugated goat anti-mouse or horse anti-goat (Invitrogen, 1:100 dilutions). Vectashield (Vector Labs) medium was used to mount #1 glass coverslips (Corning) onto immunofluorescent slides.

Microscopy and Image Preparation

All immunofluorescent images were collected by a Nikon A1 Confocal System attached to a Nikon Ti-E inverted microscope platform and using water-immersion Nikon 60x CFI Plan Apo objective lens with 1.2 NA. Image acquisition was performed at room temperature using Nikon NIS Elements 3.1 software to capture 12-bit raw files that were then rescaled to 16-bit images for further processing. All images were collected as a single scan with the pinhole adjusted to 1 Airy unit at 1024x1024 pixel density. For figure preparation, images were exported into Photoshop 7.0 (Adobe). If necessary, brightness and contrast were adjusted for the entire image and the image was cropped.

Statistical Analysis

Results are given as average value ± standard error of the mean (SEM); error bars within graphs also represent SEM. Significance was determined using single factor ANOVA followed by Student's t-test with 95% or greater confidence level. To test for significance of values from subsequent stretches or stretches with and without BDM or isoproterenol, we used a Student's paired t-test.

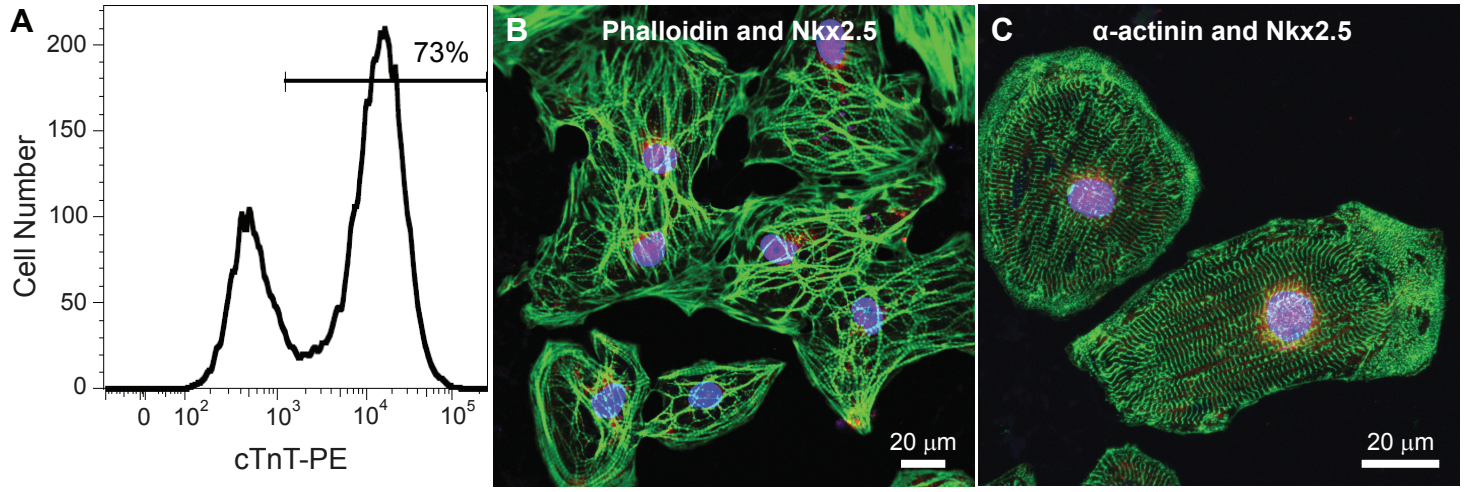

Figure 5.1. IPS cells generate human cardiomyocytes at high purity. A, Using a modified differentiation protocol, human cardiomyocytes were generated from the IMR90-iPS cell line at a purity of over 70% by cardiac troponin T (cTnT) flow cytometric analysis. **B,** These differentiated cells exhibited widespread networks of filamentous actin by phalloidin staining (green). **C,** They also displayed robust sarcomeric organization by α-actinin immunostaining (green), as well as nuclear expression of the cardiomyocyte transcription factor Nkx2.5 (red).

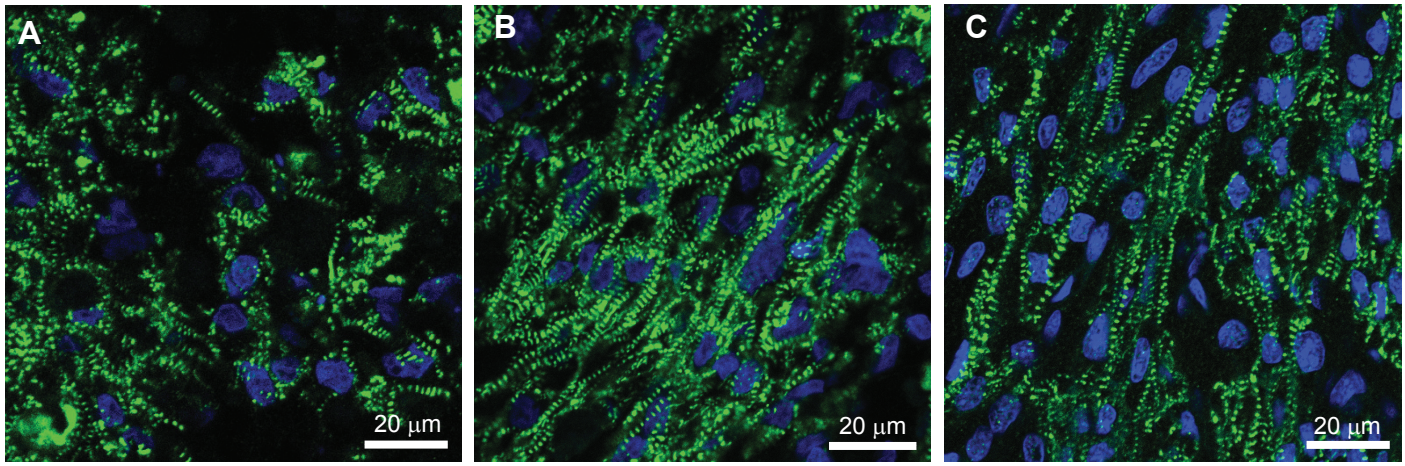

Figure 5.2. Human bioengineered cardiac tissue from iPS cell-derived cardiomyocytes. A, Human cardiac tissue constructs after 2 weeks of no stress or **B**, static stress conditioning and immunostained for α-actinin, demonstrating nascent intercellular alignment with conditioning, qualitatively similar to **C,** equivalently stained human fetal tissue.

A

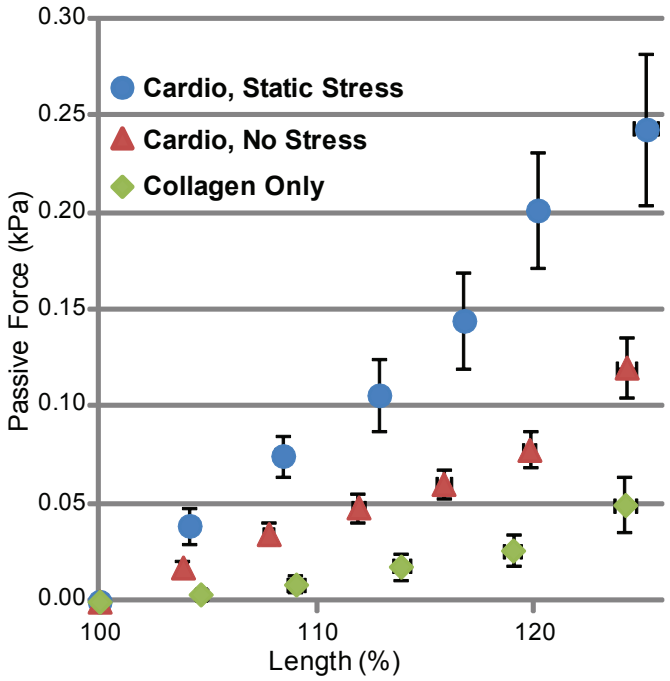

B

	Passive Force Slope (Modulus) kPa	R^2 value
Static Stress	**0.78** ±0.12*,#	**0.94** ±0.03
No Stress	**0.40** ±0.05*	**0.92** ±0.03
Collagen Only	**0.20** ±0.06	**0.88** ±0.02
Ratio of SS to CO	**3.98**	
Ratio of NS to CO	**2.04**	
Ratio of SS to NS	**1.95**	

* = significant difference to CO with p = 0.0005

= significant difference to NS with p = 0.004

Figure 5.3. Cellular responses and stress conditioning modulate matrix dynamics. A, Passive force of collagen scaffolds (green diamonds) developed over a 25% length stretch increased with the addition of iPS cell-derived cardiomyocytes in unstressed conditions (red triangles) and increased further when subjected to 2 weeks of static stress conditioning (blue circles). **B,** The differences in Young's Modulus, as calculated from the slope of the passive force over the 25% length stretch, are highly significant between these groups. Values are shown as average ± SEM.

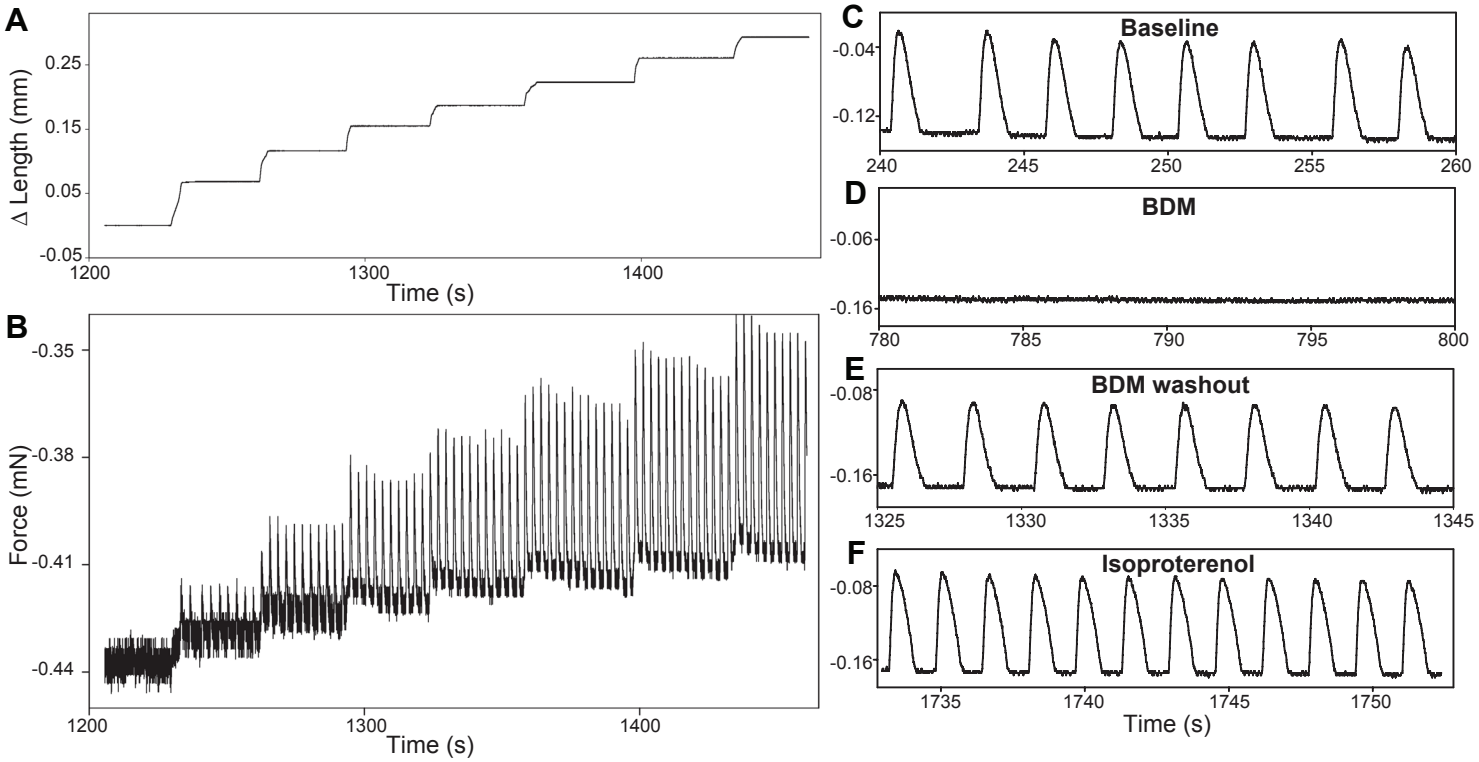

Figure 5.4. Active force increases with stretch and decreases with BDM. Representative length **(A)** and force **(B)** traces demonstrating a response of the spontaneously contracting cardiac tissue construct to a series of lengthening stretches up to 125% of slack length. Passive force increases with each stretch, and amplitude of the isometric twitch force increases markedly with increasing preparation length, in accordance with the Frank-Starling mechanism. **C,** Sample force trace at 125% slack length. **D,** Incubation with 30mM BDM reversibly inhibits spontaneous contractions. **E,** Within 3 minutes of BDM washout, contractions return. **F,** At the same preparation length, incubation with the β-adrenergic agonist isoproterenol (10 μM) increases rate markedly.

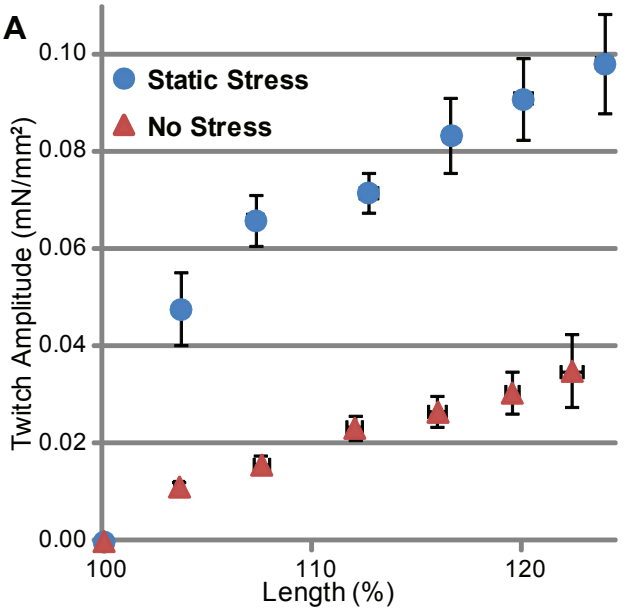

B

	Active Force Slope Average	
	mN/mm²	**R^2 value**
Static Stress	**0.38** ±0.04 *	**0.81** ±0.04
No Stress	**0.15** ±0.02	**0.92** ±0.02
Ratio of SS to NS	**2.50**	

* – indicates significant difference with $p < 0.0001$

Figure 5.5. Active force development is enhanced by stress pre-conditioning. A, Isometric twitch force amplitude measured at different preparation lengths, or the Frank-Starling response, is enhanced by 2 weeks of static stress conditioning in comparison to no stress conditioning. **B,** The average slope of these traces, an indication of the contractile response of the tissue, was significantly increased in the static stress-conditioned group. Values are shown as average ± SEM.

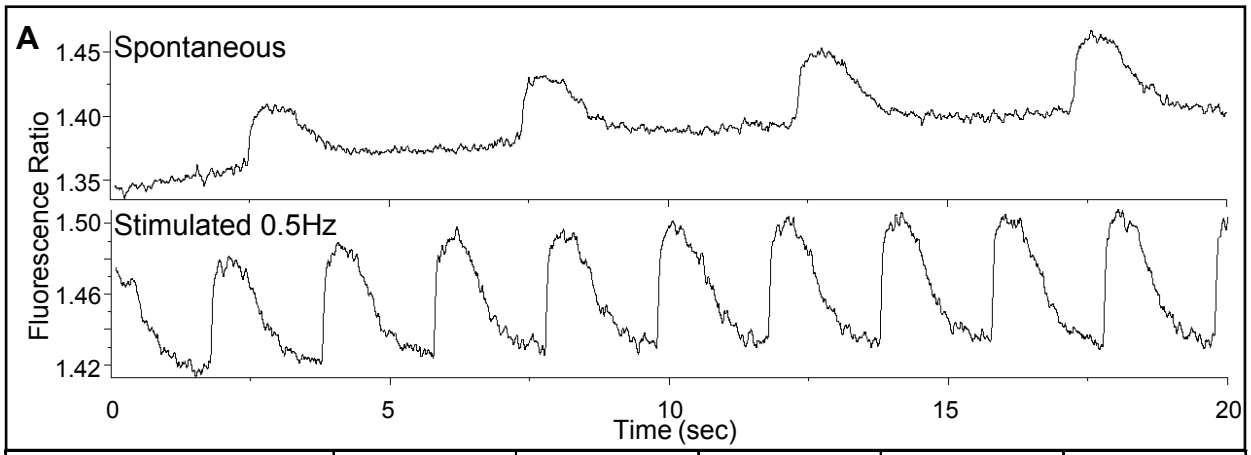

B **Spontaneous**	**dep v**	**peak t**, sec	**peak h**	**ret v**	**rate**, Hz
Static Stress	**2.22** ±0.31*	**0.51** ±0.05	**0.18** ±0.03	**-0.31** ±0.05	**0.21** ±0.01
No Stress	**1.05** ±0.30	**0.61** ±0.03	**0.21** ±0.04	**-0.40** ±0.13	**0.22** ±0.01
* = significant difference to NS with p < 0.01					
Stimulated 0.5Hz					
Static Stress	**1.91** ±0.23#	**0.52** ±0.05	**0.23** ±0.03	**-0.45** ±0.06	0.5
No Stress	**0.97** ±0.14	**0.56** ±0.02	**0.19** ±0.03	**-0.48** ±0.06	0.5
# = significant difference to NS with p < 0.005					

Figure 5.6. Calcium transient characteristics of conditioned cardiac constructs. A, Representative calcium transients in spontaneously contracting (top) and stimulated at 0.5Hz (bottom) cardiac tissue constructs recorded under low magnification. **B,** Maximum rate of calcium signal increase (departing velocity, dep v) was over 2-fold higher in stress-conditioned constructs compared to no stress-conditioned constructs. This was true for both spontaneous transients and transients elicited with 0.5 Hz stimulation. Time to peak (peak t), peak height (peak h), and maximum rate of calcium signal decay (return velocity, ret v), however, were not substantially different between the two groups. Values are shown as average ± SEM.

Table 5.1

	1st Stretch kPa	**2nd Stretch** kPa	**1st Stretch** kPa	**2nd Stretch with BDM** kPa
Static Stress	**0.76** ±0.17	**1.18** ±0.39	**0.71** ±0.17	**0.52** ±0.11
No Stress	**0.42** ±0.08	**0.45** ±0.05	**0.43** ±0.06	**0.47** ±0.06

Table 5.1. Construct stiffness calculated during 2nd stretch or with BDM. Stiffness, as determined by change in passive force over 25% length stretch, is not significantly changed with either subsequent stretches, indicating that construct integrity is not markedly diminished by multiple stretches, or with incubation with BDM, indicating that acto-myosin interaction is not a major component of passive force in tissue constructs generated with cardiomyocytes. Values are given as average ± SEM.

Table 5.2

	1st Stretch mN/mm^2	**2nd Stretch** mN/mm^2
Static Stress	**0.388** ±0.069	**0.390** ±0.058
No Stress	**0.140** ±0.017	**0.140** ±0.019

Table 5.2. Active force slope and 2nd stretch. Slope of active force amplitude over length increase also does not significantly change with subsequent stretches, indicating construct integrity or contractility is not markedly diminished by multiple stretch routines. Values are given as average ± SEM.

Chapter 6: Conclusions and Future Directions

These studies demonstrate that we can work out the biological cues operating in the developing human myocardium, and to begin to use this understanding to replicate aspects of human cardiac development *in vitro*. These include the effects of mechanical conditioning on cell and matrix alignment and force production, as well as the effect of endothelial cell interactions on cardiomyocyte proliferation. Furthermore, the ability to create these tissues using human iPS cell-derived myocardium now allows us to begin to explore important unanswered questions of human myocardial biology and disease, such as the origin of pathogenesis of human hypertrophic and dilated cardiomyopathies. These diseases affect large numbers of people, often present in childhood, and tend to become more severe with age, commonly resulting in sudden death in young adulthood or congestive heart failure similar to post-myocardial infarction disease.[118-121] Both hypertrophic and dilated cardiomyopathies are now known to have genetic determinants, and tend to present as autosomal dominant. β-myosin heavy chain mutations (MYH7) accounts for 35% of genetically determined hypertrophic cardiomyopathies; whereas myosin binding protein C (MYBPC3) accounts for 30%, and cardiac troponin C (TNNT2) for 5%.[122]

However, the mechanistic link between contractile gene mutation and the pathogenesis of disease phenotype such as myocardial disarray, increased fibrosis, or cardiac hypertrophy has not been determined, although it is clear that these histological findings are associated with the organ abnormalities – increased ventricular wall and septal thickness, or arrhythmia susceptibility – which lead to decreased effective cardiac output and sudden cardiac death, respectively. More confusingly, mutations in each of these same contractile proteins have been identified in dilated cardiomyopathy cases as well,[122] conversely leading to, in the latter set, decreased wall thickness, increased systolic and diastolic chamber diameter, and also decreased cardiac output.

The technique of inducing pluripotency in differentiated, adult human cells now theoretically could allow us to reprogram cells from these patients back to an undifferentiated, pluripotent state, then to use our current cardiac differentiation protocols to derive mutant genotype-specific cardiomyocytes, and finally to apply our current tissue engineering techniques to generate disease-producing tissue *in vitro*, comparing the functional characteristics to normal, genotype-negative engineered human tissue. This sort

of iPS cell-based approach has now been performed on a single-cell phenotyping basis for the cardiomyocyte-based diseases long-QT syndrome[123] and Leopard syndrome,[124] but has yet to be utilized for assessment of the origin of multicellular and tissue-based pathogenic phenotypes such as myocardial disarray and fibrosis found in familial hypertrophic cardiomyopathy.

The creation of a bioengineered human cardiovascular tissue disease model would allow us to directly examine the contribution of particular genetic mutations to functional differences in force production, and determine the presence or absence of aberrant calcium handling as a potential cause. These sorts of experiments, geared towards examining origins of pathogenesis, also conveniently lend themselves to drug screening in engineered human cardiovascular tissue, as has been already demonstrated on a boutique basis with a number of known arrhythmia producing compounds.[7]

Furthermore, the goal of producing functional engineered myocardium for developmental and therapeutic purposes would be greatly enhanced by an ability to generate the multiple differentiated cell types found in mature myocardium from the same genetic background. This could hypothetically be done by subjecting a single line of pluripotent cells to several specific differentiation protocols, for instance differentiating vascular endothelium using an endothelial-specific differentiation protocol,[25] and cardiomyocytes using a cardiogenic protocol,[20] and then mixing the resulting cell types, in a method analogous to our previous study (Chapter 2).[86] However, the discovery and description of a tri-potential cardiovascular progenitor population,[22] existing part-way between the pluripotent state and the differentiated cardiac and vascular fates, provides an even more attractive route to differentiated human cardiovascular tissues (Chapter 3). These KDR and PDGFRα-expressing progenitor cells can and should be used to generate 3-dimensional tissues containing myocardium with genotype-specific vasculature, both for induction of cardiomyocyte proliferation, and for “plug and play” readiness necessary for therapeutic grafting purposes.

As it is now feasible to use normal human cardiomyocytes to generate organized, engineered human myocardium,capable of producing a limited – but measurable and dynamic – level contractile function, we should focus on the goal of maturing these types of tissues to more adult developmental states. Human cardiomyocytes in engineered tissue, even when subjected to weeks of stress conditioning,[86] or implanted into myocardium *in vivo* for months,[12, 20] remain relatively immature, with only

modest increases along hypertrophy or maturation parameters. We should continue to define new methods for maturing human cardiac tissue, using not only mechanical conditioning but also assessing the potential of electrical conditioning as well as cytokine or small molecule inducement of maturation. Only when we are able to replicate contractile function in the order of magnitude of adult human myocardium will we have a potential therapy useful for human heart repair.

References

1. Madden LR, Mortisen DJ, Sussman EM, Dupras SK, Fugate JA, Cuy JL, Hauch KD, Laflamme MA, Murry CE, Ratner BD. Proangiogenic scaffolds as functional templates for cardiac tissue engineering. *Proc Natl Acad Sci U S A*. 2010;107:15211-15216
2. Caspi O, Lesman A, Basevitch Y, Gepstein A, Arbel G, Habib IH, Gepstein L, Levenberg S. Tissue engineering of vascularized cardiac muscle from human embryonic stem cells. *Circ Res*. 2007;100:263-272
3. Marsano A, Maidhof R, Wan LQ, Wang Y, Gao J, Tandon N, Vunjak-Novakovic G. Scaffold stiffness affects the contractile function of three-dimensional engineered cardiac constructs. *Biotechnol Prog*. 2010;26:1382-1390
4. Dar A, Shachar M, Leor J, Cohen S. Optimization of cardiac cell seeding and distribution in 3d porous alginate scaffolds. *Biotechnol Bioeng*. 2002;80:305-312
5. Birla RK, Huang YC, Dennis RG. Development of a novel bioreactor for the mechanical loading of tissue-engineered heart muscle. *Tissue Eng*. 2007;13:2239-2248
6. Liau B, Christoforou N, Leong KW, Bursac N. Pluripotent stem cell-derived cardiac tissue patch with advanced structure and function. *Biomaterials*. 2011;32:9180-9187
7. Schaaf S, Shibamiya A, Mewe M, Eder A, Stöhr A, Hirt MN, Rau T, Zimmermann WH, Conradi L, Eschenhagen T, Hansen A. Human engineered heart tissue as a versatile tool in basic research and preclinical toxicology. *PLoS One*. 2011;6:e26397
8. Zimmermann WH, Schneiderbanger K, Schubert P, Didie M, Munzel F, Heubach JF, Kostin S, Neuhuber WL, Eschenhagen T. Tissue engineering of a differentiated cardiac muscle construct. *Circ Res*. 2002;90:223-230
9. Zimmermann WH, Melnychenko I, Wasmeier G, Didie M, Naito H, Nixdorff U, Hess A, Budinsky L, Brune K, Michaelis B, Dhein S, Schwoerer A, Ehmke H, Eschenhagen T. Engineered heart tissue grafts improve systolic and diastolic function in infarcted rat hearts. *Nat Med*. 2006;12:452-458
10. Zimmermann WH, Didie M, Wasmeier GH, Nixdorff U, Hess A, Melnychenko I, Boy O, Neuhuber WL, Weyand M, Eschenhagen T. Cardiac grafting of engineered heart tissue in syngenic rats. *Circulation*. 2002;106:I151-157
11. Kreutziger KL, Muskheli V, Johnson P, Braun K, Wight TN, Murry CE. Developing vasculature and stroma in engineered human myocardium. *Tissue Eng Part A*. 2011;17:1219-1228
12. Stevens KR, Kreutziger KL, Dupras SK, Korte FS, Regnier M, Muskheli V, Nourse MB, Bendixen K, Reinecke H, Murry CE. Physiological function and transplantation of scaffold-free and vascularized human cardiac muscle tissue. *Proc Natl Acad Sci U S A*. 2009;106:16568-16573
13. Badie N, Bursac N. Novel micropatterned cardiac cell cultures with realistic ventricular microstructure. *Biophys J*. 2009;96:3873-3885
14. Eschenhagen T, Didie M, Munzel F, Schubert P, Schneiderbanger K, Zimmermann WH. 3d engineered heart tissue for replacement therapy. *Basic Res Cardiol*. 2002;97 Suppl 1:I146-152
15. Naito H, Melnychenko I, Didie M, Schneiderbanger K, Schubert P, Rosenkranz S, Eschenhagen T, Zimmermann WH. Optimizing engineered heart tissue for therapeutic applications as surrogate heart muscle. *Circulation*. 2006;114:I72-78
16. Shapira-Schweitzer K, Seliktar D. Matrix stiffness affects spontaneous contraction of cardiomyocytes cultured within a pegylated fibrinogen biomaterial. *Acta Biomater*. 2007;3:33-41
17. Benton JA, Kern HB, Anseth KS. Substrate properties influence calcification in valvular interstitial cell culture. *J Heart Valve Dis*. 2008;17:689-699

18. Benton JA, Fairbanks BD, Anseth KS. Characterization of valvular interstitial cell function in three dimensional matrix metalloproteinase degradable peg hydrogels. *Biomaterials*. 2009;30:6593-6603
19. Radisic M, Park H, Martens TP, Salazar-Lazaro JE, Geng W, Wang Y, Langer R, Freed LE, Vunjak-Novakovic G. Pre-treatment of synthetic elastomeric scaffolds by cardiac fibroblasts improves engineered heart tissue. *J Biomed Mater Res A*. 2008;86:713-724
20. Laflamme MA, Chen KY, Naumova AV, Muskheli V, Fugate JA, Dupras SK, Reinecke H, Xu C, Hassanipour M, Police S, O'Sullivan C, Collins L, Chen Y, Minami E, Gill EA, Ueno S, Yuan C, Gold J, Murry CE. Cardiomyocytes derived from human embryonic stem cells in pro-survival factors enhance function of infarcted rat hearts. *Nat Biotechnol*. 2007;25:1015-1024
21. Zhu WZ, Van Biber B, Laflamme MA. Methods for the derivation and use of cardiomyocytes from human pluripotent stem cells. *Methods Mol Biol*. 2011;767:419-431
22. Yang L, Soonpaa MH, Adler ED, Roepke TK, Kattman SJ, Kennedy M, Henckaerts E, Bonham K, Abbott GW, Linden RM, Field LJ, Keller GM. Human cardiovascular progenitor cells develop from a kdr+ embryonic-stem-cell-derived population. *Nature*. 2008;453:524-528
23. Murry CE, Keller G. Differentiation of embryonic stem cells to clinically relevant populations: Lessons from embryonic development. *Cell*. 2008;132:661-680
24. Mummery CL, Ward D, Passier R. Differentiation of human embryonic stem cells to cardiomyocytes by coculture with endoderm in serum-free medium. *Curr Protoc Stem Cell Biol*. 2007;Chapter 1:Unit 1F.2
25. Nourse MB, Halpin DE, Scatena M, Mortisen DJ, Tulloch NL, Hauch KD, Torok-Storb B, Ratner BD, Pabon L, Murry CE. Vegf induces differentiation of functional endothelium from human embryonic stem cells. Implications for tissue engineering. *Arterioscler Thromb Vasc Biol*. 2009;30:80-89
26. Lu SJ, Feng Q, Caballero S, Chen Y, Moore MA, Grant MB, Lanza R. Generation of functional hemangioblasts from human embryonic stem cells. *Nat Methods*. 2007;4:501-509
27. Takahashi K, Tanabe K, Ohnuki M, Narita M, Ichisaka T, Tomoda K, Yamanaka S. Induction of pluripotent stem cells from adult human fibroblasts by defined factors. *Cell*. 2007;131:861-872
28. Montgomery MO, Jiao Y, Phillips SJ, Singh G, Xu J, Balsara R, Litvin J. Alterations in sheep fetal right ventricular tissue with induced hemodynamic pressure overload. *Basic Res Cardiol*. 1998;93:192-200
29. Tobita K, Keller BB. Right and left ventricular wall deformation patterns in normal and left heart hypoplasia chick embryos. *Am J Physiol Heart Circ Physiol*. 2000;279:H959-969
30. Voronov DA, Alford PW, Xu G, Taber LA. The role of mechanical forces in dextral rotation during cardiac looping in the chick embryo. *Dev Biol*. 2004;272:339-350
31. Kira Y, Nakaoka T, Hashimoto E, Okabe F, Asano S, Sekine I. Effect of long-term cyclic mechanical load on protein synthesis and morphological changes in cultured myocardial cells from neonatal rat. *Cardiovasc Drugs Ther*. 1994;8:251-262
32. Kuruvilla L, Kartha CC. Molecular mechanisms in endothelial regulation of cardiac function. *Mol Cell Biochem*. 2003;253:113-123
33. Hsieh PC, Davis ME, Lisowski LK, Lee RT. Endothelial-cardiomyocyte interactions in cardiac development and repair. *Annu Rev Physiol*. 2006;68:51-66
34. Bhattacharya S, Macdonald ST, Farthing CR. Molecular mechanisms controlling the coupled development of myocardium and coronary vasculature. *Clin Sci (Lond)*. 2006;111:35-46

35. Bergmann O, Bhardwaj RD, Bernard S, Zdunek S, Barnabe-Heider F, Walsh S, Zupicich J, Alkass K, Buchholz BA, Druid H, Jovinge S, Frisen J. Evidence for cardiomyocyte renewal in humans. *Science*. 2009;324:98-102
36. Thomson JA, Itskovitz-Eldor J, Shapiro SS, Waknitz MA, Swiergiel JJ, Marshall VS, Jones JM. Embryonic stem cell lines derived from human blastocysts. *Science*. 1998;282:1145-1147
37. Zhang J, Wilson GF, Soerens AG, Koonce CH, Yu J, Palecek SP, Thomson JA, Kamp TJ. Functional cardiomyocytes derived from human induced pluripotent stem cells. *Circ Res*. 2009;104:e30-41
38. Zhu WZ, Santana LF, Laflamme MA. Local control of excitation-contraction coupling in human embryonic stem cell-derived cardiomyocytes. *PLoS One*. 2009;4:e5407
39. Xu C, Police S, Rao N, Carpenter MK. Characterization and enrichment of cardiomyocytes derived from human embryonic stem cells. *Circ Res*. 2002;91:501-508
40. Kehat I, Kenyagin-Karsenti D, Snir M, Segev H, Amit M, Gepstein A, Livne E, Binah O, Itskovitz-Eldor J, Gepstein L. Human embryonic stem cells can differentiate into myocytes with structural and functional properties of cardiomyocytes. *J Clin Invest*. 2001;108:407-414
41. Itzhaki I, Schiller J, Beyar R, Satin J, Gepstein L. Calcium handling in embryonic stem cell-derived cardiac myocytes: Of mice and men. *Ann N Y Acad Sci*. 2006;1080:207-215
42. Blan NR, Birla RK. Design and fabrication of heart muscle using scaffold-based tissue engineering. *J Biomed Mater Res A*. 2008;86:195-208
43. Shimko VF, Claycomb WC. Effect of mechanical loading on three-dimensional cultures of embryonic stem cell-derived cardiomyocytes. *Tissue Eng Part A*. 2008;14:49-58
44. Fink C, Ergun S, Kralisch D, Remmers U, Weil J, Eschenhagen T. Chronic stretch of engineered heart tissue induces hypertrophy and functional improvement. *FASEB J*. 2000;14:669-679
45. Weber KT, Janicki JS, Shroff SG, Pick R, Chen RM, Bashey RI. Collagen remodeling of the pressure-overloaded, hypertrophied nonhuman primate myocardium. *Circ Res*. 1988;62:757-765
46. Whittaker P, Kloner RA, Boughner DR, Pickering JG. Quantitative assessment of myocardial collagen with picrosirius red staining and circularly polarized light. *Basic Res Cardiol*. 1994;89:397-410
47. Borges LF, Gutierrez PS, Marana HR, Taboga SR. Picrosirius-polarization staining method as an efficient histopathological tool for collagenolysis detection in vesical prolapse lesions. *Micron*. 2007;38:580-583
48. Cuttle L, Nataatmadja M, Fraser JF, Kempf M, Kimble RM, Hayes MT. Collagen in the scarless fetal skin wound: Detection with picrosirius-polarization. *Wound Repair Regen*. 2005;13:198-204
49. McDevitt TC, Laflamme MA, Murry CE. Proliferation of cardiomyocytes derived from human embryonic stem cells is mediated via the igf/pi 3-kinase/akt signaling pathway. *J Mol Cell Cardiol*. 2005;39:865-873
50. Hilfiker-Kleiner D, Limbourg A, Drexler H. Stat3-mediated activation of myocardial capillary growth. *Trends Cardiovasc Med*. 2005;15:152-157
51. O'Connell TD, Ishizaka S, Nakamura A, Swigart PM, Rodrigo MC, Simpson GL, Cotecchia S, Rokosh DG, Grossman W, Foster E, Simpson PC. The alpha(1a/c)- and alpha(1b)-adrenergic receptors are required for physiological cardiac hypertrophy in the double-knockout mouse. *J Clin Invest*. 2003;111:1783-1791
52. Shyu KG. Cellular and molecular effects of mechanical stretch on vascular cells and cardiac myocytes. *Clin Sci (Lond)*. 2009;116:377-389

53. Kisanuki YY, Hammer RE, Miyazaki J, Williams SC, Richardson JA, Yanagisawa M. Tie2-cre transgenic mice: A new model for endothelial cell-lineage analysis in vivo. *Dev Biol*. 2001;230:230-242
54. Dumont DJ, Gradwohl G, Fong GH, Puri MC, Gertsenstein M, Auerbach A, Breitman ML. Dominant-negative and targeted null mutations in the endothelial receptor tyrosine kinase, tek, reveal a critical role in vasculogenesis of the embryo. *Genes Dev*. 1994;8:1897-1909
55. Gitler AD, Zhu Y, Ismat FA, Lu MM, Yamauchi Y, Parada LF, Epstein JA. Nf1 has an essential role in endothelial cells. *Nat Genet*. 2003;33:75-79
56. Gerety SS, Anderson DJ. Cardiovascular ephrinb2 function is essential for embryonic angiogenesis. *Development*. 2002;129:1397-1410
57. Chen K, Bai H, Arzigian M, Gao YX, Bao J, Wu WS, Shen WF, Wu L, Wang ZZ. Endothelial cells regulate cardiomyocyte development from embryonic stem cells. *J Cell Biochem*. 2010;111:29-39
58. Meyer D, Birchmeier C. Multiple essential functions of neuregulin in development. *Nature*. 1995;378:386-390
59. Gassmann M, Casagranda F, Orioli D, Simon H, Lai C, Klein R, Lemke G. Aberrant neural and cardiac development in mice lacking the erbb4 neuregulin receptor. *Nature*. 1995;378:390-394
60. Lai D, Liu X, Forrai A, Wolstein O, Michalicek J, Ahmed I, Garratt AN, Birchmeier C, Zhou M, Hartley L, Robb L, Feneley MP, Fatkin D, Harvey RP. Neuregulin 1 sustains the gene regulatory network in both trabecular and nontrabecular myocardium. *Circ Res*. 2010;107:715-727
61. Levenberg S, Rouwkema J, Macdonald M, Garfein ES, Kohane DS, Darland DC, Marini R, van Blitterswijk CA, Mulligan RC, D'Amore PA, Langer R. Engineering vascularized skeletal muscle tissue. *Nat Biotechnol*. 2005;23:879-884
62. Stevens KR, Pabon L, Muskheli V, Murry CE. Scaffold-free human cardiac tissue patch created from embryonic stem cells. *Tissue Eng Part A*. 2009;15:1211-1222
63. Kadler KE, Hojima Y, Prockop DJ. Assembly of collagen fibrils de novo by cleavage of the type i pc-collagen with procollagen c-proteinase. Assay of critical concentration demonstrates that collagen self-assembly is a classical example of an entropy-driven process. *J Biol Chem*. 1987;262:15696-15701
64. Holmes DF, Graham HK, Trotter JA, Kadler KE. Stem/tem studies of collagen fibril assembly. *Micron*. 2001;32:273-285
65. Velling T, Risteli J, Wennerberg K, Mosher DF, Johansson S. Polymerization of type i and iii collagens is dependent on fibronectin and enhanced by integrins alpha 11beta 1 and alpha 2beta 1. *J Biol Chem*. 2002;277:37377-37381
66. Lin IE, Taber LA. Mechanical effects of looping in the embryonic chick heart. *J Biomech*. 1994;27:311-321
67. Taber LA. Mechanical aspects of cardiac development. *Prog Biophys Mol Biol*. 1998;69:237-255
68. Arts T, Prinzen FW, Snoeckx LH, Rijcken JM, Reneman RS. Adaptation of cardiac structure by mechanical feedback in the environment of the cell: A model study. *Biophys J*. 1994;66:953-961
69. Arts T, Delhaas T, Bovendeerd P, Verbeek X, Prinzen FW. Adaptation to mechanical load determines shape and properties of heart and circulation: The circadapt model. *Am J Physiol Heart Circ Physiol*. 2005;288:H1943-1954
70. Olivetti G, Capasso JM, Sonnenblick EH, Anversa P. Side-to-side slippage of myocytes participates in ventricular wall remodeling acutely after myocardial infarction in rats. *Circ Res*. 1990;67:23-34

71. Mansour H, de Tombe PP, Samarel AM, Russell B. Restoration of resting sarcomere length after uniaxial static strain is regulated by protein kinase cepsilon and focal adhesion kinase. *Circ Res*. 2004;94:642-649
72. Senyo SE, Koshman YE, Russell B. Stimulus interval, rate and direction differentially regulate phosphorylation for mechanotransduction in neonatal cardiac myocytes. *FEBS Lett*. 2007;581:4241-4247
73. Russell B, Curtis MW, Koshman YE, Samarel AM. Mechanical stress-induced sarcomere assembly for cardiac muscle growth in length and width. *J Mol Cell Cardiol*. 2010;48:817-823
74. Vater C, Kasten P, Stiehler M. Culture media for the differentiation of mesenchymal stromal cells. *Acta Biomater*. 2010
75. Berry MF, Engler AJ, Woo YJ, Pirolli TJ, Bish LT, Jayasankar V, Morine KJ, Gardner TJ, Discher DE, Sweeney HL. Mesenchymal stem cell injection after myocardial infarction improves myocardial compliance. *Am J Physiol Heart Circ Physiol*. 2006;290:H2196-2203
76. Chacko SM, Khan M, Kuppusamy ML, Pandian RP, Varadharaj S, Selvendiran K, Bratasz A, Rivera BK, Kuppusamy P. Myocardial oxygenation and functional recovery in infarct rat hearts transplanted with mesenchymal stem cells. *Am J Physiol Heart Circ Physiol*. 2009;296:H1263-1273
77. Strauer BE, Brehm M, Zeus T, Kostering M, Hernandez A, Sorg RV, Kogler G, Wernet P. Repair of infarcted myocardium by autologous intracoronary mononuclear bone marrow cell transplantation in humans. *Circulation*. 2002;106:1913-1918
78. Katritsis DG, Sotiropoulou PA, Karvouni E, Karabinos I, Korovesis S, Perez SA, Voridis EM, Papamichail M. Transcoronary transplantation of autologous mesenchymal stem cells and endothelial progenitors into infarcted human myocardium. *Catheter Cardiovasc Interv*. 2005;65:321-329
79. Paige SL, Osugi T, Afanasiev OK, Pabon L, Reinecke H, Murry CE. Endogenous wnt/beta-catenin signaling is required for cardiac differentiation in human embryonic stem cells. *PLoS One*. 2010;5:e11134
80. Yu J, Vodyanik MA, Smuga-Otto K, Antosiewicz-Bourget J, Frane JL, Tian S, Nie J, Jonsdottir GA, Ruotti V, Stewart R, Slukvin, II, Thomson JA. Induced pluripotent stem cell lines derived from human somatic cells. *Science*. 2007;318:1917-1920
81. Xu C, Police S, Hassanipour M, Gold JD. Cardiac bodies: A novel culture method for enrichment of cardiomyocytes derived from human embryonic stem cells. *Stem Cells Dev*. 2006;15:631-639
82. Laflamme MA, Gold J, Xu C, Hassanipour M, Rosler E, Police S, Muskheli V, Murry CE. Formation of human myocardium in the rat heart from human embryonic stem cells. *Am J Pathol*. 2005;167:663-671
83. Reinecke H, Zhang M, Bartosek T, Murry CE. Survival, integration, and differentiation of cardiomyocyte grafts: A study in normal and injured rat hearts. *Circulation*. 1999;100:193-202
84. Moreno-Gonzalez A, Korte FS, Dai J, Chen K, Ho B, Reinecke H, Murry CE, Regnier M. Cell therapy enhances function of remote non-infarcted myocardium. *J Mol Cell Cardiol*. 2009;47:603-613
85. Stevens KR, Rolle MW, Minami E, Ueno S, Nourse MB, Virag JI, Reinecke H, Murry CE. Chemical dimerization of fibroblast growth factor receptor-1 induces myoblast proliferation, increases intracardiac graft size, and reduces ventricular dilation in infarcted hearts. *Hum Gene Ther*. 2007;18:401-412
86. Tulloch NL, Muskheli V, Razumova MV, Korte FS, Regnier M, Hauch KD, Pabon L, Reinecke H, Murry CE. Growth of engineered human myocardium with mechanical loading and vascular coculture. *Circ Res*. 2011;109:47-59

87. Kattman SJ, Witty AD, Gagliardi M, Dubois NC, Niapour M, Hotta A, Ellis J, Keller G. Stage-specific optimization of activin/nodal and bmp signaling promotes cardiac differentiation of mouse and human pluripotent stem cell lines. *Cell Stem Cell*. 2011;8:228-240
88. Kennedy M, D'Souza SL, Lynch-Kattman M, Schwantz S, Keller G. Development of the hemangioblast defines the onset of hematopoiesis in human es cell differentiation cultures. *Blood*. 2007;109:2679-2687
89. Haddad F, Qin AX, Bodell PW, Jiang W, Giger JM, Baldwin KM. Intergenic transcription and developmental regulation of cardiac myosin heavy chain genes. *Am J Physiol Heart Circ Physiol*. 2008;294:H29-40
90. Korte FS, Dai J, Buckley K, Feest ER, Adamek N, Geeves MA, Murry CE, Regnier M. Upregulation of cardiomyocyte ribonucleotide reductase increases intracellular 2 deoxy-atp, contractility, and relaxation. *J Mol Cell Cardiol*. 2011;51:894-901
91. Herron TJ, Vandenboom R, Fomicheva E, Mundada L, Edwards T, Metzger JM. Calcium-independent negative inotropy by beta-myosin heavy chain gene transfer in cardiac myocytes. *Circ Res*. 2007;100:1182-1190
92. Mauritz C SK, Reppel M, Neef S, Katsirntaki K, Maier L, Nguemo F, Menke S, Haustein M, Hescheler J, Hausenfuss G, Martin U. Generation of functional murine cardiac myocytes from induced pluripotent stem (ips) cells. *Circulation*. 2008;In Press
93. Narazaki G UH, Teranishi M, Okita K, Kim B, Matsuoka S, Yamanaka S, Yamashita J. Directed and systematic differentiation of cardiovascular cells from mouse induced pluripotent cells. *Circulation*. 2008;In Press
94. Wilmut I, Schnieke AE, McWhir J, Kind AJ, Campbell KH. Viable offspring derived from fetal and adult mammalian cells. *Nature*. 1997;385:810-813
95. Takahashi K, Yamanaka S. Induction of pluripotent stem cells from mouse embryonic and adult fibroblast cultures by defined factors. *Cell*. 2006;126:663-676
96. Park IH, Zhao R, West JA, Yabuuchi A, Huo H, Ince TA, Lerou PH, Lensch MW, Daley GQ. Reprogramming of human somatic cells to pluripotency with defined factors. *Nature*. 2008;451:141-146
97. Ueno S, Weidinger G, Osugi T, Kohn AD, Golob JL, Pabon L, Reinecke H, Moon RT, Murry CE. Biphasic role for wnt/beta-catenin signaling in cardiac specification in zebrafish and embryonic stem cells. *Proc Natl Acad Sci U S A*. 2007;104:9685-9690
98. Schenke-Layland K, Rhodes KE, Angelis E, Butylkova Y, Heydarkhan-Hagvall S, Gekas C, Zhang R, Goldhaber JI, Mikkola HK, Plath K, Maclellan WR. Reprogrammed mouse fibroblasts differentiate into cells of the cardiovascular and hematopoietic lineages. *Stem Cells*. 2008
99. Nakagawa M, Koyanagi M, Tanabe K, Takahashi K, Ichisaka T, Aoi T, Okita K, Mochiduki Y, Takizawa N, Yamanaka S. Generation of induced pluripotent stem cells without myc from mouse and human fibroblasts. *Nat Biotechnol*. 2008;26:101-106
100. Okita K, Ichisaka T, Yamanaka S. Generation of germline-competent induced pluripotent stem cells. *Nature*. 2007;448:313-317
101. Meissner A, Wernig M, Jaenisch R. Direct reprogramming of genetically unmodified fibroblasts into pluripotent stem cells. *Nat Biotechnol*. 2007;25:1177-1181
102. Nussbaum J, Minami E, Laflamme MA, Virag JA, Ware CB, Masino A, Muskheli V, Pabon L, Reinecke H, Murry CE. Transplantation of undifferentiated murine embryonic stem cells in the heart: Teratoma formation and immune response. *Faseb J*. 2007;21:1345-1357
103. Golob JL, Paige SL, Muskheli V, Pabon L, Murry CE. Chromatin remodeling during mouse and human embryonic stem cell differentiation. *Dev Dyn*. 2008;237:1389-1398
104. Caspi O, Huber I, Kehat I, Habib M, Arbel G, Gepstein A, Yankelson L, Aronson D, Beyar R, Gepstein L. Transplantation of human embryonic stem cell-derived

cardiomyocytes improves myocardial performance in infarcted rat hearts. *J Am Coll Cardiol*. 2007;50:1884-1893
105. van Laake LW, Passier R, Doevendans PA, Mummery CL. Human embryonic stem cell-derived cardiomyocytes and cardiac repair in rodents. *Circ Res*. 2008;102:1008-1010
106. Kroon E, Martinson LA, Kadoya K, Bang AG, Kelly OG, Eliazer S, Young H, Richardson M, Smart NG, Cunningham J, Agulnick AD, D'Amour KA, Carpenter MK, Baetge EE. Pancreatic endoderm derived from human embryonic stem cells generates glucose-responsive insulin-secreting cells in vivo. *Nat Biotechnol*. 2008;26:443-452
107. Keirstead HS, Nistor G, Bernal G, Totoiu M, Cloutier F, Sharp K, Steward O. Human embryonic stem cell-derived oligodendrocyte progenitor cell transplants remyelinate and restore locomotion after spinal cord injury. *J Neurosci*. 2005;25:4694-4705
108. Cho MS, Lee YE, Kim JY, Chung S, Cho YH, Kim DS, Kang SM, Lee H, Kim MH, Kim JH, Leem JW, Oh SK, Choi YM, Hwang DY, Chang JW, Kim DW. Highly efficient and large-scale generation of functional dopamine neurons from human embryonic stem cells. *Proc Natl Acad Sci U S A*. 2008;105:3392-3397
109. Hanna J, Wernig M, Markoulaki S, Sun CW, Meissner A, Cassady JP, Beard C, Brambrink T, Wu LC, Townes TM, Jaenisch R. Treatment of sickle cell anemia mouse model with ips cells generated from autologous skin. *Science*. 2007;318:1920-1923
110. Mummery CL, van Achterberg TA, van den Eijnden-van Raaij AJ, van Haaster L, Willemse A, de Laat SW, Piersma AH. Visceral-endoderm-like cell lines induce differentiation of murine p19 embryonal carcinoma cells. *Differentiation*. 1991;46:51-60
111. van der Heyden MA, Defize LH. Twenty one years of p19 cells: What an embryonal carcinoma cell line taught us about cardiomyocyte differentiation. *Cardiovasc Res*. 2003;58:292-302
112. Maidhof R, Marsano A, Lee EJ, Vunjak-Novakovic G. Perfusion seeding of channeled elastomeric scaffolds with myocytes and endothelial cells for cardiac tissue engineering. *Biotechnol Prog*. 2010;26:565-572
113. Dimos JT, Rodolfa KT, Niakan KK, Weisenthal LM, Mitsumoto H, Chung W, Croft GF, Saphier G, Leibel R, Goland R, Wichterle H, Henderson CE, Eggan K. Induced pluripotent stem cells generated from patients with als can be differentiated into motor neurons. *Science*. 2008;321:1218-1221
114. Okita K, Ichisaka T, Yamanaka S. Generation of germline-competent induced pluripotent stem cells. *Nature*. 2007;448:313-317
115. Freund C, Ward-van Oostwaard D, Monshouwer-Kloots J, van den Brink S, van Rooijen M, Xu X, Zweigerdt R, Mummery C, Passier R. Insulin redirects differentiation from cardiogenic mesoderm and endoderm to neuroectoderm in differentiating human embryonic stem cells. *Stem Cells*. 2008;26:724-733
116. Xu XQ, Graichen R, Soo SY, Balakrishnan T, Rahmat SN, Sieh S, Tham SC, Freund C, Moore J, Mummery C, Colman A, Zweigerdt R, Davidson BP. Chemically defined medium supporting cardiomyocyte differentiation of human embryonic stem cells. *Differentiation*. 2008;76:958-970
117. Lamba DA, Karl MO, Ware CB, Reh TA. Efficient generation of retinal progenitor cells from human embryonic stem cells. *Proc Natl Acad Sci U S A*. 2006;103:12769-12774
118. Manolio TA, Baughman KL, Rodeheffer R, Pearson TA, Bristow JD, Michels VV, Abelmann WH, Harlan WR. Prevalence and etiology of idiopathic dilated cardiomyopathy (summary of a national heart, lung, and blood institute workshop. *Am J Cardiol*. 1992;69:1458-1466
119. Grünig E, Tasman JA, Kücherer H, Franz W, Kübler W, Katus HA. Frequency and phenotypes of familial dilated cardiomyopathy. *J Am Coll Cardiol*. 1998;31:186-194
120. Sadoul N, de Chillou C, Aliot E, McKenna WJ. [evaluation of the risk of sudden death in hypertrophic cardiomyopathy]. *Arch Mal Coeur Vaiss*. 1999;92 Spec No 1:65-73

121. Maron BJ, Gardin JM, Flack JM, Gidding SS, Kurosaki TT, Bild DE. Prevalence of hypertrophic cardiomyopathy in a general population of young adults. Echocardiographic analysis of 4111 subjects in the cardia study. Coronary artery risk development in (young) adults. *Circulation*. 1995;92:785-789
122. Paul M, Zumhagen S, Stallmeyer B, Koopmann M, Spieker T, Schulze-Bahr E. Genes causing inherited forms of cardiomyopathies. A current compendium. *Herz*. 2009;34:98-109
123. Moretti A, Bellin M, Welling A, Jung CB, Lam JT, Bott-Flügel L, Dorn T, Goedel A, Höhnke C, Hofmann F, Seyfarth M, Sinnecker D, Schömig A, Laugwitz KL. Patient-specific induced pluripotent stem-cell models for long-qt syndrome. *N Engl J Med*. 2010;363:1397-1409
124. Carvajal-Vergara X, Sevilla A, D'Souza SL, Ang YS, Schaniel C, Lee DF, Yang L, Kaplan AD, Adler ED, Rozov R, Ge Y, Cohen N, Edelmann LJ, Chang B, Waghray A, Su J, Pardo S, Lichtenbelt KD, Tartaglia M, Gelb BD, Lemischka IR. Patient-specific induced pluripotent stem-cell-derived models of leopard syndrome. *Nature*. 2010;465:808-812